University of Stavanger

Faculty of Science and Technology

MASTER'S THESIS

Study program/Specialization: **Marine- and Offshore Technology**	Spring semester, 2021 **Open / ~~Restricted access~~**
Writer: **Vegard Knutsen**	
Faculty supervisor: **Professor Yihan Xing** External supervisor(s): **Ranjodh Singh**	
Thesis title: **Fatigue Analysis in Topside Pipe Systems Offshore**	
Credits (ECTS): **30**	
Key words: Fatigue, ASME B31.3, PD5500, Caesar 2, load cases, slug loads, wave loads, correlation study, expansion loop	Pages: **110** + enclosure: **13** **Stavanger, 14th June 2021**

Abstract

Safety and reliability are terms generally associated with offshore oil and gas industry, particularly regarding piping where failure could potentially cause catastrophic outcomes. Hence, codes and standards have been developed to ensure a level of quality and reliability regarding engineering practice. Such standards include methodologies and procedures with respect to many applications, where fatigue analysis is a central topic, especially when determining the design life of a structure subdued to cyclic loading. Two prominent standards in the field of offshore piping are ASME B31.3 and PD5500, where the former in 2018 added an appendix addressing the subject of fatigue analysis through an alternate method. Therefore, it is of great interest to perform a comparative study, in which results obtained from both codes were analyzed. Thus, inputs required for both methodologies were gathered through application of nodal piping software Caesar 2, which was used, amongst others, to calculate stress ranges at points of interest. For this case study, the points of interest were the elbows of an expansion loop between two oil platforms. These elbows were subdued to cyclic loading from a combination of sources, including wave displacements, slugging, and fluctuations of pressure and temperature. After stress ranges from all sources had been gathered and applied with fatigue analysis according to both codes, the results were compared and further analyzed through correlation studies with respect to the different sources of cyclic loading. The findings of which indicated that the procedure of ASME B31.3 yielded an overall more conservative output regarding estimated lifetime of structure when compared to methodology of PD5500 with S-N curve connected to weld class D. An important contributing factor of which was the constants associated with S-N curves, particularly in the case of high cyclic loading, where the former code resulted in 14 % shorter life expectancy. The most crucial factor was the method applied for calculating damage due to wave displacements, where ASME B31.3 resulted in average of 5.45 times higher instances of accumulated damage. The latter point was underlined by further analysis where more conservative weld class from PD5500 were applied. Specifically, class F2, which resulted in an overall shorter life expectancy according to PD5500 with significantly less accumulated damage attributed to wave displacements. Lastly, results from this thesis implied different impact of wall thickness, where an increase resulted in more conservative output from ASME B31.3 relative to PD5500. The main proposed reason for which was the stress outputs corresponding with increasing wall thickness that showed larger stresses from wave loads, along with decreasing stresses from slug loads.

Acknowledgement

This thesis served as graduating project of the Master of Science degree for the study program Marine- and Offshore Technology at the University of Stavanger. The entirety of the thesis was undergone in the spring semester of 2021.

I would like to extend my deepest gratitude to the department manager for piping and layout at Aker Solutions, Øystein Høie for accepting me to work on this exciting project. In addition to my thesis supervisor at Aker Solutions, Ranjodh Singh, who went beyond what could be expected to give me the best possible instructions and advice for solving the task. Additionally, I would also like to thank my supervisor at the University of Stavanger Yihan Xing for helping me in developing the scope and structure for the thesis. Lastly, I would like to thank my wife and son for the unparalleled patience, understanding, and support they have given me throughout my master studies.

<div align="right">
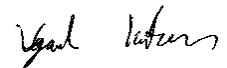
Stavanger, June 2021

Vegard Knutsen

</div>

Table of content

List of figures

List of tables

VIII

Nomenclature

A	-	S-N curve coefficient (PD5500)
C	-	Slope constant Paris section of crack growth curve
CF	-	Welded joint fatigue curve coefficient (ASME B31.3)
E	-	Elastic point
E	-	Youngs Modulus
E$_{CSA}$	-	Youngs modulus of carbon steel at ambient temperature of 21^0C
F	-	Fracture point
F	-	Force
K	-	Stress concentration factor
K$_{th}$	-	Stress concentration factor threshold value for crack initiation
I	-	Area moment of inertia
I$_p$	-	Polar area moment of inertia
L$_d$	-	Pipeline design life
L$_w$	-	Design storm period
M$_B$	-	Moment bending
M$_\theta$	-	Moment twisting
N	-	Total number of load cycles until fracture
N$_I$	-	Number of load cycles until crack initiation
N$_d$	-	Design number of stress cycles from waves
N$_g$	-	Number of load cycles during crack growth stage
N$_i$	-	Number of cycles for loading condition i
N$_{ti}$	-	Allowable number of load cycles for condition i (ASME B31.3)
N$_w$	-	Number of design cycles for storm wave height conditions
P	-	Linear section of stress-strain curve

P	-	Probability
S	-	Nominal stress
SD	-	Standard deviation
S_r	-	Nominal stress range
S_{max}	-	Maximum nominal stress
S_{min}	-	Minimum nominal stress
S_{zz}	-	Pierson-Moskowitz spectrum
T	-	Temperature in Celsius
T_E	-	Effective component thickness (ASME B31.3)
T_n	-	Nominal wall component thickness (ASME B31.3)
U	-	Ultimate tensile stress
V_0	-	Average zero up crossing period
X	-	Stochastic variable
Y	-	Yield point
Y	-	Stochastic variable
a	-	Crack length
a	-	Cross section area
cov	-	Covariance
d	-	Fatigue damage
d_t	-	Fatigue damage, all sources but waves (ASME B31.3)
d_w	-	Fatigue damage, wave loads (ASME B31.3)
dS	-	Integral operator surface of element
dV	-	Integral operator volume of element
e	-	Weld thickness (PD5500)
f	-	frequency
f	-	Specimen factor

f_I	-	Fatigue improvement factor
f_a	-	Factor related to wave fatigue
f_e	-	Environment factor
f_f	-	Maximum design stress (PD5500)
$f_{r,m}$	-	Maximum allowable stress range factor
$f_{m,k}$	-	Fatigue factor for stress ratio
f_r	-	Stress range factor
f_t	-	Temperature correction factor
h	-	Weibull stress range shape distribution parameter
k	-	Fatigue strength thickness component
m	-	Curve exponent for S-N curve for welded joint
n_i	-	Number of load cycles for source i
p_1	-	Internal pressure
p_2	-	External pressure
q	-	Weibull stress range scale distribution parameter
r	-	Radial Direction cylindrical coordinates
r_m	-	Middle surface radius
r_i	-	Inner radius
r_o	-	Outer radius
sm_i	-	Spectral moment of i grade
v	-	Poisson's ratio
$\mathbf{v}$	-	Velocity
w	-	Width plate
z	-	Longitudinal direction cylindrical coordinates
ε	-	Strain
σ	-	Local normal stress

σ_A	-	Local axial stress
σ_B	-	Local bending stress
σ_E	-	Code stress, ASME B31.3
σ_{Ei}	-	Computed stress range from load source i
$\sigma_{Ei, max}$	-	Computed maximum stress range from load source i
$\sigma_{Ei, min}$	-	Computed minimum stress range from load source i
σ_{Ew}	-	Computed maximum stress range from wave loads
σ_L	-	Longitudinal stress
σ_a	-	Allowable maximum local stress range (ASME B31.3)
σ_{aw}	-	Allowable maximum local stress range from waves
σ_c	-	Basic allowable stress at lowest temperature
σ_h	-	Basic allowable stress at highest temperature
σ_{eq}	-	Equivalent stress
σ_r	-	Local stress range
Φ	-	Surface segment
Δ	-	Range
α	-	Linear thermal expansion coefficient
θ	-	Angle cylindrical coordinates
ω	-	Angular frequency
τ	-	Torsion stress
Γ	-	Gamma function
ρ	-	Pearson correlation parameter
$\boldsymbol{\rho}$	-	Fluid density
[A]	-	Matrix representing boundary conditions of element
[B]	-	Strain displacement matrix
[**E**]	-	Youngs modulus matrix

[**F**] - Load matrix

[**N**] - Shape function matrix

[X] - Polynomial matrix

[d] - Displacement matrix

[k] - Element stiffness matrix

[u] - Vector in orthogonal coordinates

[ε] - Strain matrix

[σ] - Stress matrix

[δ] - Virtual displacement matrix

[∂] - Partial derivative for matri

Chapter 1 Introduction

This chapter presents the thoughts and concepts that initially sparked the motivation surrounding the work involved in this thesis, in addition to general information regarding the example case study. Furthermore, this chapter also includes objectives, and scope of thesis.

1.1 Background and motivation

In offshore oil production, pipelines and risers are essential parts of the production line, where often multiphase flow of oil, gas, and water is transported from wells to platforms and in between platforms and processing equipment of the same field. For pipes and risers operating in offshore setting, failure due to fatigue is a limiting factor regarding estimated design life. There are multiple sources of loading that results in accumulated damage from cyclic loading, where prominent cases includes, amongst others, pressure fluctuations, changes in temperature, slugging, and displacements caused by wave motion (Ortega & Rivera, 2013).

The mentioned sources of loading exert different impact on pipeline, wave displacements, and displacements caused by variation in temperature results in contractions and expansions of the pipeline. A natural consequence when such load cases take place, is that strain and corresponding localized stresses will occur as the pipeline resist deformation (Barker, 2018). As a result, a certain level of flexibility is advantageous for pipelines or risers that are exposed to this kind of loading. For topside bridges, acting as transportation pipelines between platforms, a solution for obtaining the required level of flexibility is to design the pipeline with an expansion loop, or another form of expansion compensator (Sutton, 2017). Generally, there are three different options of expansion compensators for pipelines, where axial joints, and bellows represents other methods than the mentioned expansion loop (Sutton, 2017). When an expansion loop experience expansion, forces and corresponding stresses are largely transmitted to supports, and fixed locations. Hence, the pipeline achieves more flexibility as the loop can expand and contract when exposed to waves or temperature variations. This yield relatively low instances of stress concentrations when compared to a standard pipe without any expansion compensator (Stewart, 2016).

1
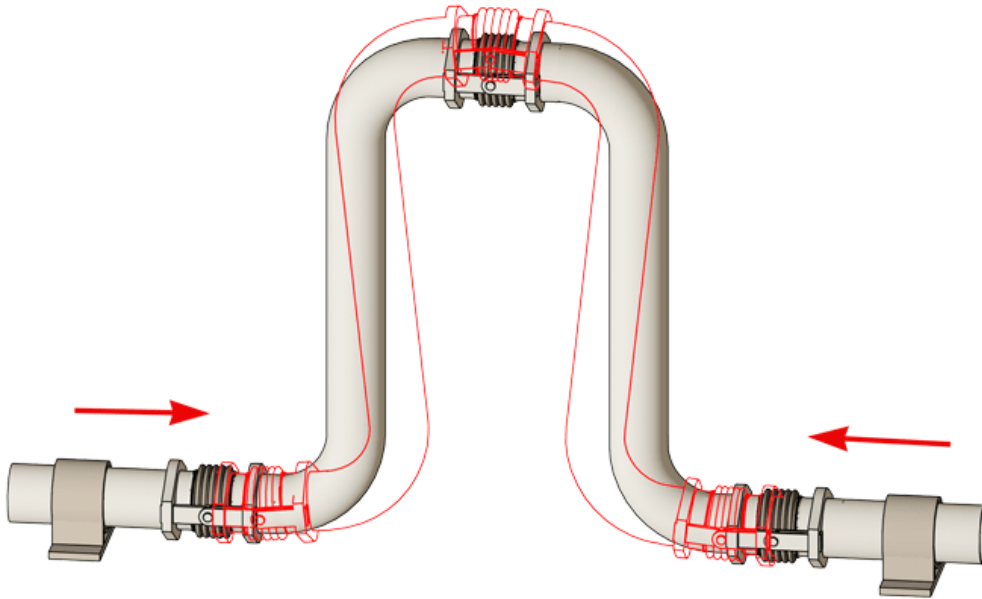
Figure 1-1: Expansion loop

Figure 1-1 shows a generic illustration of an expansion loop for the application of pipelines exposed to expansion and contraction. The red lines in the figure indicates deformed shape under contraction (Arveng Training and Engineering, 2021).

A side effect of an expansion loop, transporting multiphase flow, are stresses caused by slugging propagating at elbows of loop. This is because the curvature of pipeline will function as an obstruction to the flow, and result in accumulation of phases on either side of the bend. This will affect the state of equilibrium. Additionally, the curvature will result in flow particles accelerating in radial direction of curve (Gundersen, Andersen, & Haakonsen, 2012). In order to mitigate resulting stresses caused by cyclic loading due to slugging, a certain level of restraint and support is required. Therefore, a compromise between structural flexibility and rigidity is needed to best meet requirements of the structure's integrity in regard to fatigue from multiple sources.

Since failure of offshore pipelines would have catastrophic environmental consequences, such as gas leaks and oil spill, it is important to ensure a satisfying level of security. To assure a consensus, regarding safety in fields of engineering, codes with methodology has been developed. These calculations are applicable for a vast spectrum of utilities in marine and offshore sector. Amongst these utilities are fatigue calculations of pipeline welds. Different

standards have differing methodologies and safety factors. Hence, it is natural to assume that two selected codes might not offer the same levels of conservatism for calculations based on the same load, -and geometric inputs. Thus, gaining insight into which standard will yield the more conservative result for varying load cases will be interesting to determine the ideal code for various applications. It is believed that the comparative analysis carried out through this thesis will result in insight regarding effect of load cases on fatigue.

The codes applied for the comparative analysis of this thesis were specifically PD5500 and ASME B31.3. The former was developed by The British Standards Institution (BSI), which is the national standards body of the United Kingdom. Originally founded as engineering standards committee in 1901 in London, BSI is to this day involved in the production of technical standards (BSI Group, 2021). In addition to other services, such as supplying certification, and providing services relevant to codes and standards for various businesses. Furthermore, the institute is a non-profit body, that is operating worldwide, in 90 different offices in 31 countries (BSI Group, 2021). The code of PD5500 specifically provides specifications regarding pressure vessels manufactured from carbon, ferritic alloy and austenitic steel, nickel, and aluminum (BSi, 2003). The specifications addressed by this code generally applies to design, manufacturing, inspection, and testing. Hence, the code includes guidelines regarding fatigue analysis of welded pressure vessels subdued to cyclic loading. The specifics of these guidelines are provided in appendix C of PD5500.

The latter standard was developed by the American society of mechanical engineers (ASME). This organization was formed in 1880 as a not for profit membership organization that currently have a member status of over 110 000 engineers in more than 150 countries. The organization generally provides codes and standards for application in vast spectrum of technical fields, such as, elevators, fasteners, power plan systems, and pipelines. The standard B31.3 was specifically developed with regard to piping found in industries such as petroleum refineries (ASME , 2021). Within this field of application, it provides specific requirements regarding design, testing, construction, inspection regarding fusion welded pressure vessels for (ASME, 2018). Appendix W of the standard where added as an alternative methodology regarding fatigue analysis of pressure vessels subdued to high cyclic loading.

The principle this thesis followed to compare the fatigue standards were design by analysis. The example case for analysis was a topside piping bridge with an expansion loop between two offshore platforms supported by jacket foundation. The pipe section function as a transportation line of multiphase flow, which resulted in effects of slugging. In addition to slugging, this example case was subjected to other load cases, such as occurring stresses caused by waves displacement of platforms. Lastly, fluctuations of pressure and temperature were incorporated in analysis to obtain a broad representation of possible load cases relevant for this type of installation. Aforementioned sources of loading were utilized in combination with fatigue calculations from the standards of ASME B31.3 appendix W and PD5500 appendix C. In order to obtain a comprehensive result of the difference in utilization of standards, the analysis was performed under different combinations of load cases, where the results were statistically evaluated and compared.

1.2 Objective

The main objective of this thesis was to compare methodologies and obtained results from performing fatigue analysis provided in the codes PD5500 and ASME B31.3. Thus, gaining insight in how the codes differ in levels of conservatism regarding various sources of loading.

In order to achieve the main objective of this thesis, the following sub-objectives were defined and carried out. First, to gain understanding of methodologies and requirements of the two codes, a literature study of the two standards was done. Second, a model representing the example case of the pipeline in nodal software Caesar 2 was created, where several load cases relevant to fatigue calculations were specified. Third, outputs from stress analysis were applied to perform fatigue calculations according to methodologies from both codes. Fourth, numeric outputs from both fatigue calculations were compared to each other. Lastly, a correlation study between inputs from different load cases and outputs from fatigue analysis according to both codes was applied using excel.

1.3 Outline of thesis

- ➤ Chapter 2 contains fundamental theories relevant for the various calculations that has been included throughout the work involved with this thesis. Such as theory of elasticity, crack growth and fatigue, in addition to information surrounding application of the standards ASME B31.3 and PD5500 for fatigue analysis.

- ➤ Chapter 3 presents the methodology applied for performing stress analysis, which specifically entail general information of the nodal software Caesar 2, in addition to inputs to said software. These inputs include amongst others pipe geometry, boundary conditions, material, and loads.

- ➤ Chapter 4 includes outputs from stress analysis performed in Caesar 2.

- ➤ Chapter 5 presents the methodologies given in the two standards ASME B31.3 and PD5500, in addition to input parameter values to the respective methods. (in here is check of stresses and cycles provided by standards)

- ➤ Chapter 6 contains results from fatigue calculations according to both codes, in addition to comparison and discussion regarding the respective results.

- ➤ Chapter 7 includes correlation study of outputs from fatigue analysis, where correlation between load cases and fatigue output according to both codes are determined.

- ➤ Chapter 8 presents a summary of the thesis, before the reached conclusion based on fatigue calculations and correlation studies. Furthermore follows, suggestions and recommendations regarding future considerations when implementing these methodologies in industry. Lastly, this chapter presents the authors recommendations for future work within the field of fatigue of marine structures.

Chapter 2 Theory

2.1 Elasticity

Stress can be categorized into two overarching categories, global/nominal and local stress, where global stress is the result of the loads exerted on the geometry. For a uniform cross section under uniaxial tension, the global stress can be described through the following formula. Symbol A represents cross section area, and **F** is axial force.

$$S = \frac{F}{A} \qquad\qquad 2.1$$

Local stress, however, is the levels of stress that occur in fragmented sections of the structure, which is due to various conditions, such as geometry and resulting multiaxial stresses and strains (Schreurs, 2013). A more thorough explanation of the concept of local stresses, first requires consideration regarding theory of elasticity.

Elastic theory is a branch within solid mechanics regarding isotropic and linear elastic materials subjected to small deformations under external loading (Irgens, 2008). For an isotropic material subjected to isotropic elasticity, which is the case of general elasticity theory, it is implied that material properties are identical in all directions and that principle direction of stress and strain coincide (Boresi & Schmidt, 2003). Furthermore, materials with linear elastic properties defines that the relationship between stress and strain is linear, hence Youngs modulus E is constant and represent the steepness of the stress strain curve under yield, this linear relation is called Hooks law, and is expressed as shown in equation 2.2 (Schreurs, 2013),

$$\varepsilon = \frac{\sigma}{E} \qquad\qquad 2.2$$

where σ is stress, ε is strain, and **E** denotes Youngs modulus. An important factor, which is a consequence of linear elastic theory, is that it is only valid below yield stress of the material. This is the maximum stress level where all applied deformation is still reversible, which is also called elastic deformation (Roylance, 2001). When stresses exceeds the yield strength of material, plastic deformation will take place and the component will experience permanent changes in geometry (Callister & Rethwisch, 2011). This will cause non-linear behavior

between stress and strain at levels of stress exceeding the yield limit of the material. The linear relation between stress and strain, including the non-linear section of plastic deformation, is presented in the generic stress strain curve of figure 2-1.

P represent the maximum level at which the relation between stress and strain is linear. The symbol E at curve denotes the elasticity limit, which indicate the region of which the component is still under reversible elastic deformation. Furthermore, Y represent the yield strength of material, which defines the stress level where, if exceeded, plastic deformation will take place (Roylance, 2001). For materials that does not have a well-defined yield point, the 0.02% offset method can be used (MechniCalc, 2021). Hence, Youngs modulus would represent the linear curve drawn from offset method, which is illustrated as dashed line on figure 2-1. The letter U at the figure represent ultimate tensile strength, which is the maximum stress level the material can endure before experiencing necking. Lastly, F represents fracture point.
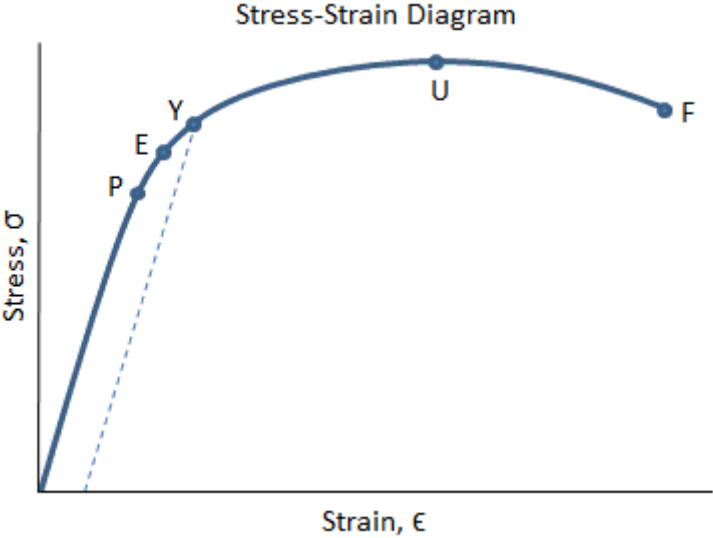
Figure 2-1: Stress-strain diagram

For isotropic, linear elastic materials the relation between stress and strain can, as shown in equation 2.2, be described mathematically through Hooks law, where the elasticity modulus acts as the stiffness constant. However, to determine the relation between stresses and strains for a three-dimensional body, subdued to triaxial strains, the concept expressed in equation 2.2 must be expanded as shown in equation 2.3 through 2.6.c, where v represents Poisson's ratio (Bell, 2015).

$$\varepsilon_{xx} = \frac{1}{E}\left[\sigma_{xx} - v\left(\sigma_{yy} + \sigma_{zz}\right)\right] \qquad\qquad 2.3$$

$$\varepsilon_{yy} = \frac{1}{E}\left[\sigma_{yy} - v(\sigma_{xx} + \sigma_{zz})\right] \qquad\qquad 2.4$$

$$\varepsilon_{zz} = \frac{1}{E}\left[\sigma_{zz} - v\left(\sigma_{xx} + \sigma_{yy}\right)\right] \qquad\qquad 2.5$$

$$\varepsilon_{xy} = \frac{(1+v)}{E}\sigma_{xy}, \qquad \varepsilon_{xz} = \frac{(1+v)}{E}\sigma_{xz}, \qquad \varepsilon_{yz} = \frac{(1+v)}{E}\sigma_{yz} \qquad 2.6.\,a - 2.6.\,c$$

Equations applied in the field of elastic theory are linear partial differential equations. Therefore, the superposition principle can be applied, which means that the sum of individual solutions to the set of equations is also a solution to the equations. Furthermore, the theory of elasticity also includes a theorem of uniqueness of solution and a theorem of existence of solution (Schreurs, 2013). The former theorem state that the solution derived from the relevant set of equations, with the given boundary conditions, must be the only solution to the problem. The latter theorem, however, merely state that a solution to the problem must exist (Irgens, 2008).

A Hookean solid subjected to strains induced by other factors than mechanic loads, such as strains caused by thermal expansion or contraction, requires an alteration of the previously presented formula as shown in equation 2.3-2.5. This alteration results in the following relation displayed in equation 2.3.a through 2.5.a, in the case of shear strains, the relation remains as in equation 2.6.a-2.6.c (Boresi & Schmidt, 2003).

$$\varepsilon_{xx} = \frac{1}{E}\left[\sigma_{xx} - v\left(\sigma_{yy} + \sigma_{zz}\right)\right] + \alpha\Delta T \qquad\qquad 2.3.\,a$$

$$\varepsilon_{yy} = \frac{1}{E}\left[\sigma_{yy} - v(\sigma_{xx} + \sigma_{zz})\right] + \alpha\Delta T \qquad\qquad 2.4.\,a$$

$$\varepsilon_{zz} = \frac{1}{E}\left[\sigma_{zz} - v\left(\sigma_{xx} + \sigma_{yy}\right)\right] + \alpha\Delta T \qquad\qquad 2.5.\,a$$

Alpha is the linear thermal expansion coefficient of the material, and delta T denotes the change in temperature in degrees of Celsius. The relation presented in the formula depends on the assumptions of thermal isotropy and thermal homogeneity, which means that the longitudinal strain is the same for all directions of the material (Callister & Rethwisch, 2011). Hence, the total strains of a Hookean solid consists of three contributing factors, namely thermal strains, elastic strains due to solid resisting thermal deformation, and elastic strains caused by external loads.

2.2 Cylindrical shell

Hollow cylindrical structures are due to their generally high strength to weight ratio applicable for a variety of applications, including pressure vessels such as offshore pipelines and risers. These structures are often subjected to wide array of different sources of stresses, such as internal pressure, external pressure, changes in temperature, and bending. For cylindrical pressure vessels under combined loading, the acting stress components are shear stress, circumferential stress and longitudinal stress (Boresi & Schmidt, 2003). The shear stress component is a result of the torsion moment exerted on the cylinder. The relation between strain and stresses for cylindrical cross-section are given by formula 2.3.b through 2.5.b (Bell, 2015).

$$\varepsilon_{rr} = \frac{1}{E}[\sigma_{rr} - v(\sigma_{\theta\theta} + \sigma_{zz})] + \alpha\Delta T \qquad 2.3.b$$

$$\varepsilon_{\theta\theta} = \frac{1}{E}[\sigma_{\theta\theta} - v(\sigma_{rr} + \sigma_{zz})] + \alpha\Delta T \qquad 2.4.b$$

$$\varepsilon_{zz} = \frac{1}{E}[\sigma_{zz} - v(\sigma_{rr} + \sigma_{\theta\theta})] + \alpha\Delta T \qquad 2.5.b$$

Equation 2.3.b through 2.5.b can be rewritten and solved with respect to stress components, and thus be applied for stress calculations based on strains, and changes in temperature.

For cylindrical structures applied as beams, there are, amongst other, three different types of stress sources of interest due to exerted mechanical loading. These sources are axial stress, bending stress, and torsional stress. Definitions of which is described through following equations respectively (Bell, 2014):

$$\sigma_N = \frac{F}{A} \qquad 2.1.b$$

$$\sigma_B(r) = \frac{M_B}{I} r \qquad\qquad 2.7$$

$$\tau(r) = \frac{M_\theta}{I_p} r \qquad\qquad 2.8$$

where M_B is bending moment, M_θ is twisting moment, the symbols I_p and I denote second polar moment of area and moment of area respectively, for hollow cylindrical cross-section, given by equations 2.7.a, and 2.8.a. The latter two equations are both functions of stress over the cross-section's radius.

2.2.1 Stress components for pressure and temperature

Stress components due to effects of pressure and temperature can for a cylindrical pressure vessel be determined through the application of equation 2.9-2.14. Equation 2.9-2.11 denotes stress components in situations of negligible effects due to change in temperature, while equation 2.12-2.14 is applicable for situations where only effects of change in temperature is considered. Base assumption for these expressions is that the pipe is close ended and computation occur far from either end (Boresi & Schmidt, 2003).

$$\sigma_{rr} = \frac{p_1 r_i{}^2 - p_2 r_o{}^2}{r_o{}^2 - r_i{}^2} - \frac{r_i{}^2 r_o{}^2}{r_m{}^2 (r_o{}^2 - r_i{}^2)} (p_1 - p_2) \qquad\qquad 2.9$$

$$\sigma_{\theta\theta} = \frac{p_1 r_i{}^2 - p_2 r_o{}^2}{r_o{}^2 - r_i{}^2} + \frac{r_i{}^2 r_o{}^2}{r_m{}^2 (r_o{}^2 - r_i{}^2)} (p_1 - p_2) \qquad\qquad 2.10$$

$$\sigma_{zz} = \frac{p_1 r_i{}^2 - p_2 r_o{}^2}{r_o{}^2 - r_i{}^2} + \frac{F}{\pi (r_o{}^2 - r_i{}^2)} \qquad\qquad 2.11$$

where r_m is middle surface curvature radius, r_i is inner radius, r_o is outer radius of cross section. Furthermore, p_1 and p_2 represents inner and outer pressure respectively, and **F** is axial force. Following set of equations presents stress distribution for a thick-walled cylinder under linearly elastic behavior for steady state change in temperature (Boresi & Schmidt, 2003).

$$\sigma_{rr} = \frac{\alpha E \Delta T}{2(1-v)\ln\left(\frac{r_o}{r_i}\right)}\left[-\ln\left(\frac{r_o}{r}\right) + \frac{r_i{}^2(r_o{}^2 - r^2)}{r^2(r_o{}^2 - r_i{}^2)}\ln\left(\frac{r_o}{r_i}\right)\right] \qquad 2.12$$

$$\sigma_{\theta\theta} = \frac{\alpha E \Delta T}{2(1-v)\ln\left(\frac{r_o}{r_i}\right)}\left[1 - \ln\left(\frac{r_o}{r}\right) - \frac{r_i{}^2(r_o{}^2 + r^2)}{r^2(r_o{}^2 - r_i{}^2)}\ln\left(\frac{r_o}{r_i}\right)\right] \qquad 2.13$$

$$\sigma_{zz} = \sigma_{rr} + \sigma_{\theta\theta} \qquad 2.14$$

2.3 Primary and secondary stresses

Primary stresses are defined as stress caused by solely mechanical loading, which mean stresses that are induced by forces, such as gravity and pressure. Another characteristic of primary stresses is that they are not self-limiting, which mean that the structure is unable to contain continuing deformation until stresses reach equilibrium, once stress levels of plastic deformation is reached. Most primary stresses tend not to by cyclic of nature, but static, however, some types such as pulsating in pressure can be classified as cyclic primary stress. Secondary stresses are normal, or shear stress usually caused by displacements, for example displacements due to thermal expansion, vibration, or movement of foundation. Unlike primary stresses, secondary stresses are generally self-limiting, which means that stress dissipate as structure reach yield (Rezkallah, 2021; Hexagon, 2017).

2.4 Sources of loading

2.4.1 Slugging

Slugging is a phenomenon that occur in transportation pipelines of multiphase flow, where accumulation of either the gas or liquid phase results in sections where there is difference in density from the ambient fluid (Mokhatab & Towler, 2007). This phenomenon is particularly relevant regarding the systems integrity in piping sections with bends. Under ideal production conditions, the pipe is transporting a mixture of liquid and gas that have a uniform density throughout the pipeline, which leaves the piping system in equilibrium. However, the reality of the state of the multiphase flow of the system is not that simple, in fact there are many factors that may result in slugs. These factors can be related to events that causes change in pressure or

temperature, which in turn affect the density of the gas or liquid (Kansao et al, 2008). Additionally, changes in direction regarding flow will cause the particles of fluid to experience acceleration perpendicular to the direction of flow (Ortega & Rivera, 2013). Hence, when slugging occurs in pipeline bends, it causes the forces acting before and after each bend to become out of balance with respect to the state of equilibrium. When expressing slugging induced forces mathematically, it is easily seen that curvature of the pipe cross-section is vital, as presented in equation 2.15 through 2.15.b (Hou, Tijsseling, & Bozkus, 2014). Where both horizontal and vertical component of the slugging force is redundant for sections without curvature.

$$\boldsymbol{F} = DAF \cdot \boldsymbol{\rho v}^2 \pi r_i{}^2 \sqrt{2(1 - cos\theta)} \qquad\qquad 2.15$$

$$\boldsymbol{F}_x = DAF \cdot \boldsymbol{\rho v}^2 \pi r_i{}^2 (1 - cos\theta) \qquad\qquad 2.15.a$$

$$\boldsymbol{F}_y = DAF \cdot \boldsymbol{\rho v}^2 \pi r_i{}^2 sin\theta \qquad\qquad 2.15.b$$

DAF is acronym for dynamic amplification factor and is a dimensionless number that is used in equations containing expressions for static loads in order to factor in the effects of dynamic loading (El-Reedy, 2015). Furthermore, $\mathbf{v}$ represents the velocity of the flow, r_i is inner diameter of cross-section, and the symbol $\boldsymbol{\rho}$ is density of the fluid.

2.4.2 Waves

In the case of marine structures, waves will cause displacements in potentially three lateral directions, depending on the response of the vessel. The response displacement of the vessel depends not only on the size and direction of the wave, but also the vessels mass and geometry (Journee & Massie, 2001). A floating vessel has 6 degrees of freedom, namely, heave, sway, surge, yaw, roll and pitch. The first three are relative to motion in 3D space, while the latter three are related to rotating motion among the axis of the 3 dimensional coordinate system (Gudmestad, 2015). Hence, the motion response of a vessel when encountering waves is a result of different combinations of the mentioned 6 degrees of freedom. The motion response of a vessel can be obtained for various angles of incoming waves combined with wave heights. This

is done in order to determine displacements of defined points on vessel. For the further determination of the incoming angle and wave heights these displacements become critical.

For wave loads a comprehensive study of the area in question is necessary to establish a good understanding of expected wave heights. These expected values are determined through statistical methods, where the wave data of a certain location is recorded and analyzed over a long period of time (Journee & Massie, 2001). Parameters and variables, with respect to the wave field, required for evaluating wave induced displacements are explained further in chapter 2.8.1.

2.4.3 Thermal and displacement loads

A well-known property of metallic alloys is that they expand over increase in temperatures and shrink during decrease, where the rate of change relative to change in temperature depends on the material (Callister & Rethwisch, 2011). When these displacements occur in proximity to restraints, it results in stresses propagating in the structure. The significance of these displacements depends on factors such as material temperature coefficient of expansion (α), ambient temperature, and in the case of pressure vessels, operating temperature of content fluid (Braestrup, et al., 2005). In the case of constant strain, linear displacements caused by change in temperature can be determined mathematically as shown in equation 2.16 (The Process Piping, 2021),

$$u(x) = \varepsilon_t \times x = \alpha \Delta T \times x \qquad\qquad 2.16$$

where x is length of subject, and ε_t is strain caused by thermal expansion or contraction, and T is temperature in degrees Celsius. Consequently, the stress range applicable for fatigue analysis from thermal expansion is determined based on the strain range given by the change in temperature. For a hollow cylindrical cross-section only subjected to stresses induced by changes in temperature, the stress components can be expressed as shown in equation 2.12-2.14.

2.4.4 Pressure

Operating pressure within a pipeline is usually a source for fatigue loading since there will typically be fluctuations off the pressure level. Hence, load cycles occur from variations in

pressure, where one load cycle is defined as significant deviation from the steady state status of operating pressure.

2.5 FEA

Finite element method is a numerical approach to solving engineering problems related to topics such as structural mechanics. The methodology of this form of analysis includes following steps. The first step is to define the geometry representing the structure of analysis. After the geometry has been defined, it can be divided into a network of nodes with interconnecting elements. Once the nodal network has been defined, loads and boundary conditions can be assigned to the nodes for analysis. The principle of a generic FEA system can be presented in the following matter (Dong, 2001),

$$[\boldsymbol{F}] = [k] \cdot [d] \qquad 2.17$$

where the F-matrix represent the loads applied to the system, d-matrix represent nodal displacement, and k-matrix is the stiffness matrix of the system. To establish the systems stiffness matrix, it is necessary to evaluate the shape functions of the elements the system consists of. This can be done through interpolation, where the level of interpolation depends on the base element and the number of nodes it contains. For beam elements with one node on each end, the interpolation is done through a polynomial that represent bending, axial and shear forces and displacements that may occur in that element. The process of interpolation results in a matrix of the elements shape functions, which is presented in equation 2.18 through 2.18.b for the case of beam element (Zienkiewicz, Taylor, & Zhu, 2005).

$$[N] = [X] \cdot [A]^{-1} \qquad 2.18$$

where $[X]$ represents the polynomial degree of which the shape functions are interpolated. In the case of generic beam element, it is as follows.

$$[X] = [1 \ \ x \ \ x^2 \ \ x^3], \qquad \frac{d}{dx}[X] = [0 \ \ 1 \ \ 2x \ \ 3x^2] \qquad 2.19 - 2.20$$

15

Furthermore, $[A]$ can be represented as shown in equation 2.18.a.

$$[A] = \begin{bmatrix} X_{(0)} \\ X_{x(0)} \\ X_{(L)} \\ X_{x(L)} \end{bmatrix} = \begin{bmatrix} 1 & 0 & 0 & 0 \\ 0 & 1 & 0 & 0 \\ 1 & L & L^2 & L^3 \\ 0 & 1 & 2L & 3L^2 \end{bmatrix} \qquad 2.18.\,a$$

As a result, the shape functions matrix can be defined as follows.

$$[N] = \begin{bmatrix} 1 & x & x^2 & x^3 \end{bmatrix} \cdot \begin{bmatrix} 1 & 0 & 0 & 0 \\ 0 & 1 & 0 & 0 \\ 1 & L & L^2 & L^3 \\ 0 & 1 & 2L & 3L^2 \end{bmatrix}^{-1} = \begin{bmatrix} 1 & x & x^2 & x^3 \end{bmatrix} \cdot \frac{1}{L^3} \cdot \begin{bmatrix} L^3 & 0 & 0 & 0 \\ 0 & L^3 & 0 & 0 \\ -3L & -2L^2 & 3L & -L^2 \\ 2 & L & -2 & L \end{bmatrix} \quad 2.18.\,b$$

When deriving element matrices, it is necessary to apply certain mechanical principles, specifically the principle of virtual work and the principle of virtual displacement. A virtual displacement is defined as a small and admissible change in the systems configuration (Hughes, 2000). In other words, change that does not break with assigned the boundary conditions. The principle of virtual work states that the amount of strain energy accumulated in the system is equal to that of the total work done by body forces in volume and traction forces on surface. Thus, the principle of virtual work can be described as the following equation (Cook, Malkus, & Plesha, 1989),

$$\int [\delta\varepsilon]^T \cdot [\sigma]\, dV = \int [\delta u]^T \cdot [F] dV + \int [\delta u]^T \cdot \emptyset dS \qquad 2.19$$

where the first term of the equation represents total work exerted on geometry, the second and third term of the equation, however, represent work caused by body forces and surface forces respectively. Mathematical notation of terms in principle of virtual work are displayed in equation 2.20-2.22 (Zienkiewicz, Taylor, & Zhu, 2005).

$$[\varepsilon] = [\partial] \cdot [u], \qquad u = [u, v, w]^T = [N] \cdot [d], \qquad [\sigma] = [\varepsilon] \cdot [E] \qquad 2.20 - 2.22$$

For one element, the matrix representing strain is:

$$[\varepsilon] = [\partial] \cdot [N] \cdot [d] = [B] \cdot [d] \qquad\qquad 2.20.a$$

where $[B]$ is strain displacement matrix for the element.

$$[B] = [\partial] \cdot [N] \qquad\qquad 2.23$$

Equation 2.20.a, 2.21, 2.22, and 2.23 can be substituted into the original expression representing the principle of virtual work. This is the expression that need to be solved for an arbitrary element in order to establish the element stiffness matrix. This expression is valid for any virtual displacements (Hughes, 2000).

$$\int [\delta]^T \cdot [B]^T \cdot [d]^T \cdot [\varepsilon] \cdot [E] \, dV = \int [\delta]^T \cdot [N]^T \cdot [d]^T \cdot [F] dV + \int [\delta]^T \cdot [N]^T \cdot [d]^T \cdot \phi dS$$

$$\rightarrow [\delta d]^T \cdot \left\{ \int [B]^T \cdot [B] \cdot [d] \cdot [E] \, dV - \int [N]^T \cdot [F] dV - \int [N]^T \cdot \phi dS \right\} = 0$$

$$\rightarrow \int [B]^T \cdot [B] \cdot [d] \cdot [E] \, dV - \int [N]^T \cdot [F] dV - \int [N]^T \cdot \phi dS = 0 \qquad 2.19.a$$

Hence, by applying equation 2.19.a along with the generic expression of a FEA presented in equation 2.17, the expression for determining a systems stiffness matrix is obtained,

$$[k] \cdot [d] = [F] = \int [N]^T \cdot [F] dV + \int [N]^T \cdot \phi dS \qquad\qquad 2.24$$

where $[F]$ in this case represents the systems reaction forces, thus, the final expression for the systems stiffness matrix is defined as following,

$$[k] = \int [B]^T \cdot [B] \cdot [E] \, dV \qquad\qquad 2.24.a$$

Once the systems stiffness matrix is determined, the loads and boundary conditions can be applied to the relevant matrices in equation 2.24.a to perform finite element analysis. The application of boundary conditions entails determining nodal restraints for model in accordance

with the system under evaluation (Hughes, 2000). The loads acting on the system is similarly applied at each respective node for both horizontal and vertical direction. Lastly, Support reactions and displacements of undefined nodes in the system can be determined through solving the set of equations derived from the three matrices. Naturally, for any realistic system this process becomes a set of equations of a magnitude so large that solving without the use of computer software is futile. Hence, special software packages have been developed in order to handle these structural calculations.

2.6 Fatigue

Structural failure can generally be divided into two categories, fracture caused by exceeding ultimate tensile limit of structures material, and fatigue induced fracture. The latter term is defined as cyclic loading of relatively lower stresses, usually lower than yield strength of material (Berge & Ås, 2017). Consequently, fatigue is cycle by cycle process of damage accumulation, where each cycle might be insignificant. However, with millions of such cycles, the damage may result in significant weakening of the structures integrity. Furthermore, fatigue life is generally represented through crack growth, and how crack initiate and continue to grow over continued load cycling until finally the size of the crack overcome the structure and causes final failure (Ziegler & Muskulus, 2016). Thus, total fatigue life can be generally described through a simple equation displaying the three stages of a component's life before fatigue fracture, as shown in equation 2.25 (Berge & Ås, 2017), where N is total number of load cycles before fracture, N_I is crack initiation and N_g is crack growth.

$$N = N_I + N_g \qquad\qquad 2.25$$

Furthermore, crack initiation and growth are commonly defined through application of crack growth diagram, which represent the two stages, in addition to fracture as displayed in figure 2-2.
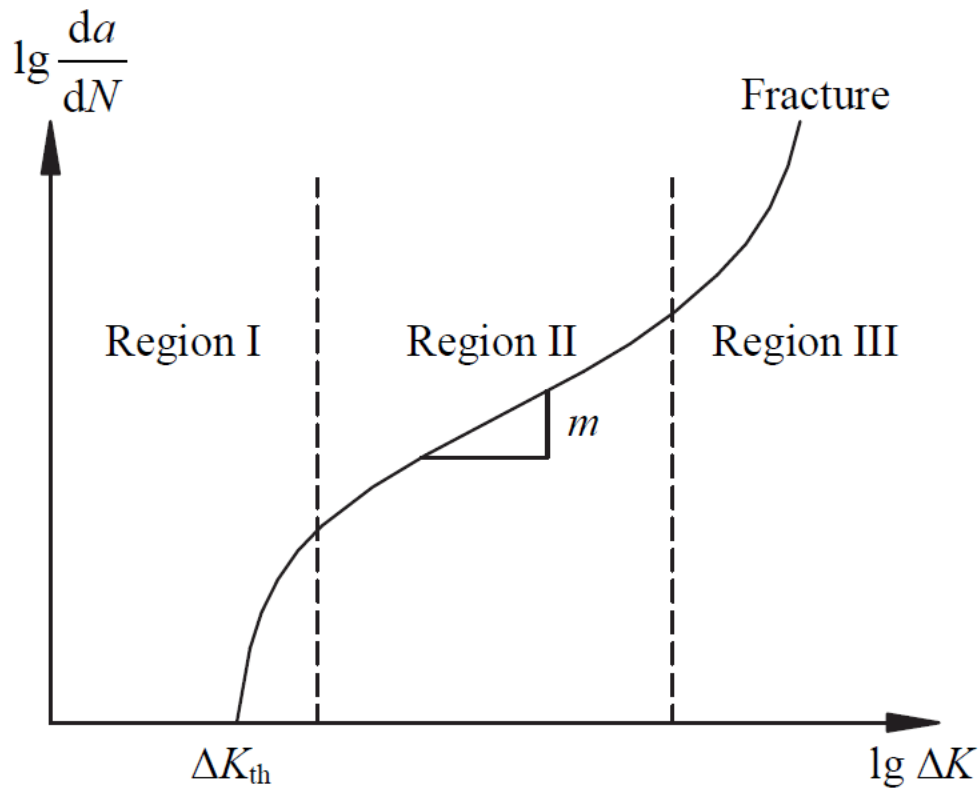
Figure 2-2: Crack growth curve

The vertical axis of the diagram represents change in crack length (a) with respect to load cycles (N). The horizontal axis, on the other hand, depends on change in K-value, which is a linear elastic parameter that is defined as the stress intensity factor. The stress intensity factor is an analytical approach to determine the impact of stresses located at the weld toe. Mathematically, K is defined as shown in equation 2.26 (Keprate et al, 2016). Hence, it is solely dependent on nominal stresses and geometry of crack and component of analysis. K_{th} indicates the threshold value for initiation of cracks, and is defined as equation 2.26, but with the threshold stress range that initiates crack growth (Ziegler & Muskulus, 2016).

$$K = S\sqrt{\pi a} \times f\left(\frac{a}{w}\right) \qquad 2.26$$

In this equation, S is nominal stress, the parameter a is the length of crack, w is width of component under evaluation, and f is a specimen factor determined through the relation between a and w.

19

As can be observed in the generic crack growth diagram, only a certain portion of the curve is approximately linear (region 2), which makes this part most ideal for consideration. This linear section of the crack growth curve is commonly referred to as the Paris section, and is denoted by equation 2.27, which defines the rate of crack growth (Paffumi, Nilsson, & Taylor, 2008).

$$\frac{da}{dN} = C(\Delta K)^m \qquad\qquad 2.27$$

where C and m are material constants that defines the linear section of the relevant crack growth curve.

Of the two phases, crack initiation and growth, which one is dominant depends on the physical characteristics of the component. These characteristics include amongst other, production method and whether there is a welded or bolted connection included in the structure. For a machined component, the number of load cycles initiating cracks represents the majority of fatigue cycles. For components with welded connections, however, the crack growth phase dominates the process (Berge & Ås, 2017). The reason for this difference is due to material defects in connecting joint after completed welding process (Berge & Ås, 2017; Callister & Rethwisch, 2011), which means that these weld defects in practice affect the component in the same manner as a small crack with respect to fatigue. For machined components with smooth surfaces, the initiation stage is most prominent. In these cases, cracks propagate in slip planes located at the surface of the component. Slip planes are flaws in the atomic structure of a metallic alloy that take the form as gaps between the planes of the atomic structure, which leads to dislocations more easily taking place and further lead to plastic deformation (Callister & Rethwisch, 2011). Due to the large number of crystalline grains, a component of a crystallin material is statistically bound to have slip planes located somewhere at its surface. Although a structure is bound to have slip planes that can cause crack initiation, the total amount of load cycles until fracture is still considerably higher than that of a welded connection with inherent defects (Berge & Ås, 2017). Hence, the concept of weldability is introduced. An important aspect of weldability is reducing the occurrence of weld defects as much as possible (Bjork, Samuelsson, & Marquis, 2008). This is achieved through good choice of materials, good workmanship, inspections, and quality control. However, despite efforts such as these, the process of welding will always cause impurities in the structure, whether it is introduction of slag, lack of weld penetration or porosity forming in weld (Bjork, Samuelsson, & Marquis,

2008). Therefore, whenever a welded connection is present in a structure, it represents a location of great interest considering fatigue fracture analysis. This is especially represented in standards such as PD5500, where fatigue calculations are largely based on weld classes that are defined in mentioned code (BSi, 2003).

It is not only the state of structure and method of manufacturing that affect crack initiation and growth. There are multiple other contributing factors affecting the fatigue life of a structure. Firstly, corrosion is a natural process of the metal returning to its original form, in the case of steel alloys, iron oxide. This process is greatly accelerated when the metal is submerged in seawater (Berge & Ås, 2017). Chemically, the process of corrosion involves oxidation, where electrons transfers from the material to the environment (seawater or air), thus, degrading the material (Chopra, 2000). There are different ways of protecting the structure against the accelerating effect of corrosion when submerged. One of such method is coating the surface area of the structure with protective layer of paint, which insulates the structure and protects it against seawater (Braestrup, et al., 2005). The second contributing factor is the frequency of load cycles. Since failure caused by fatigue is defined as the number of load cycles that causes fracture in structure, the frequency of the cyclic loading is highly relevant for the structure's lifespan. High frequent loading will reduce the design life relative to low frequent loading, which will have the same number of cycles over a longer period. Thirdly, the orientation of loading will influence the fatigue life, whether it is uniaxial loading, bending or torsion (Berge & Ås, 2017). Fourthly, the operating temperature is an important factor also regarding estimation of a structures design life. All metallic alloys experience increasing brittleness and hardening under low temperatures. This ductile to brittle transition temperature is a threshold, that varies with different materials. However, change in temperature will usually result in an alteration of the materials Youngs modulus, even if the material has yet to reach the transitional phases of ductile to brittle (BSi, 2003; Callister & Rethwisch, 2011). Generally, increase in temperature lead to decrease in magnitude of Youngs modulus, and oppositely for decrease in temperature, an increase in Youngs modulus is experienced. Hence, relevant temperatures regarding design of structure is highly relevant for estimation of fatigue. Lastly, resulting stress range from applied load cycle, these ranges are considered as a sinusoidal function, which is shown in equation 2.28 (Berge & Ås, 2017),

$$S_r = S_{max} - S_{min} \qquad 2.28$$

where S_{max} is the largest instance of nominal stress caused by applied external loading. Furthermore, S_{min} is lowest nominal stress acting on the same component before returning to equilibrium. Thus, one load cycle is defined as an applied load resulting in the occurrence of an individual stress range. However, load cycles are not always stress ranges of identical amplitude. On the contrary, it is often the case that there is varying amplitude, depending on different sources of loading. For marine structures that is exposed to harsh environment and irregular loading from various sources, it is necessary to account for all relevant loadings and incorporating them into the fatigue analysis. A method for handling these irregular loading amplitudes, is through rain flow counting (Lee & Tjhung, 2012; Berge & Ås, 2017). This is a counting method that can be applied through the following steps. First, present all the load cycles as stress ranges with peaks and valleys, this stress cycle plot is to represent a pagoda rooftop when rotated 90 degrees. Secondly, each stress peak is to be imagined as a source of rain that run down the rooftop off the edge. The occurrences of half cycles are counted when; the rain flow reaches the end of the time history, intersect with a past flow of greater magnitude, or it continue to flow, but there are peaks of greater size at later stage. Thirdly, this process is repeated for the valleys of the plot. Fourth, all half-cycles get a stress value equal to the difference in stress from initiation to termination of cycle. Lastly, matching half-cycles, same magnitude, but opposite orientation, are paired up and counted as whole load cycles (Lee & Tjhung, 2012).

The rain flow method is not the only way of handling load cycles of varying amplitude. This can also be achieved through minor summation, which is a simple and precise method of addressing the problem of variable stress amplitude through load history. This method is based on the premise that damage inflicted on structure is constant for each load cycle for a given stress range, which is given by equation 2.29 (Berge & Ås, 2017),

$$d = \frac{1}{N} \qquad\qquad 2.29$$

where N is the estimated number of load cycles until failure for a source of loading with constant amplitude. Hence, for a series of varying stress ranges, the sum of cumulated damage is determined through equation 2.29.a (ASME, 2018; BSi, 2003).

$$d = \sum_{i=1}^{n} \frac{n_i}{N_i} \qquad\qquad 2.29.a$$

In this case, Ni is calculated number of load cycles until failure for a given source of loading, and ni is the actual amount of load cycles for the same source.

The definition of minor sum can be expanded further to an expression for equivalent stress range. This expression entail combining the damage caused by all loadings and combining them into one nominal stress range that is equivalent to that estimated damage. The equivalent stress range is determined through the following formula (Paffumi, Nilsson, & Taylor, 2008).

$$\Delta\sigma_{eq} = \frac{1}{n} \sum_{i=1}^{n} [(\Delta\sigma_i)^m]^{\frac{1}{m}} \qquad\qquad 2.30$$

Fatigue data is normally presented in a stress-life diagram (SN-diagram), where S denotes the nominal stress range and N is the number of cycles to failure. The SN-diagram is generally related to the linear Paris section of a crack growth diagram (Berge & Ås, 2017), which makes constants representing crack growth curve relevant for corresponding SN-diagrams .

A conventional SN-diagram consists of two zones, namely low-cycle fatigue (LCF) and high-cycle fatigue (HCF). The former denotes structures undergoing less than 10^7 load cycles before failure, which imply relatively high nominal stress range, a result of which is that cyclic plastic behavior can be detected for LCF. However, cases falling in the classification of LCF are not generally considered by standards regarding marine structures. HCF is relevant for structures exposed to cyclic stress ranges exceeding that of 10^7 load cycles (ASME, 2018; BSi, 2003). Furthermore, in HCF range, the relationship between number of cycles and nominal stress range is log-linear, which mathematically be described as shown in equation 2.31 (Berge & Ås, 2017).

$$N(\Delta S)^m = constant \qquad\qquad 2.31$$

Another mathematical method of considering fatigue is through probability, specifically through the application of a Weibull distribution function. The two parameter Weibull distribution is often applied to represent stress spectrum for cyclic loads in marine conditions, particularly regarding structures subjected to wave loads. In this approach, a maximum allowable stress range is determined and considered proportional to the maximum allowable

wave height of a wave spectrum with defined Weibull parameters (ASME, 2018; Berge & Ås, 2017). Hence, probability of exceeding stress range over defined period can be calculated, the Weibull method is expressed as shown in equation 2.32,

$$\boldsymbol{P} = \exp\left[-\left(\frac{\Delta S}{q}\right)^h\right] \qquad 2.32$$

where h is shape parameter, and q is scale parameter of the Weibull distribution, which can be determined through various methods of statistical inference, more of which is described in chapter 2.8.1.

Welded connections exposed to cyclic loading requires consideration about stress concentrations, in particular hot-spot stress and notch stress. The former term is defined by stress concentrations occurring because of the nominal shape of the structure, such as curves, holes, and edges (Berge & Ås, 2017), whilst the latter is a result of stress concentrations due to weld geometry which results in local stresses (Boresi & Schmidt, 2003). In the case of notch-stress, the outcome due to weld geometry is increasing local stresses as distance to the weld decreases, where max notch stress is at the weld toe. Notch-stress at the weld toe, and hot-spot stress will typically be higher than that of the stress due to the nominal geometry of the component (Boresi & Schmidt, 2003). The effect of stress concentrations can be determined through relation described in equation 2.33,

$$SCF = \frac{\sigma_{max}}{S} \qquad 2.33$$

where S is nominal stress exerted on structure, and σ_{max} is maximum local occurring stresses. Thus, it is important to consider concentrations of stress when performing fatigue analysis, since the local stresses occurring at these hot spots are bound to be of greater magnitude than the nominal stresses. Stress concentrations are factored into fatigue estimations as shown in equation 2.31.a.

$$N(SCF \times \Delta S)^m = constant \qquad 2.31.a$$

$$\rightarrow N(\Delta \sigma)^m = constant$$

Therefore, when conducting a fatigue analysis with respect to local stresses obtained from analysis, it is the weak spots with high occurring stresses that are of interest, and the main subject of fatigue calculations.

2.7 Standards

2.7.1 Theory fatigue PD5500

The PD5500 standard describes, amongst others, a simplified fatigue analysis where designed curves are applied in correspondence with simple calculations. This process is divided in to three steps. Firstly, the number of different cases which may result in cyclic loading is determined, along with corresponding frequency and expected number of cycles. Secondly, these variables are used to establish the various maximum stress ranges occurring at the given cases, examples of this is temperature and mechanical loading.

$$N = A \cdot \sigma_r^{-m} \qquad 2.34$$

Once acquired, stress range values can be utilized along with SN-curve from standard, based on weld class. This is represented in equation 2.34, which determines expected load cycles (N) for given stress range. Weld classes used to determine appropriate SN-curve, is based on factors such as quality of workmanship, type of weld (butt, fillet etc), and for what type of application the weld is intended. Table 2-1 presents values for SN-curve parameters corresponding with the different weld classes (BSi, 2003).

Table 2-1: S-N curve coefficients for various weld classes.

| Class | Constants of S-N curve | | | | Stress range at N=10^7 cycles |
| | For N < 10^7 cycles | | For N > 10^7 cycles | | |
	m	A[a]	m	A[a]	N/mm^2
C[b]	3.5	4.22×10^{13}	5.5	2.55×10^{17}	78
D	3	1.52×10^{12}	5	4.18×10^{15}	53
E	3	1.04×10^{12}	5	2.29×10^{15}	47
F	3	6.33×10^{11}	5	1.02×10^{15}	40
F2	3	4.31×10^{11}	5	5.25×10^{14}	35
G	3	2.50×10^{11}	5	2.05×10^{14}	29
W	3	1.58×10^{11}	5	9.77×10^{13}	25

[a] For **E**=209 000 N/mm^2

[b] If S_r > 766 N/mm^2 or N < 3 380, use class D curve

The last step of the procedure is to check whether the number of estimated cycles of each case (ni) has a satisfactory relation to the number of cycles obtained through calculations and curves provided by standards (Ni). This last step is performed through the following calculation (BSi, 2003),

$$\sum \frac{n_i}{N_i} \leq 0.6 \left(\frac{22}{e}\right)^{0.75} \qquad 2.35$$

where e is component wall thickness. PD5500 annex C does not include methods that explicitly factor in the effects of corrosion. For structures in corrosive environment, where adequate protection against corrosion is not apparent, the code accounts for the effects of corrosion through the application of an adjusting factor. Furthermore, the code specifies that under such conditions frequent and comprehensive inspection and testing is necessary in order to ensure that the stress levels are conservative (BSi, 2003).

Regarding operating temperatures, this code is only applicable for temperatures below creep for aluminum and steel, which results in maximum design temperatures of 350 C, 430 C and

100 C for ferritic steel, austenitic stainless steels and aluminum respectively (BSi, 2003). Furthermore, given that the structure follows the requirements given by code about sub-zero temperatures, the code does not offer any restrictions regarding application of SN-curves for structures operating at sub-zero temperatures. The mentioned requirements are in place to ensure that the structure is protected against brittle fracture (BSi, 2003).

Factors such as wind loads and pulsation of pressure in piping can lead to vibrations in the pipeline, since vibration results in a high frequency in cycling loading affecting the structure it can accelerate the fatigue process, even in cases of low stress amplitude (Ortega & Rivera, 2013). This is especially the case for welded joints. Since vibrations are generally hard to predict at design stage, the standard recommends inspection of plant at initial startup, followed by further alterations of design in case of vibrations (BSi, 2003). Thus, effects of vibrations are prevented in design instead of accounted for in fatigue calculations.

The code specifies conditions for when a detailed analysis is necessary, which is the case when the previously described simplified method is valid, or when the total number of stress fluctuations from all load cases exceed the number derived from equation 2.36 (BSi, 2003),

$$N \leq \frac{6 \times 10^9}{f_f^3} \left(\frac{22}{e}\right)^{0.75} \left(\frac{E}{2.09 \times 10^5}\right)^3 \qquad\qquad 2.36$$

where f_f is maximum design stress.

For a detailed fatigue analysis, the assessment is generally performed for weak links in the pressure vessel structure, such as welds and bolt connections. The code supply SN-curves for various weld classes which are based on test specimens. Tests comparing the test specimens to actual welded connections of pressure vessels under cyclic loading show that the obtained curves are conservative to a satisfactory level (BSi, 2003). Furthermore, when applying the fatigue curves presented in the standard, it is important to account for all operational load cycles. This is conducted similarly to the simplified method through application of formula 2.34 in combination with SN-curves. In situations where the variation in stress does not start and end at the same place, or when the superposition of a combination of loads result in a higher stress amplitude than that of individual load sources, a counting technique is required (Berge & Ås,

2017). The standard acknowledges the rainflow method, which explained in section 2.6, as acceptable for this purpose. The SN-curves presented in PD5500 is based on a material with a Youngs modulus of 209 000 N/mm^2, however, it is applicable for all ferritic and austenitic steels, in addition to aluminum (BSi, 2003). As a result, adjustments to the initial formula need to be made to account for the effects of material. This is executed through inclusion of equation 2.37 to the general expression of the SN-curve:

$$\sigma = \frac{\sigma_r \times 2.09 \times 10^5}{E} \qquad\qquad 2.37$$

where S$_r$ is the obtained stress range from stress analysis.

In addition to the criteria for allowable damage caused by fatigue, the parameter of plate thickness needs to be incorporated in analysis. For plates containing surface welds, these is generally a correlation between increase in plate thickness with decease in fatigue life (BSi, 2003). The S-N curves of the standard cover plate thicknesses up to 22 mm, and as for plates thicker than this, it is necessary to perform adjustments to the calculations through application of an adjustment factor as shown in equation 2.36.a.

$$N_i = A \left(\frac{22}{e}\right)^{\frac{m}{4}} \left(\frac{\sigma_r \times 2.09 \times 10^5}{E}\right)^{-m} \qquad\qquad 2.36.a$$

The stresses to be considered in a fatigue analysis according to PD5500 are those who fall into the category of primary and secondary stresses. These stress categories are defined by the standard as those caused by pressure, other mechanical loads and thermal effects (BSi, 2003). Application of the SN-curves require the full stress range, and these design curves factors in stress concentrations that occur in welds, depending on type and shape of the weld (BSi, 2003).

2.7.2 Theory fatigue ASME B31.3

ASME 31.3 appendix W contains methodology relevant for fatigue design, in this methodology the code differentiates between two categories of cyclic loading. Specifically, loading that can be portrayed as a series of stress range cycle pairs, through the principle of minor sums, and load cycles that are required to be portrayed through application of statistical methods. The

former category includes all cyclic stress, except those induced by wave loads, the latter method, however, is meant only for wave loads, and specifically applies a 2-parameter Weibull distribution function for this purpose.

In the case of loading from all other sources than waves, the fatigue life, expressed as number of allowable cycles for given load case, is determined through the application of equation 2.38 (ASME, 2018),

$$N_{ti} = \frac{f_I}{f_E} \left(\frac{CF \cdot f_{M,k} \cdot f_t}{\sigma_{Ei} \cdot T_E^k} \right)^m \qquad\qquad 2.38$$

where CF, k and m are material constants dependent on number of load cycles, parameter value and further explanation is provided in table 2-3 and 2-4, information from which was extracted from the code (ASME, 2018).

Table 2-2: Coefficients applicable for fatigue analysis for stress range sources of corresponding load cycles less than 10 000 000.

Fatigue material coefficients (-3σ)			
Material	CF (SI Units)	m	k
Ferritic steels and austenitic stainless steel	14 137	3.13	0.222
Aluminum	2 303	3.61	0.222

Table 2-3: Coefficients applicable for fatigue analysis for stress range sources of corresponding load cycles more than 10 000 000.

Fatigue material coefficients when Nti $> 10^7$			
Material	CF (SI Units)	m	k
Ferritic steels and austenitic stainless steel	$CFa[(f_E/f_I)10^7]^{ax}$	5	0.222

where CFa is CF from table 2-3, and variable ax is determined through equation 2.47,

$$ax = \frac{1}{m_2} - \frac{1}{m_1} \qquad 2.47$$

where m1 is selected m value from table 2-3, and m2 is the m coefficient from table 2-4.

Furthermore, f_E is environmental correction factor, for structures located in air, in absence of effects of corrosion, this factor is 1 (ASME, 2018). Next, T_E denotes the thickness factor, which follow specified guidelines provided in the standard, where the factor is equal to the wall thickness for thicknesses between 16 mm and 150 mm, and equal to 16 mm or 150 mm for anything less or above. The standard accounts for effects of temperature by implementation of the temperature correction factor f_t, which mathematically is the ratio between the Youngs modulus of the material at reference temperature and relevant temperature of load case, given by equation 2.39 (ASME, 2018).

$$f_t = \frac{E}{E_{CSA}} \qquad 2.39$$

In cases where a load results in a combination of maximum and minimum stress ranges which exceed the materials yield stress, the factor $f_{M,k}$ is applied to account for this effect, which is done as displayed in equation 2.40, for load cases where stress range is below yield stress, $f_{M,k}=1$ (ASME, 2018).

$$f_{M,k} = \left(1 - \frac{\sigma_{Ei,min}}{\sigma_{Ei,max}}\right)^{0.2778} \qquad 2.40$$

Lastly, σ_{Ei} is obtained stress range from analysis for given cycles of loading, which shall not exceed the defined maximum allowable stress range, which is determined in accordance with guidelines presented in paragraph 319 of the standard, allowable maximum stress range is defined through equation 2.41 (ASME, 2018),

$$\sigma_A = f_r(1.25\sigma_c + 0.25\sigma_h) \qquad 2.41$$

where σ_c is basic allowable stress at the lowest temperature expected through displacement cycle, σ_h is basic allowable stress at the maximum temperature expected throughout displacement cycle. Furthermore, f_r is stress range factor, which is calculated through equation 2.42 (ASME, 2018).

$$f_r = 6.0(N)^{-0.2} \leq f_m \qquad\qquad 2.42$$

N is expected total number of load cycles through the design life of the structure, and f_m is the maximum allowable value for stress range factor, which is 1.2 for ferrous alloys with SMTS less than 517 MPa for temperature below 371 degrees Celsius. For other conditions, the maximum allowable stress range factor is 1. However, the appendix regarding fatigue calculations specifically state that the calculations shall be done based on a maximum allowable stress range factor of 1 (ASME, 2018).

In cases where σ_h is larger than stresses from sustained loads σ_L, equation 2.43 shall be applied for maximum allowable stress range instead of equation 2.41 (ASME, 2018).

$$\sigma_A = f_r[1.25(\sigma_c + \sigma_h) - \sigma_L] \qquad\qquad 2.43$$

The code applies table A1 in appendix A for determining magnitude of basic allowable stress range for given temperatures (ASME, 2018). Once allowable load cycles from every source relevant to fatigue (except wave) is calculated, the accumulated damage is calculated through the following formula, where N_i represents design value for number of load cycles for given load case.

$$d_t = \sum_{i=1}^{n} \frac{n_i}{N_{ti}} \qquad\qquad 2.44$$

Loads caused by waves is represented statistically through a 2-parameter Weibull distribution. The characteristics regarding application of this distribution is that it is suitable for random processes, such as natural phenomena (Walpole et al, 2012). The two parameters that define this distribution are those representing shape and scale of the probability density function. Shape parameter reflect the failure rate of the observed phenomena and how it changes over time, a shape parameter larger than 1 suggest that the failure rate increase over time, while a

shape parameter less than 1 indicate the opposite. In the case of wave loads, increasing failure rate mean that, as time goes by, the probability of the measured wave heights to be above the accepted criteria increases (Journee & Massie, 2001).

For shape parameter equal to 1, constant failure rate is suggested, and the distribution is reduced to an log-normal distribution with one parameter (Journee & Massie, 2001). The scale parameter determines the steepness and width of the probability density function, where increasing value yields a wider curve. This indicates a higher level of uncertainty regarding prediction of outcome. In order to utilize a Weibull distribution in the case of wave loads, it is necessary to gather a large amount of relevant wave height data (Journee & Massie, 2001). From this data the Weibull distribution is fitted through statistical inference, where the mentioned parameters are determined. Statistical inference methods include amongst others, method of moments and maximum likelihood estimator (Walpole et al, 2012). This initial statistical process is something that needs to be performed by the user as the standard does not address this through the guidelines. Therefore, a method for defining this parameter is described in detail in chapter 2.8.1.

The procedures described in this section of the code is primarily intended for floating structures. However, the standard also states that it can be utilized for other situations that fit the application of a Weibull distribution (ASME, 2018). Furthermore, the significant wave height and zero up crossing period of the field is to be presented in a scatter diagram, where the shape parameter h and zero up crossing period of the distribution function is determined. As a probability function of a long-term stress range, the distribution can be described mathematically as in equation 2.32.a (ASME, 2018),

$$P = exp\left[-\left(\frac{\sigma_{EW}}{q}\right)^h\right] \qquad 2.32.a$$

where **P** is probability of exceeding the measured stress range σ_{EW}, which is deemed to be proportional to wave height, specifically the stress range is derived from displacement caused by waves. According to the code, this stress range shall not exceed the allowable maximum probable stress range (ASME, 2018).

$$\sigma_{aw} = \left(\frac{d_w f_a}{N_d}\right)^{\frac{1}{m}} \times \frac{[\ln(N_w)]^{\frac{1}{h}}}{\left[\Gamma\left(1 + \frac{m}{h}\right)\right]^{\frac{1}{m}}} \qquad 2.45$$

Furthermore, the parameter q is determined through equation 2.46 (ASME, 2018),

$$q = \frac{\sigma_{aw}}{[\ln(N_w)]^{\frac{1}{h}}} \qquad 2.46$$

where the maximum allowable stress range during wave load cycles and design storm wave height associated cycles is determined through equation 2.47.a, and 2.47.b respectively (ASME, 2018).

$$N_w = 3.156 \times 10^7 \times V_0 \times L_w \qquad 2.47.a$$

$$N_d = 3.156 \times 10^7 \times V_0 \times L_d \qquad 2.47.b$$

V_0 is average zero-up crossing frequency, which is a parameter determined through statistical analysis of the wave spectrum, by method described in chapter 2.8.1.

Equation 2.45 can be rewritten with respect to d_w to estimate damage caused by wave displacements, where maximum measured stress range is set equal to, or less than the maximum allowable stress range (ASME, 2018).

$$d_w = \frac{\sigma_{aw}^m \times N_d}{f_a} \times \frac{\Gamma\left(1 + \frac{m}{h}\right)}{[\ln(N_w)]^{\frac{m}{h}}} \qquad 2.45.a$$

The parameter f_a is determined through equation 2.49, which is calculated similarly to the former category that is based on application of fatigue curves through equation 2.38 (ASME, 2018).

$$f_a = \left(\frac{f_I}{f_E}\right) \times \left(\frac{CF \cdot f_{M,k} \cdot f_t}{T_E^k}\right)^m \qquad 2.49$$

As with other sources of fatigue than waves, values for the material parameters CF, m and k that are required for equation 2.49 were extracted from ASME B31.3 appendix W and are presented in table 2-2 and 2-3. Furthermore, the code defines the parameter f1=1, unless otherwise is specified in engineering design. Total fatigue damage caused by cyclic loading of all sources are calculated and summed through following relation, where a combined value of 1 indicate failure (ASME, 2018).

$$d_w + d_t \leq 1 \qquad\qquad 2.50$$

2.7.3 Code stress

Standards offer methodology of calculating stresses based on obtained stress components from analysis, such method offered in ASME B31.3 takes the form of equation 2.51 (ASME, 2018; Hexagon, 2017).

$$\sigma_E = \sqrt{(|\sigma_A| + \sigma_B)^2 + (2\tau)^2} \qquad\qquad 2.51$$

The symbol σ_A of the equation is axial stress range, σ_B is bending stress range, and τ is torsional stress range. This stress is defined as code stress and is relevant for obtaining stress ranges applicable for fatigue analysis.

2.8 Statistics

2.8.1 Wave statistics

When performing statistical analysis of wave fields, there are certain parameters that are particularly useful regarding fatigue. Two of such are shape parameter h for a 2-parameter Weibull distribution, and mean zero up crossing period (ASME, 2018). The former can be determined through statistical inference of gathered wave data, in which the following methodology is applied. First, mean wave height µ is set equal to the equation for first moment according to method of moments, shown in equation 2.52. Second, variance from wave data is set equal to second equation from method of moments, as shown in equation 2.53 (Walpole et al, 2012). Thus, parameter h can be determined through assistance of the two equations, as shown in equation 2.53.a.

$$\mu = q \times \Gamma\left(1 + \frac{1}{h}\right) \qquad\qquad 2.52$$

$$SD^2 = q^2 \times \left[\Gamma\left(1 + \frac{2}{h}\right) - \Gamma^2\left(1 + \frac{1}{h}\right) \right] \qquad 2.53$$

$$\rightarrow SD^2 = \left(\frac{\mu}{\Gamma\left(1 + \frac{1}{h}\right)} \right)^2 \times \left[\Gamma\left(1 + \frac{2}{h}\right) - \Gamma^2\left(1 + \frac{1}{h}\right) \right] \qquad 2.53.a$$

Zero up crossing period is defined as the average period of a wave crossing the mean water line going up, from through to crest (Gudmestad, 2015). The mathematical definition of mean zero up crossing period is described through equation 2.54,

$$V_0 = 2\pi \sqrt{\frac{sm_0}{sm_2}} \qquad 2.54$$

where sm_0 and sm_2 denote spectral moments of 0 and 2nd order, that are calculated based on the wave spectrum, the following equation is used to determine these moments (Journee & Massie, 2001).

$$sm_n = \int_0^\infty \omega^n\, S_{zz}(\omega)d\omega \qquad 2.55$$

where $S(\omega)$ represent the mathematical interpretation of the wave spectrum, several different formulas are applicable for this, where one viable candidate is the Pierson-Moskowitz spectrum. This representation is valid for fully developed sea states. The Pierson-Moskowitz spectrum is described as shown in equation 2.56 (Journee & Massie, 2001),

$$S_{zz}(f) = 0.3125 h_s^2 t_p^{-4} f^{-5} exp\left[-1.25 t_p^{-4} f^{-4}\right] \qquad 2.56$$

where t_p is spectral peak period and represents h_s significant wave height. Significant wave height is defined as the average wave height of the highest one-third of the recoded waves, which can be calculated through equation 2.57 (Gudmestad, 2015).

$$h_s = 4SD \qquad 2.57$$

Lastly, the conversion between the Pierson-Moskowitz spectrum with respect to frequency to angular frequency is done through the following relation.

$$S_{zz}(f) = 2\pi \times S_{zz}(\omega) \qquad\qquad 2.56.a$$

2.8.2 Correlation

Statistical analysis is generally described as the method of collecting data and uncover patterns and trends (Løvås, 2013), naturally this is of great importance whenever conducting scientific research or performing comparative analysis. The toolbox of statistics is vast and include various methods and theorems, one such tool is Pearson correlation factor. This factor is a method of conducting correlation studies of multivariable data. More specifically, the Pearson correlation factor is a way of determining the extent of which the outcome of two variables change with respect to each other (Walpole et al, 2012). The magnitude of the correlation parameter indicates the percentage of which the variations of variable **Y** is accounted for by a linear relationship to the variable **X**. Thus, a correlation parameter value of 1 would indicate a perfect linear relationship between the two variables (Artusi, Verderio, & Marubini, 2002). Hence, a change in one parameter would be paired with a proportional increase in the other variable. For a correlation parameter value of -1, it would be the same linear relationship, however, with a decreasing trend. A correlation approaching 0 indicate that there is a completely random relationship between the variables. A more precise categorization of correlation factor values with assigned correlation implications was extracted from (Kent state University, 2021; Artusi, Verderio, & Marubini, 2002) and is presented in table 2-4.

Table 2-4: Values correlation parameters.

Correlation value	Correlation implication
$0 \leq \rho < 0.2$	Little to no correlation
$0.2 \leq \rho < 0.4$	Small correlation
$0.4 \leq \rho < 0.6$	Moderate correlation
$0.6 \leq \rho < 0.8$	High correlation
$0.8 \leq \rho \leq 1.0$	Very high correlation

Mathematically, Pearson correlation factor can be expressed as displayed in equation 2.58 (Walpole et al, 2012).

$$\rho_{X,Y} = \frac{cov(X,Y)}{SD_X \times SD_Y}$$ 2.58

The factor cov(**X, Y**) represents covariance of variable **X** and **Y**, which is a measure of the joint variability of a set of statistical variables. This is mathematically defined as shown in equation 2.59 (Walpole et al, 2012). Furthermore, SD represents standard deviation of sample of variable **X** and **Y** respectively. Generally, standard deviation can be defined as a way of expressing the spread of the collected sample of data, where a low value for standard deviation suggests that the gathered data is centered around the mean value. Oppositely a large value implies a large dispersion in sample, the expression for standard deviation is defined as equation 2.60 (Løvås, 2013).

$$cov(X,Y) = \frac{1}{n}\sum_{i=1}^{n}\left(x_i - \mu(X)\right)\left(y_i - \mu(Y)\right)$$ 2.59

$$SD = \sqrt{\frac{1}{n}\sum_{i=1}^{n}\left(x_i - \mu(X)\right)^2}$$ 2.60

In equations above, n represents the sample number and μ(**X**) represents expected value from sample of the variable **X**, and is expressed through equation 2.61 (Løvås, 2013). Similarly, μ(**Y**) is expected value with respect to variable **Y** and is expressed, as with variable **X**, through application of equation 2.61, but with respect to variable **Y**.

$$\mu(X) = \frac{1}{n}\sum_{i=1}^{n}x_i$$ 2.61

Chapter 3 Method stress analysis

The purpose of this thesis is to compare the two standards ASME and PD5500 with respect to fatigue analysis. Therefore, utilizing the procedures regarding fatigue listed in the standards is a large part of the work that needs to be performed. The remaining main tasks that this thesis consisted of was to determine the parameters required to perform the fatigue analysis and to further examine the difference in fatigue analysis results. In order to secure valid and reliable results for both tasks, it is imperative to make a good selection of applied methods. Method chosen for these tasks are further explained in this chapter.

3.1 Numerical software

When applying the methods described in the standards it is important to supply a reliable and conservative estimation of stress due to different load cases. Since complicated piping cases such as the example case of this project pose a challenge regarding precise calculations, it was necessary to use numerical software. Throughout the work on this thesis the piping software Caesar 2 was utilized.

Caesar 2 is a nodal based software that is specifically developed for stress and displacement calculation for pipe systems. Unlike other FEA software that utilizes a mesh of elements and nodes to determine local stress and displacements of the entire structure, a nodal based software only evaluate the nodes of the system (Zienkiewicz, Taylor, & Zhu, 2005). These nodes represent locations of interest along the pipeline, which include welded areas, locations with structural support or loads, amongst others. Load cases are assigned to the piping system model, which are series of loads that occur in the system at the same time, which mean that these loads must be analyzed simultaneously. Caesar 2 recognizes three different kinds of load cases, namely operating load cases, sustained load cases and expansion load cases (Hexagon AB, 2021). Operating load cases incorporate loads under hot operations, which mean that primary loads such as weight, pressure and other forces are included. In addition to the primary loads, operating load cases also include secondary loads, which mainly involve loads caused by displacements or thermal expansion (Hexagon, 2017). Sustained load cases, on the other hand, represent the load cases after initial installation before start of operations (Hexagon AB, 2021). Hence, these load cases involve only primary loads such as weights and pressure. Lastly, expansion load cases represent the range between the displacement extremes, usually between

the operating and sustained cases. These load cases are used to meet expansion stress requirements, in addition to application in fatigue calculations, for cases such as wave displacements and thermal expansion (Hexagon AB, 2021).

After assigning material and geometric properties to all the elements in the pipeline system, the software automatically generates stiffness matrix for the entire system (Hexagon, 2017). In order to assure conservative result from analysis, the software have incorporated in its algorithm a procedure for assigning stress concentration factors to exposed nodes, such as bends. However, the software also allows for customized inputs in this regard.

Once the model was defined and assigned with geometry and material properties, as well as load cases representing all operational loads, the analysis could be performed. The software generally gives nodal solutions in terms of displacements, moments, forces, reaction forces and stresses, where the focus of this analysis was stress outputs. Solutions were obtained for all load cases relevant for fatigue analysis.

3.2 Procedure stress analysis

The methodology involved in this thesis was divided into three different stages, stress analysis, fatigue life analysis and statistical comparison of results.

Regarding stress analysis, the following step by step procedure was applied for obtaining the required data needed for fatigue life calculations. First, a model of the piping system was created in Caesar 2 with assigned loads, which is elaborated in chapter 3.3 through 3.4. Secondly, several load cases, representing the different load combinations occurring in operating conditions were generated, and a full overview of which is presented in table 3-9. Thirdly, analysis of piping system for load cases relevant to fatigue was performed, in addition to cases from sustained loads, which was applied to estimate allowable stress range according to ASME B31.3. Output stresses with corresponding nodes were recorded for all respective load cases once results had been obtained. Lastly, nodes of highest occurring stresses located at elbows were identified and selected for further fatigue analysis. It was important to include all elbows since these locations were exclusively exposed to slugging loads, which was anticipated to cause a substantial part of the systems fatigue damage, along with the wave displacements. Additionally, nodes representing supports in expansion loop were evaluated for further fatigue

analysis with respect to different weld class. Furthermore, to broaden the understanding of how methodology impact design, additional simulations were performed for changes in pipe diameter. However, this was primarily done in order to collect data for correlational studies with respect to design and fatigue. For the alternate simulations of variations in diameter, all relevant data regarding load cases were the same as the original simulation. More information about specifics regarding values of changes in diameter is displayed in appendix.

3.3 Geometry and material input

The example case of this study was a pipe bridge, with an expansion loop, between two platforms, named here Platform 1 and Platform 2.

Generally, when two anchors are applied to a marine system consisting of pipeline bridge, such as the example case of a pipeline between two platforms, an expansion loop is advised (Barker, 2018). Furthermore, expansion loops should preferably be situated in the middle of the piping section that is under exposure of wave displacements and thermal expansion (DST Group Limited, 2021). Thus, enabling desired flexibility as pipe expands.

Restraints were assigned to act as guides for loop, which was generally beneficial to focus the direction of expansion in longitudinal direction of the bridge (Engineers Edge, 2021; Spirax Sarco, 2021). Hence, the expansion loop of this case had been equipped with restraints acting in lateral direction of bridge before and after the loop, which was the x-direction with respect to model. Additionally, to further prevent unwanted displacements of bridge, a restraint in x-direction was placed at node 350, in order to support and guide loop by preventing lateral displacements from occurring. Figure 3-1 shows the location of nodes where guiding restraints were modelled. Further detailed information of boundary conditions and modelling of displacements and pipe geometry follows later in chapter.
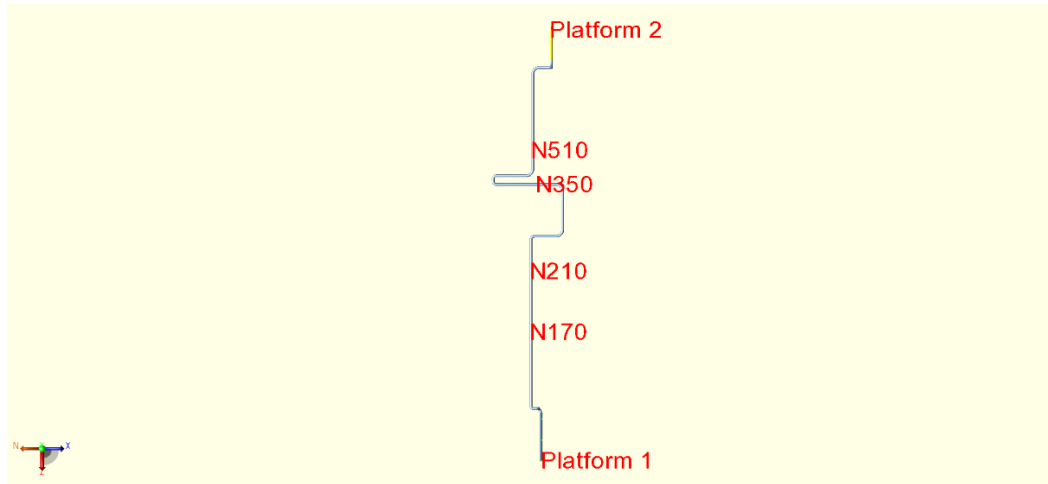
Figure 3-1: Expansion loop with guiding nodes

The bridge between platform 1 and 2 consists of two different types of pipes, where the former was a duplex stainless-steel ranging from node 10 to 105, while the latter was of super duplex stainless steel, spanning the remaining section of bridge from node 105 to 700. The main difference of the two pipe sections, other than the material properties, was the wall thickness, which were of 38.89 mm and 24.61 mm respectively. Specifics regarding geometric specifications and material properties are listed in table 3-1 and 3-2 respectively. The intersecting point of the different pipes was located shortly off the deck of platform 1, at the start of bridge span, which is illustrated in figure 3-1. Therefore, the main pipe segment of study was that of the super duplex material. The entire bridge span from the deck of platform 1 to the deck of platform 2 was modelled in zx-plane and divided into 23 elements. Every element starts and ends at either an elbow or support. All nodes of relevance regarding stress analysis are illustrated in figure 3-2, which portray a top view of the expansion loop.
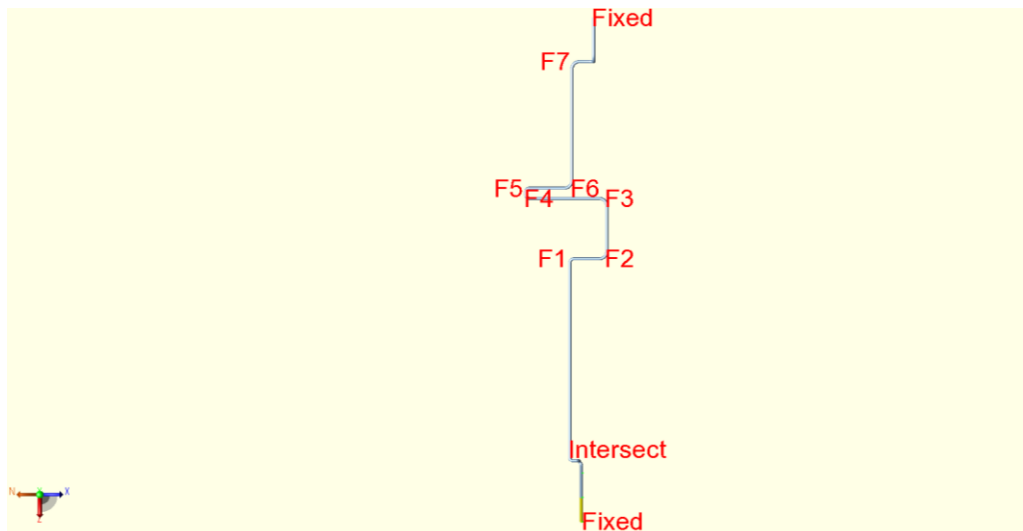
Figure 3-2: Top-view of pipe showing intersecting point of the two pipes, locations of slug loads, and locations of fixed nodes.
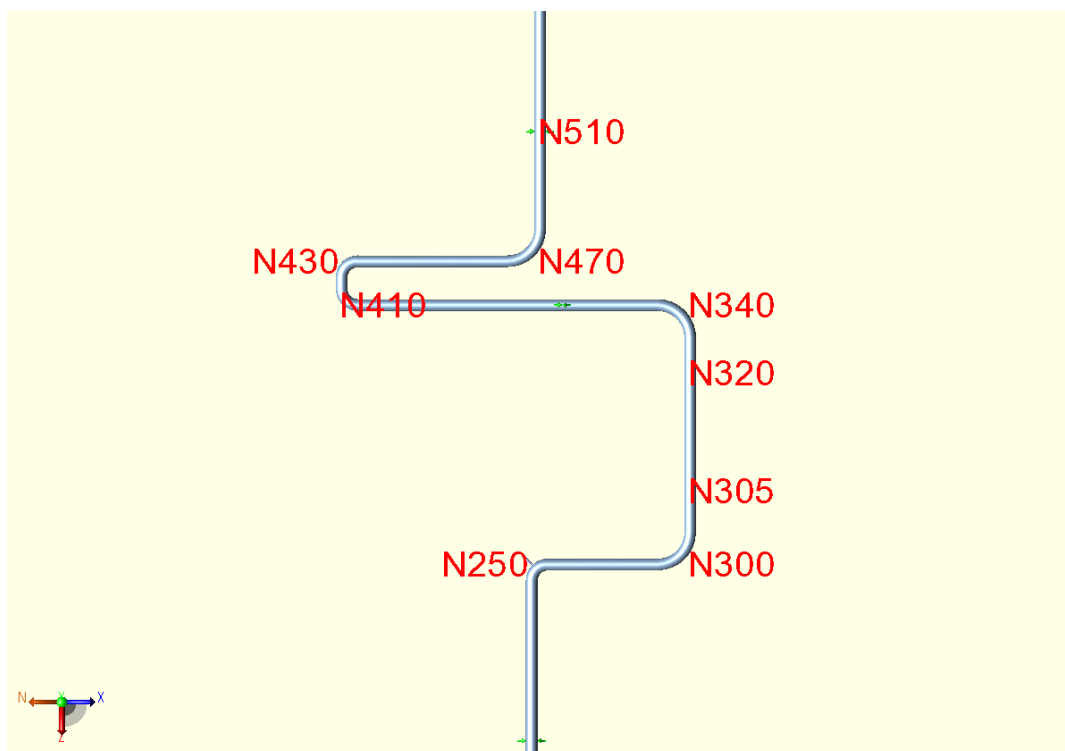
Figure 3-3: Top-view of expansion loop with nodes relevant for analysis.

Table 3-2 displays geometric specifications of the two pipe sections, in addition to information such as mill tolerance and corrosion allowance.

Table 3-1: Geometric specifications for both pipe cross-sections applied in simulation.

Pipe	Nominal Size (in)	Outer diameter (mm)	Wall thickness (mm)	Schedule	Corrosion allowance	Mill tolerance (mm)
Section 1	24	610	38.89	100	0	0.3
Section 2	24	610	24.61	60	0	0.3

Through assigning the aforementioned geometric and material specifications to piping input section of software, the following model, presented in figure 3-3 and 3-4, was created.
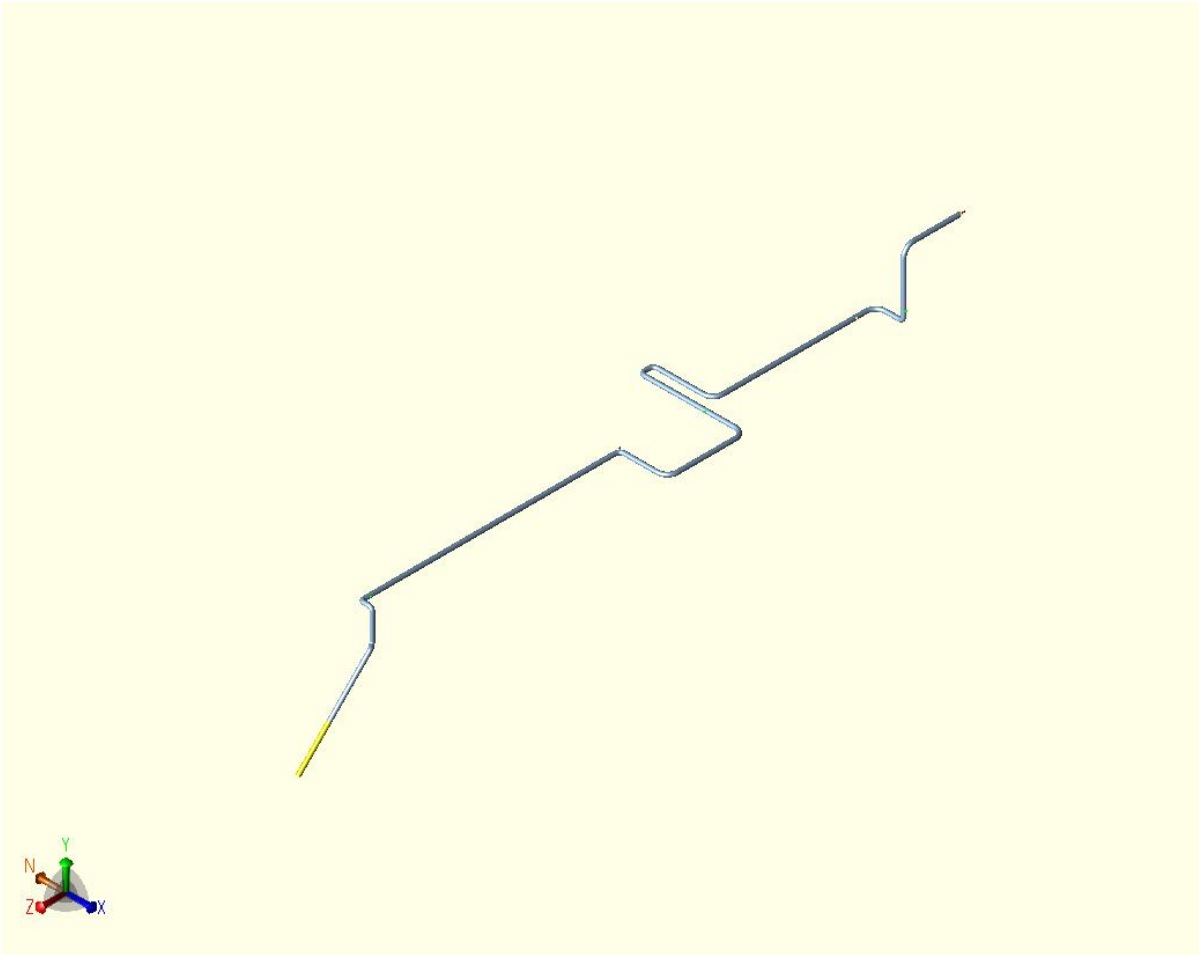
Figure 3-4: Model of bridge
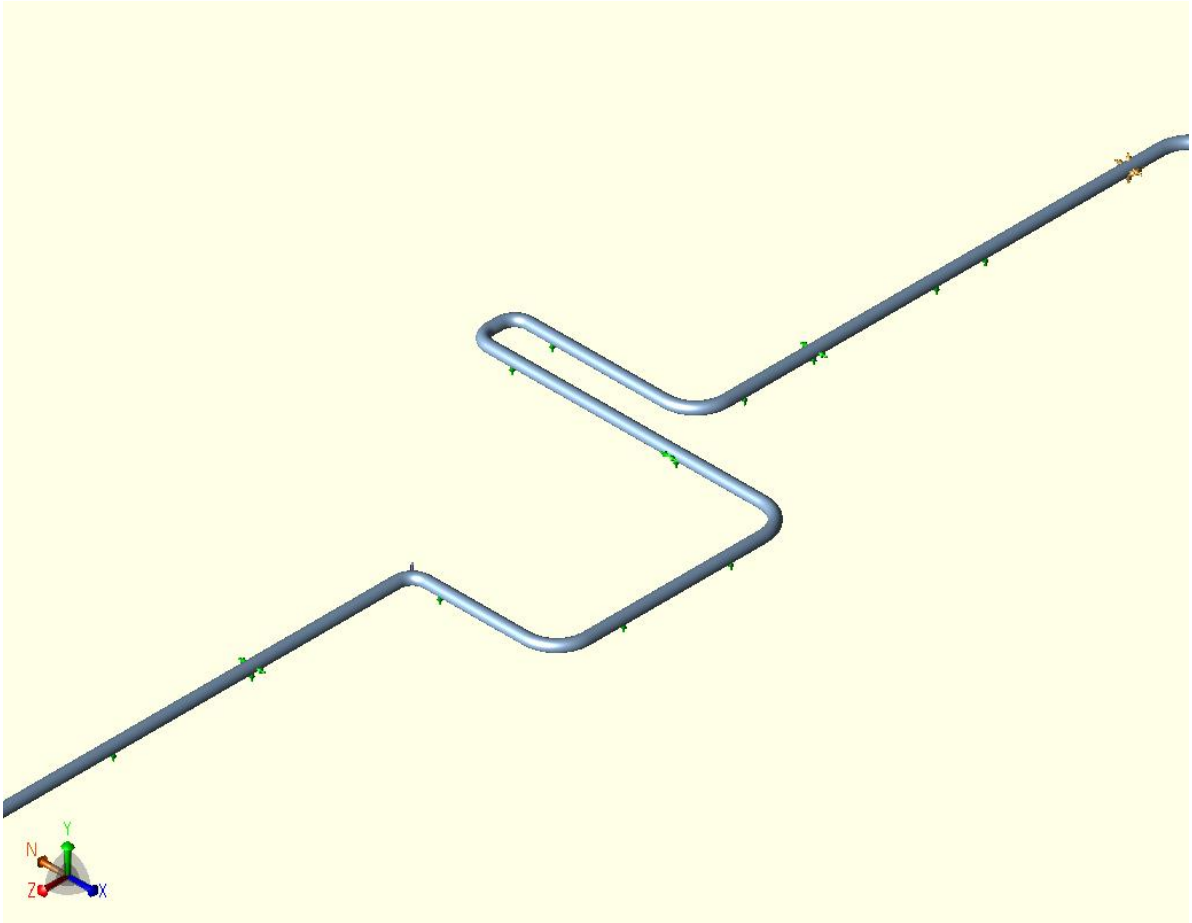
Figure 3-5: Expansion loop

3.3.1 Material data

Table 3-2 displays the two material types used in model, where A790 S31803 was assigned to pipe section 1 between node 10 and 105, whereas material of type A790 S32760 were applied to the section 2 spanning from node 105 to node 700.

Table 3-2: Material properties for both sections of piping applied to model.

Properties	Material	
	A790 S31803	A790 S32760
SMYS (MPa)	448	552
SMTS (MPa)	620	752
Youngs modulus (GPa)	201. 370	201. 370
Density (kg/m^3)	8027.1997	8027.1997

3.4 Load inputs used in calculations

Relevant load cases regarding stress cycles resulting in fatigue for this example case is slugging, wave motions and changes in temperature and internal pressure. Each of these loads needs to be evaluated and determined at the initial stage of the process through a stress analysis.

3.4.1 Slugging

The reason why slugging poses a threat to the structural integrity of the bridge is mainly due to two reasons. Firstly, the dynamic nature of slugs. Forces caused by slugging typically occur over short time periods, which substantially increase the impact forces (Ortega & Rivera, 2013). In a static analysis, however, the dynamic effects are factored into the simulation through application of dynamic amplification factor (DAF). In this case the value for DAF was set at 2, which is a common value applied for marine situations (El-Reedy, 2015). Second, the design of the loop is mainly to mitigate stresses due to longitudinal displacements of bridge caused by wave motions. Hence, a certain flexibility is required in order to let the loop serve its purpose, and a result of which is naturally a lack of restraint, which in turn reduce the strength of the joint. The result of these two factors is that there need to be made a compromise between flexibility and rigidity regarding slugging and wave displacements. Loads due to slugging were applied to nodes 250, 300, 340, 410, 430, 470 and 620. The resultant slug force was decomposed into a radial and axial component of equal magnitude that were exerted on every elbow of the loop.

The slugging data applied for this study was categorized into four different classes based on frequency and magnitude of force. Class A is the highest occurring class, but of lowest force, followed by class B, then C and finally class D, which is the class of highest slug force, but lowest occurrence. Points of interest at this bridge regarding slugging are the bends, and it is at those locations that slugging can cause displacements in the structure. The occurrences of the different classes of slugs with belonging force at the seven different sections are represented in table 3-3. Since there were four different categories of slug loads occurring alternately occurring at each elbow, four different Caesar files had to be created, where each file represented a category of slugs.

Table 3-3: Slug loads with connecting load cycles, assigned with category and node at which it appear.

Slug category	Branch	50 years cycles	Slug force (N)	F Axial = F Radial (N)	Caesar Node No.
A	F1	291 981 750	4707	3328	250
B		117 165 000	6315	4465	
C		19 162 500	8129	5748	
D		1 752 000	9781	6916	
A	F2	88 421 250	4396	3109	300
B		61 265 250	8355	5908	
C		68 820 750	11966	8461	
D		30 441 000	14736	10420	
A	F3	22 283 250	6551	4632	340
B		65 535 750	11353	8028	
C		117 548 250	15127	10696	
D		14 289 750	18595	13149	
A	F4	162 114 750	7675	5427	410
B		124 665 750	11216	7931	
C		85 464 750	16323	11542	
D		17 629 500	20437	14451	
A	F5	116 234 250	2393	1692	430
B		89 571 000	5092	3600	
C		32 466 750	7657	5415	
D		4 653 750	9911	7008	
A	F6	7 719 750	6126	4332	470
B		19 764 750	9453	6684	
C		149 303 250	12559	8881	
D		48 837 000	14157	10011	
A	F7	24 582 750	9092	6429	620
B		81 851 250	12674	8962	
C		244 842 000	15877	11226	
D		41 938 500	18888	13356	

3.4.2 Waves

The displacements of platforms, which causes the cyclic strain and corresponding stress on the piping system was in a large degree caused by waves. For the purpose of modelling displacements caused by waves at a specific field in a fatigue analysis, it was necessary to statistically evaluate the relevant field over an extended time period in order to obtain wave heights. In addition, a response analysis needs to be performed to determine displacements of vessel when exposed to the measured waves from different angles. Table 3-4 presents data representing bridge displacements due to both 100-year wave and 1000-year wave.

Table 3-4: Bridge displacements from 100-year, and 1000-year wave.

Return period (years)	Wave angle (from North)	Wave height (m)	Wave period (s)	Platform 1 – Max Movement (m)	Platform 2 – Max Movement (m)	Max Relative Movement (m)
100	235 deg	27.1	16.3	+0.314 /+0.002	+0.250 /-0.017	+0.331 /-0.239
100	245 deg	27.1	16.3	+0.314 /+0.002	+0.251 /-0.017	+0.331 /-0.241
100	255 deg	27.1	16.3	+0.307 /+0.003	+0.247 /-0.017	+0.322 /-0.239
10 000	235 deg	34.5	18.3	+0.489 /-0.027	+0.407 /-0.046	+0.520 /-0.433
10 000	245 deg	34.5	18.3	+0.491 /-0.028	+0.409 /-0.046	+0.522 /-0.436
10 000	255 deg	34.5	18.3	+0.481 /-0.027	+0.402 /-0.045	+0.504 /-0.426

Since 10 000-year wave is defined as an accidental load case, it will not be considered in the fatigue analysis, as the case would not give a good representation of the cyclic loading taking place. Hence, what is left of the wave displacement data are those caused by the 100-year return wave. These displacements will serve as maximum on a range that is the summation of the largest positive, and largest negative relative movements between Platform 1 and Platform 2. Hence, the maximum displacement range becomes 0.572 m. When modelling wave displacements, the bridge was defined as fixed at the platform 1 and pinned at platform 2. This was an approximation that was applied to simplify the modelling. Thus, all displacements were simulated through movements of only Platform 2. Furthermore, the positive direction of displacement was defined in the direction of Platform 2, where the bridge was moving away

from Platform 1. Negative direction of displacement occurred when the bridge moved towards Platform 1. Hence, the displacements are exerted on the restraints at Platform 2 in east-west direction. Since parts of the pipe was defined through boundary conditions as fixed at deck of Platform 2, it was necessary to take special consideration when modelling the mentioned wave displacements. There is a simple application in Caesar that allows for moving anchors, where fixed nodes are assigned connecting nodes that are then assigned the desired displacements, which in this case was 0.331 m in the positive direction, and 0.241 in the negative direction. The specific nodes that was assigned with the aforementioned longitudinal displacements was 590 and 700, which were the only nodes with restraints in this direction, other than nodes 10 and 100 at Platform 1. Placement of platforms and fixed nodes relative to bridge is illustrated in figure 3-6.
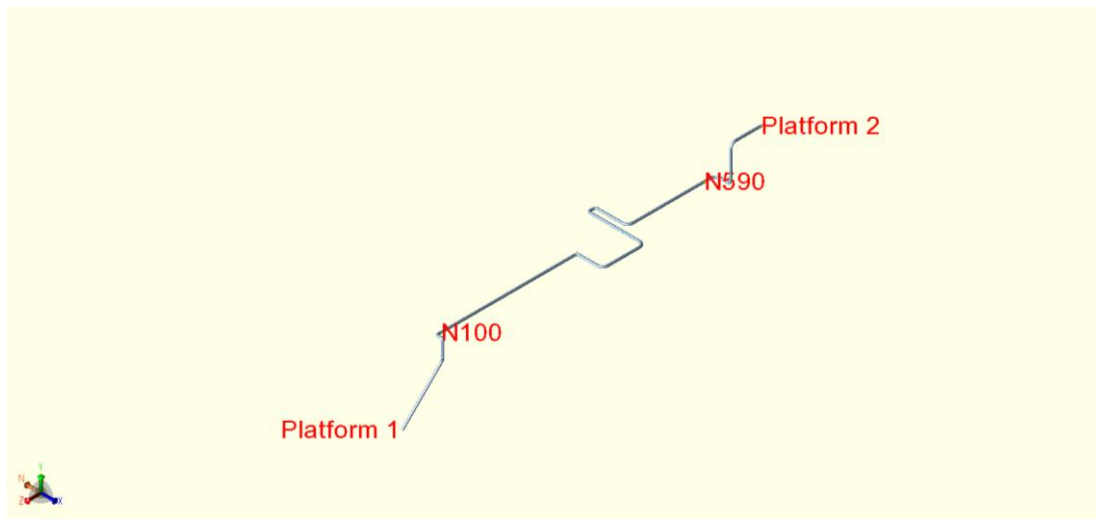
Figure 3-6: Locations of the two platforms joint by bridge, N100 and N590 represent fixed points at deck of each platform.

For expansion load cases, such as wave displacements and thermal expansion, stress analysis was performed with and without effects of friction on supports. In analysis where frictional effects were considered, it was however, only considered in horizontal directions relative to bridge. The reason for this was that only longitudinal movements was considered, not rotational. Hence, vertical motion would be negligible. Frictional force at supports are modelled in Caesar 2 by simply assigning relevant nodes with a coefficient of friction corresponding to surface layer of support and pipe, then the software calculates frictional response at these nodes based on normal force multiplied with coefficient. In this particular case, the magnitude of friction coefficient was 0.15, which is representing that of stainless-steel surface towards another

surface of stainless-steel (Engineering toolbox, 2021). After frictional forces has been inserted into piping model, it is necessary to specify in load cases whether friction should be neglected or included in analysis. To ensure a conservative result, the higher stress value of the two were applied in further analysis.

3.4.3 Pressure and temperature variations

Stress ranges caused by changes in temperature were applied in stress analysis, where two instances were considered. First, maximum change in temperature, which was the range between maximum and minimum design temperature. Second, partial change in temperature, which was the range between maximum operating temperature and installation temperature.

Stress cycles due to changes in pressure that were apt for consideration in further fatigue analysis were mainly those that were estimated to occur on a regular basis. In order to both increase conservatism, and to gain additional data for correlational studies, full pressure range cycles on weekly basis were incorporated as well. Hence, an approximation of a 10 percent change in design pressure, and full design pressure change were included in the stress analysis. Specifics regarding these load cases are shown in table 3-5.

Table 3-5: Design parameters regarding stresses caused by changes in processing pressure and temperature.

Max design pressure	202 barg
Max operating pressure	15 barg
Max design temperature	+ 90 ºC
Min design temperature	- 29 ºC
Max operating temperature	+ 80 ºC
Installation temperature	+ 4 ºC

3.4.4 Code stress

The code that has been considered when performing stress analysis is ASME B31.3. Hence, code stress and allowable stress were calculated in Caesar based on formulas provided in said code, and these equations are provided in chapter 2.6.3 as equation 2.50.

3.4.5 Allowable stress

Table 3-6: Maximum allowable stress for both sections of pipes, for maximum and minimum design temperature.

Pipe material	Allowable stress cold	Allowable stress hot
A790 S32760	206.850 MPa	206.850 MPa
A790 S31803	250.288 MPa	247.696 MPa

3.5 Boundary conditions

Boundary conditions with relevant nodes are listed in table 3-7. Locations of nodes with restraints are additionally displayed in figure 3-6 and 3-7, where figure 3-6 shows the section starting at Platform 1 until midsection of bridge, whilst figure 3-7 shows location of nodes for bridge leading up to platform 2. Lastly, figure 3-8 presents the entire bridge with all restraint nodes.
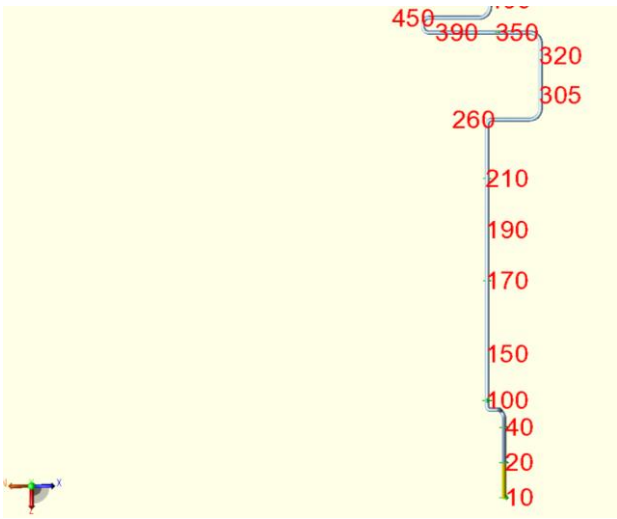
Figure 3-7: Restraint nodes from Platform 1 until mid-point of loop.
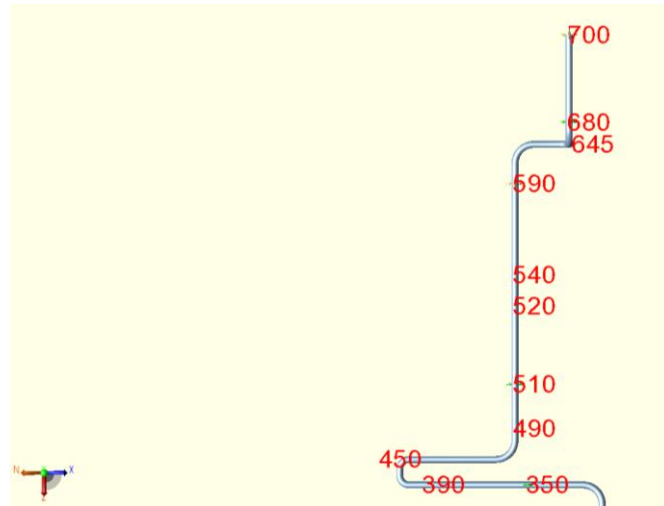
Figure 3-8: Location of restraint nodes from mid-point of loop until Platform 2.
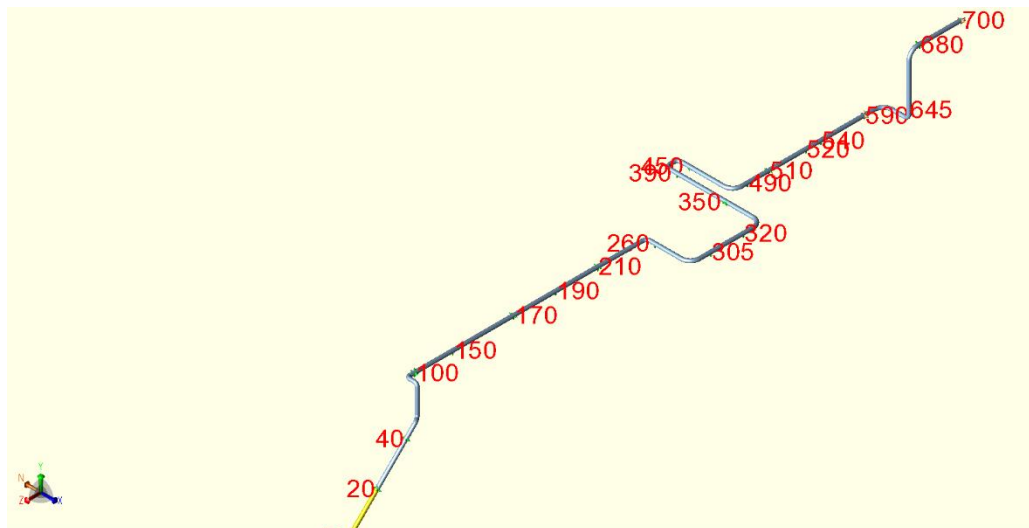
Figure 3-9: Bridge with all restraint nodes.

The boundary conditions in table 3-7 represent six directions in total. Y-axis was defined as vertical; x-axis was oriented in the longitudinal direction of the pipe and z-axis was horizontal and perpendicular to x-direction.

Table 3-7: Boundary conditions for restraint nodes.

Boundary conditions:	+X	-X	+Y	-Y	+Z	-Z
Nodes:	10, 20, 40, 100, 170, 210, 350, 510, 590, 680, 700	10, 20, 40, 100, 170, 210, 350, 510, 590, 680, 700	10, 40, 100, 150, 170, 190, 210, 260, 305, 320, 350, 390, 450, 490, 510, 520, 540, 590, 645, 680, 700	20, 590	10, 100, 590, 700	10, 100, 590, 700

3.6 Load cases

Table 3-9 presents the total of load cases applied in initial stress analysis. Out of these load cases L17 through L27 and L34 through L37 were utilized in further fatigue analysis, while L1 and L2 were relevant for determining allowable stress. For cases where friction multiplier is equal to 1, it is implied that frictional forces at supports has been accounted for in calculations. Designations for load cases is presented in table 3-8.

Table 3-8: Designations relevant for load cases.

W	Deadweight
P1	Maximum design pressure
P2	Maximum operating pressure
P3	10% deviation of maximum design pressure
T1	Maximum design temperature
T2	Minimum design temperature
T3	Maximum operating temperature
T4	Installation temperature

D1	Longitudinal displacement from positive 100-year wave				
D2	Longitudinal displacement from negative 100-year wave				
F1	Slugging force at node 250				
F2	Slugging force at node 300				
F3	Slugging force at node 340				
F4	Slugging force at node 410				
F5	Slugging force at node 430				
F6	Slugging force at node 470				
F7	Slugging force at node 620				

Table 3-9: Load cases for stress analysis.

Case No.	Load Case	Stress Type	Combination method	Elbow stiffening pressure	Case description	Friction multiplier
L1	W+P1	SUS		PMax	Sustained stress with max design pressure	0
L2	W+P2	SUS		P2	Sustained stress with max operating pressure	0
L3	W+D1+P1	OPE		None	Sustained stress with positive 100-year wave displacement	0
L4	W+D2+P1	OPE		None	Sustained stress with negative 100-year wave displacement	0
L5	W+T1+P1	OPE		PMax	Max design temperature with max design pressure	0

L6	W+T2+P1	OPE	PMax	Min design temperature with max design pressure	0
L7	W+T3+P2	OPE	PMax	Max operating temperature with max operating pressure	0
L8	W+T4+P2	OPE	PMax	Installation temperature with max operating pressure	0
L9	W+T3+P3	OPE	P2	Max operating temperature with 10% design pressure drop	0
L10	W+P2+T3+F1	OPE	P2	Max operating pressure and temperature with slug force F1	0
L11	W+P2+T3+F2	OPE	P2	Max operating pressure and temperature with slug force F2	0
L12	W+P2+T3+F3	OPE	P2	Max operating pressure and temperature with slug force F3	0
L13	W+P2+T3+F4	OPE	P2	Max operating pressure and temperature with slug force F4	0

L14	W+P2+T3+F5	OPE		P2	Max operating pressure and temperature with slug force F5	0
L15	W+P2+T3+F6	OPE		P2	Max operating pressure and temperature with slug force F6	0
L16	W+P2+T3+F7	OPE		P2	Max operating pressure and temperature with slug force F7	0
L17	L10-L7	OCC	Algebraic	PMax	Stress amplitude due to slug force F1	
L18	L11-L7	OCC	Algebraic	PMax	Stress amplitude due to slug force F2	
L19	L12-L7	OCC	Algebraic	PMax	Stress amplitude due to slug force F3	
L20	L13-L7	OCC	Algebraic	PMax	Stress amplitude due to slug force F4	
L21	L14-L7	OCC	Algebraic	PMax	Stress amplitude due to slug force F5	
L22	L15-L7	OCC	Algebraic	PMax	Stress amplitude due to slug force F6	
L23	L16-L7	OCC	Algebraic	PMax	Stress amplitude due to slug force F7	
L24	L3-L4	EXP	Algebraic	None	Max displacement range due to 100-year wave (without friction)	
L25	L5-L6	EXP	Algebraic	None	Full thermal displacement range (without friction)	

L26	L7-L8	EXP	Algebraic	None	Partial thermal displacement range (without friction)	
L27	L7-L9	OPE	Algebraic	PMax	10% variation in design pressure	
L28	W+D1+P1	OPE		None	Sustained stress with positive 100-year wave displacement	1
L29	W+D2+P1	OPE		None	Sustained stress with negative 100-year wave displacement	1
L30	W+T1+P1	OPE		PMax	Max design temperature with max design pressure	1
L31	W+T2+P1	OPE		PMax	Min design temperature with max design pressure	1
L32	W+T3+P2	OPE		PMax	Max operating temperature with max operating pressure	1
L33	W+T4+P2	OPE		PMax	Installation temperature with max operating pressure	1
L34	L28-L29	EXP	Algebraic	None	Max displacement range due to 100-year wave (with friction)	

L35	L30-L31	EXP	Algebraic	None	Full thermal displacement range (with friction)
L36	L32-L33	EXP	Algebraic	None	Partial thermal displacement range (with friction)
L37		OPE	Algebraic	PMax	Full pressure range

Chapter 4 Results stress analysis

Results from stress analysis in Caesar, for each respective load case is displayed in table 4-1 through 4-7, and the stresses that were included in outputs were namely axial, bending, torsional, hoop and code stress. The code stress was determined by the software, through application of equation 2.50 from chapter 2.7.3,

$$\sigma_E = \sqrt{(|\sigma_A| + \sigma_B)^2 + (2\tau)^2}$$

where the three elements of the equation represent axial stress, bending stress, and torsional stress.

Since code stress was the most relevant output for further fatigue analysis, it was the only output that was presented in aforementioned tables. The output from Caesar included stresses from three nodes of every elbow, from which the largest stress at the three nodes was chosen for further fatigue analysis of each elbow. Additionally, to the elbows, node 305, 320, and 510 representing locations of pipe supports within loop were included in analysis. In the case of thermal expansion and wave displacements, load cases both with and without friction were applied, where the higher output of the two were utilized in the fatigue assessment.

Table 4-1: Obtained stresses from all slug loads under category A, both elbow nodes and support nodes have been included in the presented results.

Node	F1	F2	F3	F4	F5	F6	F7
250	4.192	1.694	5.218	0.129	0.214	0.1994	0.0794
300	2.615	5.8318	5.04	0.882	0.415	0.1374	0.0446
305	0.5615	2.0332	1.9414	0.8103	0.2194	0.0301	0.0038
320	0.4479	0.45	0.3056	1.288	0.2534	0.0642	0.0385
340	1.8416	3.3328	3.711	2.052	0.527	0.3	0.1494
410	0.6126	1.7668	2.093	1.613	0.888	1.2488	0.5108
430	0.7564	1.935	2.261	5.3122	2.503	0.9796	0.3676
470	0.6056	0.9914	1.079	11.1534	2.437	2.537	0.9112
510	0.0696	0.0286	0.0564	3.7897	0.4146	0.7665	1.1764

Table 4-2: Slug load category B output from stress analysis.

Node	F1	F2	F3	F4	F5	F6	F7
250	5.6242	3.219	9.0442	0.1886	0.4554	0.3076	0.1108
300	3.5084	11.082	8.7344	1.289	0.8834	0.212	0.0622
305	0.7533	3.8637	3.364	0.8103	0.4668	0.0464	0.0249
320	0.6009	0.8552	0.5296	1.288	0.5392	0.0991	0.0054
340	2.4708	6.3332	6.432	2.9988	1.1216	0.4628	0.2082
410	0.8218	3.3574	3.6272	2.3574	1.8892	1.927	0.712
430	1.0148	3.677	3.9186	7.7632	5.3254	1.5114	0.5124
470	0.8126	1.8842	1.8706	16.2994	5.1856	3.9144	1.2704
510	0.0933	0.0543	0.0977	3.7897	0.8821	1.1827	1.6398

Table 4-3: Slugging category C stress range output for all relevant nodes for further fatigue analysis.

Node	F1	F2	F3	F4	F5	F6	F7
250	7.2404	4.61	12.05	0.2744	0.685	0.4086	0.1388
300	4.5166	15.8708	11.64	1.8758	1.329	0.2818	0.078
305	1.5646	7.846	5.7944	0.9379	0.7021	0.0617	0.0067
320	0.9698	5.5334	4.4829	1.1793	0.811	0.1317	0.0673
340	3.1808	9.07	8.569	4.364	1.687	0.615	0.2608
410	1.0578	4.8082	4.833	3.4306	2.842	2.5604	0.8918
430	1.3064	5.266	5.221	11.298	8.01	2.0082	0.6418
470	1.0462	2.6984	2.492	23.7206	7.8	5.201	1.5912
510	0.1201	0.0777	0.1302	5.5152	1.3269	1.5714	2.0541

Table 4-4: Stress ranges obtained from output due to slugging category D.

Node	F1	F2	F3	F4	F5	F6	F7
250	8.7116	5.6772	14.8134	0.3436	0.8866	0.4606	0.1652
300	5.4344	19.5454	14.306	2.3486	1.7196	0.3176	0.0926
305	2.3336	13.629	11.022	2.953	1.8174	0.1392	0.008
320	1.8614	3.0166	1.735	4.6936	2.0992	0.2968	0.0801
340	3.8272	11.17	10.5348	5.464	2.1836	0.6932	0.3104
410	1.2728	5.9214	5.941	4.2952	3.6774	2.886	1.061
430	1.572	6.4852	6.4184	14.1454	10.3666	2.2636	0.7636
470	1.2586	3.323	3.0638	29.6992	10.0948	5.8628	1.8932
510	0.289	0.1914	0.3202	13.8104	3.4344	3.5426	2.4438

Table 4-1 through 4-4 presents the results from stress analysis with regards to slug loads category A through D respectively. The higher instances of stress ranges occurred for category D slugs, while the lowest stress ranges were the case for category A. Furthermore, node 470 was the elbow that was exposed to the highest instances of stress concentrations throughout this analysis.

Table 4-5: Stress ranges due to 100-year wave displacements, obtained from nodal analysis of both elbow nodes and nodes at support locations of loop

Node	With friction	Without friction
250	46.5228	47.31725479
300	77.639	78.06023249
305	60.967	61.2535
320	74.932	75.0176
340	108.975	108.4722624
410	166.306	164.1873164
430	165.497	163.252389
470	25.4929	24.71007598
510	21.9907	20.236

Stress ranges applicable as inputs for fatigue analysis, regarding load cases both with and without effects of friction, should be the output with the largest stress range from each node. Hence, for 100-year wave, further fatigue analysis of node 250 and 300 were performed for stress ranges without frictional forces. For the remaining nodes, however, stress ranges from outputs that included friction, were utilized. For maximum displacements due to change in temperature, stress ranges from analysis that included effects of friction was applied for fatigue analysis for all nodes except node 470. Lastly, as can be seen in the right section of table 4-6, displacements caused by minor fluctuations in temperature resulted in generally higher stresses when effects of friction were included. The only two exceptions were node 410 and 470, that experienced slightly higher stress ranges from simulations without frictional effects on supports.

Table 4-6: Obtained stress ranges due to thermal expansion and contraction, table display both the case of maximum displacement and that of partial displacements. Both cases have been evaluated with and without effects of friction.

Node	Full range (with friction)	Full range (without friction)	Partial range (with friction)	Partial range (without friction)
250	14.29	13.93	7.72	7.70
300	22.35	22.16	10.55	10.52
305	17.7253	17.65	13.1035	13.05
320	20.5688	20.52	15.1722	15.12
340	29.65	29.44	13.96	13.95
410	47.71	47.46	23.12	23.15
430	46.91	46.70	22.74	21.63
470	8.26	8.33	3.88	3.90
510	9.3159	9.32	6.6672	6.67

Table 4-7: Stress ranges obtained from analysis due to fluctuations in pressure.

Node	Full range	10% fluctuations
250	106.23	11.02
300	106.23	11.02
305	106.23	11.02
320	106.23	11.02
340	106.23	11.02
410	106.23	11.02
430	106.23	11.02
470	106.23	11.02
510	106.23	11.02

Since the input of stress analysis software based the calculations on a section of pipe with uniform cross-section, of the same material. That additionally were undergoing the identical changes in pressure over the entire length of pipe, the output would naturally be the same for all nodes.

As can be seen in tables presented in this chapter, the hot spot regarding this set of load cases were 470. However, for stress ranges induced by causes of expansion, such as wave displacements and temperature variations, node 410 was the node under exposure to the highest instances of stress concentrations. Furthermore, since the number of load cycles associated with the four slug categories varied to a great extent, a full fatigue analysis of all elbows was warranted.

Chapter 5 Method fatigue analysis

5.1 Stress and load cycle input

Once stresses had been obtained from software, the fatigue analysis of selected the nodes could be performed. Two different codes were compared, which meant two different paths to follow. However, inputs such as number of load cycles, and magnitude of stress ranges are shared by both methods. Hence, this section of the chapter includes a presentation of such. Another general element for both standards was that the global hot spot of the pipeline was defined as the elbow node that would experience the shortest fatigue life due to high cases of local stresses. This spot will act as the structures weak link and will ultimately determine the overarching fatigue life of the structure. The dominating load cases, regarding fatigue, were those caused by wave displacements and slugging. Thus, the elbow nodes located in the loop of the bridge will all be considered in the fatigue analysis. All elbows as modelled in Caesar consists of three nodes, one at each end and one in center. In this analysis, all three nodes of each bend were evaluated, where the node of highest occurring stresses represented the elbow in further fatigue calculations. These nodes included the following, 248, 249, 250, 298, 299, 300, 338, 339, 340, 408, 409, 410, 428, 429, 430, 468, 469 and 470. Additionally, node 305, 320 and 510 were selected to represent fatigue calculations for support locations.

5.1.1 Temperature and pressure variations

Load cycles with paired load cases caused by fluctuations in temperature and pressure is presented in table 5-1, where the two values for load cycles are derived from. To be specific, one cycle every day for 50 years, and one cycle every week for 50 years. Stress ranges valid for each of the load cases presented in table 4-6 and 4-7, where the higher instance between the cases with or without friction were selected. The cycle numbers were applied in accordance with each code, presented in chapter 5.2 and 5.3, to determine accumulated damage due to cyclic loading from these sources, and corresponding design life.

Table 5-1: Load cycles applicable for variations in pressure and temperature.

Load cases	Cycles	Description
Maximum temperature range	2 600	Max design temperature to min design temperature (with and without friction)
Partial temperature range	18 300	Max operating temperature to installation temperature (with and without friction)
Full pressure range	2 600	Design pressure to operating pressure
Partial pressure range	18 300	10% fluctuation of design pressure

5.1.2 Slugging

Stresses determined from Caesar analysis with respect to slugging load cases can be considered as the amplitude of a single load cycle under given conditions. However, for a fatigue analysis in accordance with both ASME B31.3 and PD5500, the full stress range is required in the calculations (ASME, 2018; BSi, 2003). Hence, assumptions need to be made in order to convert the result to a corresponding stress range from each respective amplitude. A conservative assumption is simply to multiply the stress amplitude with 2, hence implying that every time a slug load is exerted on an elbow, the tension created will be followed by compression stresses of equal magnitude.

Table 5-2: Load cycles relevant for fatigue calculations, in regard to slug loads, which are values that are relevant for both codes. The stress ranges corresponding to the respective load cycles are presented in table 4-1 through 4-4.

Slug Category Name	Slug Category	Branch	50 Years Cycles
5380_to_ 8032	A	F1	291 981 750
8032_to_ 10683	B		117 165 000
10683_to_ 13334	C		19 162 500

13334_to_ 15985	D		1 752 000
4257_to_ 9441	A	F2	88 421 250
9441_to_ 14625	B		61 265 250
14625_to_ 19808	C		68 820 750
19808_to_ 24992	D		30 441 000
5794_to_ 12273	A	F3	22 283 250
12273_to_ 18753	B		65 535 750
18753_to_ 25232	C		117 548 250
25232_to_ 31711	D		14 289 750
6269_to_ 13284	A	F4	162 114 750
13284_to_ 20300	B		124 665 750
20300_to_ 27315	C		85 464 750
27315_to_ 34330	D		17 629 500
1561_to_ 5465	A	F5	116 234 250
5465_to_ 9370	B		89 571 000
9370_to_ 13274	C		32 466 750
13274_to_ 17178	D		4 653 750
6543_to_ 10867	A	F6	7 719 750
10867_to_ 15190	B		19 764 750
15190_to_ 19514	C		149 303 250
19514_to_ 23837	D		48 837 000
9802_to_ 15051	A	F7	24 582 750
15051_to_ 20300	B		81 851 250
20300_to_ 25550	C		244 842 000
25550_to_ 30799	D		41 938 500

5.1.3 Wave

The scatter diagram of the met ocean analysis report shows the amount of wave cycles for the various heights; however, it does not divide into categories for the different directions. Since waves of same height but different direction will result in a large difference in relative longitudinal displacements, it was necessary to make appropriate adjustments with respect to this aspect.

Table 5-3: This table represents how difference in incoming wave angle will result in difference in displacement of bridge.

	Bridge movement with respect to wave direction			
Global angles (degrees)	Original max bridge movement (mm)	Platform 1 max movement (mm)	Platform 2 max movement (mm)	Adjusted max bridge movement (mm)
335 and 155	133	52	-42	94
20 and 200	658	257	-206	463
65 and 245	803	314	-251	565
110 and 290	520	203	-163	366

$$Bridge\ mvmt(direction) = \frac{Orig\ movement\ (wave\ angle) \times Adj\ movement\ (245^o)}{Orig\ movement\ (245^o)}$$

The relation above was applied to determine the adjusted max bridge movement for all eight directions based on the originally obtained max bridge movements.

Table 5-3 displays the result of initial response analysis, regarding bridge displacements subjected to 100-year wave, where the assumed maximum displacement range were as shown in the column "original max bridge movement". Furthermore, adjusted max bridge movements was considered proportional to the values obtained from previous analysis, described through forementioned relation. However, it was centered around the adjusted maximum longitudinal bridge displacement value, of the 100-year wave, of 565 mm. With defined angles of incoming waves, data representing distribution between wave number with respect to direction could be evaluated to determine the number of load cycles of each direction. Thus, scatter diagram displayed in table 5-4 was applied to estimate distribution of wave numbers between directions, which is ultimately presented in table 5-5.

Table 5-4: Scatter diagram with respect to significant wave height and direction.

H_s (m)	Wave direction								
	335°	20°	65°	110°	155°	200°	245°	290°	Omni
0-1	3.79	2.45	0.45	0.81	1.17	1.45	1.77	2.89	14.77
1-2	8.60	5.34	0.81	2.48	3.66	3.92	4.52	6.30	35.63
2-3	5.18	2.77	0.26	1.91	2.68	2.95	3.74	4.17	23.65
3-4	2.44	1.06	0.07	1.32	1.72	1.86	2.45	2.33	13.25
4-5	1.19	0.46	0.02	0.86	1.04	0.97	1.22	1.12	6.87
5-6	0.57	0.18	0.00	0.43	0.48	0.49	0.61	0.56	3.32
6-7	0.29	0.08	0.00	0.24	0.22	0.19	0.26	0.26	1.53
7-8	0.14	0.04	0.00	0.09	0.09	0.06	0.09	0.12	0.64
8-9	0.05	0.01	0.00	0.04	0.02	0.01	0.03	0.05	0.21
9-10	0.02	0.01	0.00	0.02	0.00	0.00	0.01	0.03	0.08
10-11	0.02	0.01	0.00	0.00	0.00	0.00	0.00	0.01	0.04
11-12	0.00	0.00	0.00	0.01	0.00	0.00	0.00	0.00	0.01
12-13	0.00	0.00	0.00	0.00	0.00	0.00	0.00	0.00	0.00
14+	0.00	0.00	0.00	0.00	0.00	0.00	0.00	0.00	0.00
Total %	22.28	12.40	1.62	8.20	11.07	11.89	14.70	17.83	100.00

Calculations of incoming waves regarding angles resulted in the following distribution of wave cycles for all applied directions. The percentages of each direction were applied to the total number of every wave height, in order to obtain load cycle number with respect to both direction and height.

Table 5-5: Breakdown of waves with respect to angles.

Global angles (degrees)	Wave distribution (percentage)	Wave distribution (total number of cycles)
335 and 155	33.36	168831563
20 and 200	24.29	122929217
65 and 245	16.32	82593858
110 and 290	26.04	131785789

With wave numbers distributed over angles determined, along with new values for maximum movements for each direction, displacements for smaller wave heights could be calculated. This was conducted through the assumption of proportional relation equivalent to that of the following equation,

$$RBM = \left[\left(\frac{WH}{MWH}\right)^{1.7}\right] \times Maximum\ relative\ deflection$$

where RBM is an acronym for relative bridge movements, WH denote wave height from 1 to 28 m, MWH is maximum wave height (in this case 28 m). Lastly, maximum relative deflection represents the value of maximum longitudinal displacement range, which was applied in stress analysis.

The foregoing expression is an estimation of wave displacements for marine fixed leg steel jacket structures, where the exponent number 1.7 is the constant representing this feature. This specific value was obtained from DNV-RP-D101 Appendix J. Thus, the mentioned relation was applied between the different wave heights for each respective direction. Furthermore, for every wave height, it was assumed that the displacement relation with respect to directions would be proportional to that of the displacements of different directions of the 100-year wave, which can be described with the following equation,

$$Stress\ range = (RBM/MRBM) \times Maximum\ stress\ range$$

where RBM is relative bridge movement for a specific direction, MRBM is maximum relative bridge movement for the same direction, and maximum stress range was that obtained from stress analysis. With the established displacements and defined relation with stress ranges, stresses for all wave heights could be calculated for every direction. This was highly applicable for PD5500 in particular, since minor sum principle was applied for wave loads, as shown in detail in chapter 5.2. For ASME B31.3, which is displayed in chapter 5.3, another approach was applied, however, acquired data was still utilized. Example of output values from this methodology can be found in the appendix, where stress ranges at all elbow nodes for wave heights ranging from 1 to 28 m, for the 4 main directions are presented, for load case without friction.

5.2 Fatigue calculations according to PD5500

Before initiating the fatigue analysis according to PD5500, it was necessary to determine if a simplified analysis could be performed, or if the code require a detailed analysis. This was conducted through utilization of equation 2.36.

$$N \leq \frac{6 \times 10^9}{f_f^3}\left(\frac{22}{e}\right)^{0.75}\left(\frac{E}{2.09 \times 10^5}\right)^3 \qquad\qquad 2.36$$

In this case, maximum design stress range from any source is that of maximum displacement range due to 100-year wave, which is a stress range of 166.306 MPa. Furthermore, Youngs modulus for operating temperature is 195 000 N/mm², and thickness e is 24.61 mm. Hence, the expression becomes:

$$N \leq \frac{6 \times 10^9}{166.306^3}\left(\frac{22}{24.61}\right)^{0.75}\left(\frac{195000}{2.09 \times 10^5}\right)^3 = 974$$

Since the total number of load cycles from all sources far exceed the result from equation 2.36, a detailed consideration of fatigue calculations according to PD5500 was required.

The next step when applying fatigue calculations in accordance with PD5500 was to determine weld class of the structure and apply corresponding SN-curve for further calculations. The standard includes specifications and definitions regarding the different weld classes. Generally, since the concern of a fatigue analysis is the weak link of the structure, the SN-curve representing an appropriate weld class of the hot spot of the structure is applied. The welded connections of the pipe elbows, were defined as fully penetrated butt welds of class D. However, additional analysis was performed on the basis of weld class F2, which corresponds with welded supports. This extra analysis was performed on nodes representing supports located in expansion loop and were mainly performed in order to establish comparative data regarding multiple S-N curves from PD5500.

Table 5-6: Numeric values for coefficients representing the SN-curve of a class D and F2 weld.

| Class | Constants S-N curve | | | | Stress range at $N = 10^7$ cycles (MPa) |
| | For $N < 10^7$ cycles | | For $N > 10^7$ cycles | | |
	m	A	m	A	
D	3	1.52×10^{12}	5	4.18×10^{15}	53
F2	3	4.31×10^{11}	5	5.25×10^{14}	35

Hence, constants from selected weld class could be assigned to equation 2.36.a, as displayed below, for stress ranges of both over and under 10 000 000 cycles. In addition to constants from S-N curve, values for wall thickness (**e**), and Youngs Modulus (**E**) were defined as 24.61 mm and 195 000 N/mm² respectively. In the case of maximum displacement due to change in temperature, Youngs modulus was set as 204 100 N/mm².

$$N_i = A \left(\frac{22}{e}\right)^{\frac{m}{4}} \left(\frac{\sigma_r \times 2.09 \times 10^5}{E}\right)^{-m} \qquad 2.36.a$$

Under 10 000 000 load cycles:

$$\rightarrow N = 1.04 \times 10^{12} \times \left(\frac{22}{24.61}\right)^{\frac{3}{4}} \left(\frac{S_r \times 2.09 \times 10^5}{195\,000}\right)^{-3} \qquad 2.36.b$$

Over 10 000 000 load cycles:

$$\rightarrow N = 2.29 \times 10^{15} \times \left(\frac{22}{24.61}\right)^{\frac{5}{4}} \left(\frac{S_r \times 2.09 \times 10^5}{195\,000}\right)^{-5} \qquad 2.36.c$$

The next stage of the fatigue analysis included implementation of all relevant stress ranges to obtain allowable load cycles from the two instances of equation 2.36.a, which are noted as 2.36.b and 2.36.c. For the load cases related to variation in pressure or temperature, the implementation of stress ranges was straight forward. Obtained stress ranges from Caesar analysis was applied directly to equation 2.36.a for all relevant elbow nodes. Similarly, the process of determining fatigue induced by slugging was based on applying stresses obtained at elbow nodes, from all slug loads for each category, where every stress range was multiplied with 2 before inserted into equation, as explained in chapter 5.1.2. Regarding wave loads, the

applied method for PD5500 was according to methodology in chapter 5.1.3. A full list of stress ranges for all wave heights and directions with corresponding number of cycles are presented in appendix. Last stage of methodology included summation of accumulated damage from all viable stress ranges according to equation 2.35, where right side of equation represent allowable fatigue and n_i represents occurring load cycles.

$$\sum \frac{n_i}{N_i} \leq 0.6 \left(\frac{22}{e}\right)^{0.75} \qquad\qquad 2.35$$

$$\rightarrow \sum \frac{n_i}{N_i} \leq 0.6 \left(\frac{22}{24.61}\right)^{0.75} = 0.5516$$

5.3 Fatigue calculations according to ASME B31.

The initial step of the fatigue analysis according to ASME B31.3 included a check of various factors and parameters. While some of the parameters listed in methodology are restricted to either accumulated damage caused by waves, or all other sources of loading than waves, there are some that overlap. Hence, these factors were determined in the first stage of the analysis. First, there was the fatigue improvement factor f_I, which remained 1, since nothing in design indicated that a reduction in conservatism should be considered for fatigue calculations. Second, since the structure of the case study is located entirely above sea level, the environmental factor f_E, was set equal to 1, for the purpose of all calculations in this analysis. Third, pipe cross-sectional geometry was uniform for all nodes considered in analysis, hence, following requirement from standard was accounted for (ASME, 2018).

$$16\ mm < T < 150\ mm \rightarrow T_E = T_n = 24.61\ mm$$

Fourth, since both materials used in model were steel, the fatigue material coefficients were determined based on two conditions, for stress ranges with an amount of corresponding cycles less than 10 000 000, information from table 2-2 were applied. For stress ranges that had corresponding load cycles that exceeded 10 000 000, table 2-3 was used. This resulted in the following values for the different coefficients.

Less than 10 000 000 cycles:

$$CF = 14\,137, \qquad m = 3.13, \qquad k = 0.222$$

More than 10 000 000 cycles:

$$CF = CFa[(f_F/f_I)10^7]^{\left(\frac{1}{m_2} - \frac{1}{m_1}\right)} = 14\,137 \times [(1/1)10^7]^{-0.1195} = 2060.32$$

$$m = 5.0, \qquad k = 0.222$$

Fifth, fatigue factor for stress ratio was controlled based on the following requirement listed in code (ASME, 2018).

$$\left(\sigma_{Ei,max} + \sigma_{Ei,min}\right) > \sigma_{yi}$$

Since wave displacements, by far represent the largest instances of stresses of any of the load cases and is the only stress range that is remotely close to yield strength of structure, the control was performed on the basis of only that stress range.

$$(166.306 + 2.82) = 169.126 \, MPa$$

$$\rightarrow 169.126 \, MPa < S_{yi} = 448 \, MPa$$

Hence, the factor $f_{M,k}$ will be equal to 1 throughout the fatigue analysis, for all load cases. Lastly, temperature correction factor f_t was determined for the relevant temperatures and corresponding load cases. For all load cases other than full temperature displacement range, the factor was based on operational temperature, shown in equation 2.39.a, while the factor for full temperature displacement was determined as shown in equation 2.39.b.

$$f_t = \frac{E}{E_{CSA}} = \frac{201370}{195430} = 1.0304 \qquad\qquad 2.39.\,a$$

$$f_t = \frac{E}{E_{CSA}} = \frac{201370}{204100} = 0.9866 \qquad\qquad 2.39.\,b$$

With coefficients and factors applicable for stress ranges from all other sources than waves determined, the next step was to go through the relevant obtained stress ranges from analysis, and corresponding load cycles, in order to determine whether they met criteria from code. First, a check needed to be conducted to determine whether the basic allowable stress at maximum temperature exceeded the stress due to sustained loads. This was represented in load case 1 and 2 of Caesar analysis. The output from stress analysis indicated a basic allowable stress range, representing equation 2.43, of 206.850 MPa, which was above the highest occurring stress ranges from analysis. Second, determine whether number of load cycles is within maximum requirement for every stress range. This step was performed through application of equation 2.38.

$$N_{ti} = \frac{f_I}{f_E} \left(\frac{CF \cdot f_{M,k} \cdot f_t}{\sigma_{Ei} \cdot T_E^k} \right)^m \qquad 2.38$$

When inserting numeric values for factors and coefficients in equation, it yields the following two equations, 2.38.a for stress ranges less than 10 000 000 load cycles, and 2.38.b for stress ranges with more than 10 000 000 load cycles.

$$N_{ti} = \frac{1}{1} \left(\frac{14\ 137 \cdot 1 \cdot 1.0304}{S_{Ei} \cdot 24.61^{0.222}} \right)^{3.13} \qquad 2.38.a$$

$$N_{ti} = \frac{1}{1} \left(\frac{2060.32 \cdot 1 \cdot 1.0304}{S_{Ei} \cdot 24.61^{0.222}} \right)^{5} \qquad 2.38.b$$

For the specific load case of full temperature range, the number of load cycles indicate equation 2.38.a, however, temperature correction factor is different. Hence, a third expression is defined as equation 2.38.c.

$$N_{ti} = \frac{1}{1} \left(\frac{14\ 137 \cdot 1 \cdot 0.9866}{S_{Ei} \cdot 24.61^{0.222}} \right)^{3.13} \qquad 2.38.c$$

Third, summation of accumulated damage caused by all stress ranges, other than wave loads, is performed through equation 2.44.

$$d_t = \sum_{i=1}^{n} \frac{n_i}{N_{ti}} \qquad\qquad 2.44$$

The fourth step of fatigue methodology according to ASME B31.3 included the evaluation of wave loads. When utilizing fatigue analysis in accordance with ASME B31.3, stress range caused by wave induced longitudinal displacements, which as previously mentioned was applied through a Weibull cumulative distribution function. This function was utilized to describe the probability of exceeding the relevant stress range under the conditions of the wave spectrum, over a given design period. Furthermore, the stress range appearing in the equation is deemed to be proportional to the parameter representing wave height of a standard Weibull cumulative function.

Hence, the application of this method provides the probability of exceeding a prescribed maximum stress range over a defined period, which in this case corresponds to the probability of a 100-year wave height occurring during the lifetime of structure, of 50 years. Furthermore, the stress output from Caesar software regarding maximum displacement range caused by said 100-year wave will serve as maximum allowable probable stress range. This means that the expression for fatigue induced by wave displacements, according to ASME B31.3, can be reduced to equation 2.45.a,

$$d_w = \frac{\sigma_{aw}^m \times N_d}{f_a} \times \frac{\Gamma\left(1 + \frac{m}{h}\right)}{[\ln(N_w)]^{\frac{m}{h}}} \qquad\qquad 2.45.a$$

where parameter f_a is determined through equation 2.49 with respect to both cases of low cyclic loading and high cyclic loading.

$$f_a = \left(\frac{f_I}{f_E}\right) \times \left(\frac{CF \cdot f_{M,k} \cdot f_t}{T_E^k}\right)^m \qquad\qquad 2.49$$

Low cyclic loading:

$$f_a = \left(\frac{1}{1}\right) \times \left(\frac{14\,137 \cdot 1 \cdot 1.0304}{24.61^{0.222}}\right)^{3.13} = 1.161 \times 10^{12}$$

High cyclic loading:

$$f_a = \left(\frac{1}{1}\right) \times \left(\frac{2060.32 \cdot 1 \cdot 1.0304}{24.61^{0.222}}\right)^5 = 1.232 \times 10^{15}$$

To account for wave heights with number of occurrences exceeding 10 000 000 cycles, and those below said number, the equation for fatigue damage needed to be utilized twice. Furthermore, parameters N_w and N_d were defined based on recorded cycles in scatter diagram, which accounted for 100 years of data. As a result, N_w was assigned the total number of recorded wave heights, and N_d was defined as half that number. Thus, N_w was 504960000, and N_d 252480000.

Table 5-7: The Weibull shape parameter h was extracted from wave statistics based on met ocean data. A summary of this study with respect to this parameter is presented in table.

Direction	Sector Prob.	Weibull parameters		
		Shape	Scale	Location
-	(%)	-	(m)	(m)
0º	18.46	1.104	1.44	0.72
30º	1.65	1.263	1.03	0.54
60º	0.93	1.384	1.20	0.49
90º	1.32	1.284	1.19	0.59
120º	8.19	1.584	2.83	0.46
150º	7.43	1.739	2.65	0.36
180º	7.19	1.469	2.13	0.52
210º	8.46	1.685	2.65	0.31
240º	8.72	1.560	2.48	0.43
270º	13.08	1.396	2.33	0.53
300º	11.18	1.166	1.67	0.65
330º	13.40	1.216	1.88	0.62
0º – 360º	100.00	1.324	2.07	0.55

As presented in table 5-7, the analysis resulted in numerous values of Weibull parameters depending on direction of incoming waves. For the purpose of fatigue calculations utilized in this thesis, the value representing the entire spectrum of incoming waves will be applied. Thus, shape parameter h=1.324. Hence, accumulated damage from wave heights from the four

different directions could be performed. Table 5-8 and 5-9 summarize stress ranges with respect to different nodes and angles applied to the relevant equations regarding high cycle, or low cycle load. Additionally, the presented stress ranges were subtracted from load cases with and without frictional effects, where the higher stress range from the two scenarios were chosen.

Table 5-8: Maximum stress range with load cycles less than 10 000 000 for every direction.

Node	Direction							
	65 and 245		20 and 200		335 and 155		110 and 290	
	Stress	Cycles	Stress	Cycles	Stress	Cycles	Stress	Cycles
250	39.45	8131245	30.03	4914302	4.33	5268364	29.40	6748554
300	78.61		59.83		8.63		58.57	
305	61.25		46.62		6.72		45.64	
320	75.01		57.09		8.23		55.90	
340	109.24		83.14		11.98		81.40	
410	166.30		126.57		18.25		123.92	
430	165.50		125.95		18.16		123.32	
470	25.50		19.40		2.80		19.00	
510	22.00		16.74		2.41		16.39	

Table 5-9: Maximum stress range with load cycles more than 10 000 000 for every direction.

Node	Direction							
	65 and 245		20 and 200		335 and 155		110 and 290	
	Stress	Cycles	Stress	Cycles	Stress	Cycles	Stress	Cycles
250	0.44	40427310	0.67	56550306	0.10	59320364	0.66	71709775
300	0.88		1.34		0.20		1.31	
305	0.15		1.02		0.69		1.05	
320	0.18		1.25		0.84		1.28	
340	1.23		1.86		0.27		1.83	
410	1.86		2.82		0.41		2.76	
430	1.85		2.81		0.40		2.75	
470	0.28		0.42		0.06		0.42	
510	0.05		0.37		0.25		0.38	

The last step of this fatigue analysis was to sum the two expressions for accumulated damage, and check if it fulfilled requirement for all elbow nodes, in addition a calculation of estimated design life of hot spot node was executed.

$$d_w + d_t \leq 1 \qquad\qquad 2.49$$

Chapter 6 Results fatigue analysis

6.1 Comparison of the two results

The following chapter includes a portrayal of the obtained results from the fatigue analysis that were made according to PD5500 and ASME B31.3. These calculations were performed on elbow nodes located at expansion loop of the bridge, in addition to analysis of nodes located at supports of the loop. A summary of fatigue calculations according to PD5500 and ASME B31.3 is presented in table 6-1 through 6-10, where the nodes representing elbows of expansion loop was 250, 300, 340, 410, 430 and 470, while nodes 305, 320 and 510 represented selected supports at the loop. The cells marked "years" represents the number of years until fatigue related failure.

Table 6-1: Fatigue caused by pressure variations; results are based on both load cases.

		10% Pressure change	
Node	Max stress range	PD5500	ASME B31.3
		di	di
All	11.0238	2.16E-05	3.41E-05

		Full pressure range	
Node	Max stress range	PD5500	ASME B31.3
		di	di
All	106.2284	0.002746	0.005816

Table 6-1 shows the results from fatigue calculations from the load cases related to variations in pressure. All nodes in expansion loop were subjected to the same levels of accumulated damage for both cases of pressure fluctuations.

Table 6-2: Fatigue outputs from both cases of temperature displacements, according to both codes.

	Maximum temperature variation		
Node	Max stress range	PD5500	ASME B31.3
		di	di
250	14.2903	6.68506E-06	1.0908E-05
300	22.3553	2.55931E-05	4.4261E-05
340	29.6495	5.97081E-05	0.00010712
410	47.7144	0.000248846	0.00047493
430	46.9123	0.000236506	0.00045039
470	8.33023	1.3242E-06	2.0143E-06
	Partial temperature variation		
Node	Max stress range	PD5500	ASME B31.3
		di	di
250	7.7234	7.42822E-06	1.1189E-05
300	10.55	1.89329E-05	2.9697E-05
340	13.9618	4.38817E-05	7.1385E-05
410	23.1543	0.000200149	0.00034772
430	22.7395	0.000189584	0.0003286
470	3.9014	9.5746E-07	1.3196E-06

Table 6-2 represents the results from fatigue analysis based on changes in temperature, the results regarding design life across the different nodes are approximately the same between the two methods. Nodes 410 and 430 were hot spot nodes for both temperature ranges, however, the total fatigue caused by the two load cases was not substantial.

Table 6-3: Fatigue caused by instances of slug category A at elbows.

Node	Max stress range	PD5500	ASME B31.3
		di	di
250	5.2184	0.000181232	0.000378001
300	5.8318	0.000274321	0.000572094
340	3.711	2.51467E-05	5.26281E-05
410	2.0928	1.49111E-05	4.45378E-05
430	5.3122	0.000279268	0.000588882
470	11.1534	0.011006879	0.023066762

Table 6-4: Fatigue due to all slugs from category B at elbows.

Node	Max stress range	PD5500	ASME B31.3
		di	di
250	9.0442	0.001808629	0.003771766
300	11.082	0.005307376	0.011068153
340	6.432	0.000539848	0.001125813
410	3.6272	3.079E-05	6.42104E-05

Node			
430	7.7632	0.001557391	0.003247827
470	16.2994	0.055966623	0.116714385

Table 6-5: Fatigue caused by slugging category C on elbow nodes.

Node	Max stress range	PD5500	ASME B31.3
		di	di
250	12.05	0.011829252	0.024669058
300	15.8708	0.03675522	0.07665038
340	9.07	0.00381415	0.007954137
410	4.8328	0.000214083	0.000446456
430	11.298	0.006828747	0.014240864
470	23.7206	0.250433359	0.522260833

Table 6-6: Fatigue caused by accumulated damage on elbows from slugging category D.

Node	Max stress range	PD5500	ASME B31.3
		di	di
250	14.8134	0.005058164	0.011592927
300	19.5454	0.037382085	0.078273641
340	11.17	0.002902298	0.006272509

410	5.941	0.000145693	0.000936677
430	14.1454	0.004307043	0.022697343
470	29.6992	0.158896243	0.344050405

The results from fatigue analysis regarding slugging is presented in table 6-3 through 6-6, where the slugging categories are presented separately, from A to D respectively. As can be seen in all four tables, the methodology related to ASME B31.3 resulted in a more conservative output than PD5500.

Table 6-7: Accumulated damage caused by all categories of slugging.

Node	Max stress range	PD5500		ASME B31.3	
		di	years	di	years
250	14.8134	0.018877	1461.05	0.04041175	1237.2639
300	19.5454	0.079719	345.9734	0.16656427	300.18443
340	11.17	0.007281	3787.801	0.01540509	3245.681
410	5.941	0.000405	68020.19	0.00149188	33514.752
430	14.1454	0.012972	2126.095	0.04077492	1226.2441
470	29.6992	0.476303	57.90568	1.00609238	49.697225

Table 6-5 shows the total accumulated damage due to all stress ranges caused by slugging, of all four categories. The table also presents expected lifetime of specific node when subjected to the prescribed levels of fatigue. As indicated by results in table, the node exposed to the highest degree av fatigue was 470, in which PD5500 yielded an expected design life of 57.9 years,

whereas the method of ASME B31.3 resulted in a design life of 49.7 years. The difference in outcome between the codes is visualized in figure 6.1, which shows how level of accumulated damage vary from node 250 to node 510.
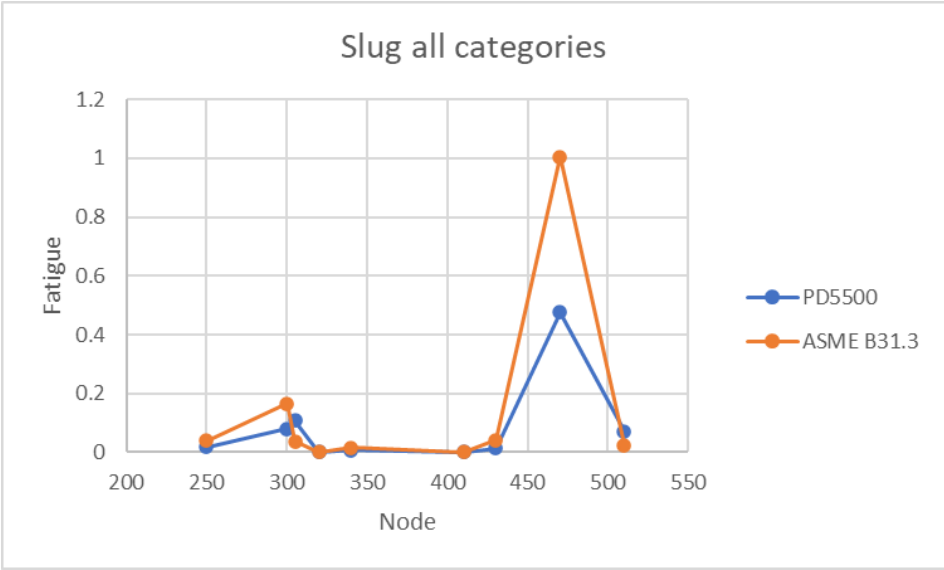
Figure 6-1: Comparison fatigue slugging, all categories

Table 6-8 contains results from fatigue analysis based on wave loads according to both codes, where node 410 and 430 represents the elbows that are under highest exposure regarding fatigue induced by wave displacements. In addition, the results obtained through ASME B31.3 is significantly more conservative than PD5500.

Table 6-8: Fatigue of elbows caused by wave displacements according to both codes.

Node	Max stress range	PD5500	ASME B31.3
		di	di
250	47.31725479	0.000263	0.00264339
300	78.06023249	0.001182	0.02286699
340	108.975	0.003215	0.06355402
410	166.306	0.011428	0.23864465
430	165.497	0.011262	0.23502984

470	25.4929	4.12E-05	0.0006736

The different levels of conservatism evident in the outputs from fatigue analysis with respect to wave displacements is presented in figure 6-2. In this graph, fatigue output for node 250 through 510 is plotted with respect to outcome from both standards.
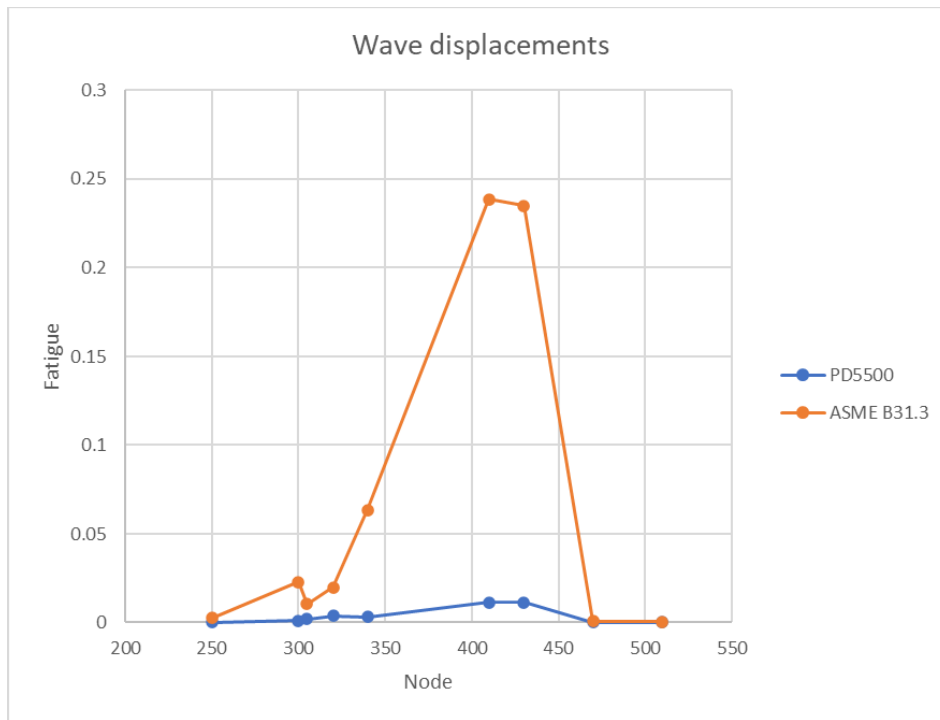
Figure 6-2: Comparison between wave fatigue output from both standards, for all nodes

Design life were calculated based on allowable damage criteria from codes, presented in table 6-9.

Table 6-9: Allowable damage according to both codes, which were applied in determining total fatigue and design life of all nodes included in analysis.

Standard	PD5500	ASME B31.3
Max damage (d)	0.5516	1

The total sum of accumulated damage from all sources is presented in table 6-10, in addition to design life (years), which were based on information in table 6-9. The results show that it is mainly slugging that poses a threat to the structural integrity of the pipe. This is evident when considering node 470, which were exposed to large stress ranges from slugging. A secondary

cause for fatigue were wave displacements. This is evident for node 410 which experienced the most fatigue from displacements due to waves and thermal changes.

Table 6-10: Design life and total accumulated damage caused by all sources of loading according to methodologies of both codes.

Node	PD5500		ASME B31.3	
	di	years	di	years
250	0.022	1258.5	0.0431113	1159.788
300	0.081	340.7	0.1895393	263.7975
340	0.011	2590.2	0.0791717	631.5389
410	0.012	2208.3	0.2409918	207.476
430	0.025	1111.3	0.2765703	180.7858
470	0.491	56.2	1.0068034	49.66213

Figure 6-3 contains a comparison between accumulated damage from all sources of loading according to both ASME B31.3 and PD5500. Calculations based on ASME B31.3 generally resulted in a more conservative output. This was particularly evident for nodes where wave displacements and high cycle loading such as slugging were prominent.
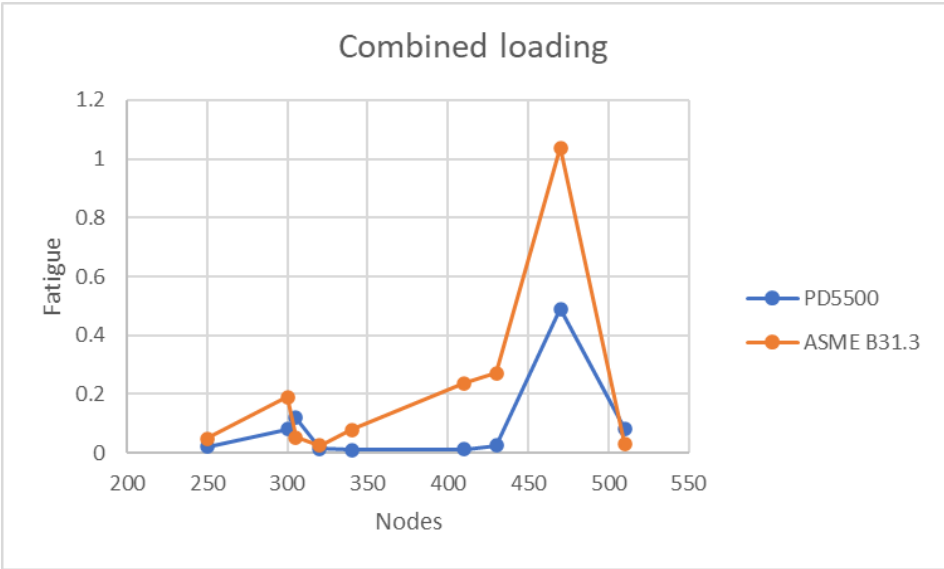
Figure 6-3: Comparison fatigue combined loading

Table 6-9 through 6-11 present calculated ratio between the two codes with regard to design. The reason for this was the fact that the codes have difference in allowable accumulated damage, as shown in table 6-9.

Table 6-11: Fatigue output ASME B31.3 to PD5500 ratio, slugging fatigue.

Node	Category A	Category B	Category C	Category D	Sum
250	2.08		2.08		
		2.08		2.30	2.14
300	2.08		2.08		
		2.08		2.10	2.09
340	2.09		2.08		
		2.08		2.16	2.12
410	2.98		2.08		
		2.08		6.43	3.68
430	2.11		2.08		
		2.08		5.27	3.14
470	2.09		2.08		
		2.08		2.16	2.11

Table 6-12: Fatigue output ASME B31.3 to PD5500 ratio, all sources except slugging. Only elbow nodes.

Node	Wave	Thermal (Partial)	Thermal (Max)	Pressure	Combined	Design life
250				1.85		
	10.04	1.03	1.11		2.23	0.81
300				1.85		
	19.35	1.07	1.18		2.34	0.77
340				1.85		
	19.76	1.11	1.23		7.48	0.24
410				1.85		
	20.88	1.19	1.30		18.95	0.10
430				1.85		
	20.87	1.19	1.30		10.95	0.16
470				1.85		
	16.66	0.94	1.04		2.11	0.86

When evaluating the results from fatigue analysis according to both methodologies, the overarching pattern is clearly that ASME B31.3 gave a more conservative result than that of PD5500. The method of the former code resulted in an estimated life of 49.6 years, which is approximately 7 years shorter than what were obtained with PD5500, and more importantly, a couple of months shy of the desired lifetime of 50 years. However, closer inspection of fatigue outputs from various sources showed varying degree of conservatism in comparison to PD5500. Table 6-2, which represents the results from accumulated damage due to two cases of temperature fluctuations, shows that the method of ASME B31.3 did not result in much higher results of fatigue than that of PD5500, especially when factoring in allowable damage. Similar differences were found when observing results from fatigue caused by both instances of pressure variations. Slugging showed a larger difference in outcome compared to both pressure and temperature, in which results from ASME B31.3 were more conservative. However, the biggest difference in outcome regarding the two standards where that of fatigue caused by wave loads.

Table 6-13: Average ratio between the codes, with respect to all sources of loading, in addition to combined loading and design life.

Fatigue ASME B31.3 to PD5500 ratio						
Slugging All categories	Wave	Thermal (partial)	Thermal (max)	Pressure	Total fatigue	Design life
2.55	17.93	1.20	1.09	1.85	7.34	0.49

As presented in table 6-13, there are generally not significant differences between outputs when considering fluctuations in temperature, and to a certain degree pressure, where ASME B31.3 comparatively gave 1.85 times higher accumulation of damage. Results such as these could simply suggest variations due to difference of integrated safety factors. However, the relatively high average ratio of the two code outputs regarding slugging and waves deserved further inspection. Especially interesting was the fact that slugging induced fatigue showed such a gap in ratio, when compared to thermal or pressure variations, considering that fatigue from slugging was calculated through the same methodology in ASME B31.3. The two mentioned observations suggested the following implications. Firstly, the specific methods for determining damage caused by waves show vast variation in results. Secondly, what mainly separated slug loads from pressure and temperature variation, as mere stress ranges with load cycles, was the number of cycles. The load spectrum from temperature and pressure fluctuations solely stayed within the range of 10 000 000 load cycles. This was not the case for slugging, where oppositely the majority of stress ranges occurred over vast amounts of load cycles, mostly exceeding 10 000 000 cycles. This observation would suggest that the methodology of ASME B31.3 regarding high cyclic loading includes coefficients of proportionally higher levels of conservatism when compared to S-N curves of low cyclic loading. In other words, the data suggest that with application of ASME B31.3, the degree of conservatism increase when structures are subjected to stress ranges of high accounts of corresponding load cycles. However, unlike ASME B31.3, PD5500 supply multiple S-N curves for various weld classes, where the range of connecting curve coefficients vary greatly. Which is highly relevant since any practical comparison of the two codes would to a great extent depend on the assumption of applied weld class. Hence, further fatigue analysis of nodes located at supports in the extension loop was included, in order to investigate the relation between weld class in PD5500 and output.

The supports were selected due to increase in margin of safety regarding weld class. While fully penetrated butt welds belong to weld class D, welds meant for supports belong to class F2. Since the supports of the expansion loop were located exclusively at straight sections, the effects of slug loads were expected to be much lower than of the elbows. The results of which is displayed in table 6-14 through 6-17.

Table 6-14: The table presents fatigue caused by wave displacements on support nodes of expansion loop, where calculations were conducted according to both codes. For PD5500, weld class F2 were utilized. Furthermore, estimated design life based on wave displacement alone have been calculated with ratio.

Max stress range	Node	PD5500	ASME B31.3	Ratio	
		di	di	di	Years
305	61.25	0.00201	0.01047	5.2003	0.3486074
320	75.20	0.00369	0.01975	5.33914	0.3395421
510	22.00	9.3E-05	0.00042	4.5519	0.3982635

Table 6-15: Fatigue calculations due to fluctuations in temperature of support nodes in expansion loop. Both maximum thermal displacements and partial displacements are presented.

Max temperature displacement					
Max stress range	Node	PD5500	ASME B31.3	Ratio	
		di	di	di	Years
17.7253	305	4.5E-05	2.14E-05	0.47580	3.8101011
20.5688	320	7.0E-05	3.41E-05	0.48509	3.7371154
9.3159	510	6.5E-06	2.86E-06	0.43763	4.1424230
Partial temperature variation					
Max stress range	Node	PD5500	ASME B31.3	Ratio	
		di	di	di	Years
17.7253	305	0.000128	5.85E-05	0.45748	3.96271942
20.5688	320	0.000199	9.26E-05	0.466281	3.88792036
9.3159	510	1.69E-05	7.06E-06	0.41901	4.32654296

Table 6-16: Fatigue analysis based on all sources of slug loads exerted on support nodes in expansion loop. For calculation according to PD5500, weld class F2 were applied.

Max stress range	Node	PD5500	ASME B31.3	Ratio	
		di	di	di	Years
13.629	305	0.108547	0.037113	0.341904	5.3022681
4.6936	320	0.000539	0.000187	0.347364	5.2189247
13.8104	510	0.072229	0.024718	0.34222	5.2973698

Table 6-17: Fatigue analysis based on all sources of cyclic loading exerted on support nodes in expansion loop. For calculation according to PD5500, weld class F2 were applied. The results are displayed in table as total accumulated damage, design life and ratio between the two codes.

Node	PD5500		ASME B31.3		Ratio	
	damage	Years	damage	Years	damage	Years
305	0.120495	228.8954	0.053514	934.3289	0.444122	4.08190345
320	0.014268	1933.066	0.025914	1929.47	1.816243	0.99814004
510	0.082106	335.9163	0.031002	1612.809	0.377584	4.80122474

As can be seen in table 6-17, when applying weld class F2 and methodology of PD5500, the results of fatigue calculations becomes relatively more conservative for all sources of loading than that of class D. The difference in outputs compared to ASME B31.3 was more conservative for all load cases except wave loads. For wave loads, the outcome was approximately a third of the design life of that estimated by PD5500.

Fatigue analysis resulted in several observations, which can be summarized through the following points. Firstly, constants representing S-N curve resulted in variation in outputs from calculations according to the two codes. The most noticeable change in ratio took place in the shift from low cyclic loading to high cyclic loading. This was particularly evident when comparing results from slugging, which were mostly stress ranges over cycles extending 10 000 000 cycles, to results from variations in temperature and pressure. Where the ratio for low cyclic loading were approximately 1.05, with respect to estimated fatigue life from load case. Average ratio with respect to design life for high cyclic loading were 0.75, when not including wave loads. The specifics surrounding the mentioned outputs were based on weld

class D for PD5500, but a similar trend was observed when conducting the same comparisons, but for weld class F2. However, in this instance, the relation was reversed, in which the increasing degree of conservative output were for the results based on PD5500. Thus, the S-N curve constants representing ASME B31.3 have an approximate level of conservatism that leaves it somewhere in the middle of the S-N curves representing weld class D and F2 from PD5500.

Secondly, regarding obtained outputs from fatigue caused by waves, there were significant differences between results from ASME B31.3 and PD5500 for the elbows, and the supports. The change in weld class resulted in a change of ratio from ASME B31.3 having, on average, 17.93 times more accumulated damage from waves, to 5 times more for weld class F2. This large occurring difference over a change in weld class heavily suggested that the applied method of Weibull distribution for determining damage from waves were in this case a lot more conservative than the method of minor sums. This was likely due to the methodology of PD5500 based the analysis on fatigue contribution from exact measured wave cycles for all recorded wave heights. A statistical distribution function for the wave field in question, represents the frequentist probability that the distribution of wave heights over number of wave cycles will correspond with the curve of a cumulative density function (Walpole et al, 2012). This mean that for a Weibull model applied for stress range, the shape and scale parameters from obtained wave data will determine the expected number of stress ranges over corresponding load cycles. However, since the approach was through expected values, and not the actual reported wave heights, a certain degree of deviance from recorded data was to be expected. For example, the probabilistic approach accounted for the 100-year wave height coming from all four directions, admittedly through low levels of probability, but were nevertheless accounted for. For minor sum approach of PD5500, however, the only incoming angle that were accounted for in regard to the 100-year wave was 65/245. To summarize the difference in applying the two methods for wave loads, was that PD5500 only accounted for fatigue due to stress ranges of recorded load cycles, with the precise number of cycles. While the method of ASME B31.3 left open possibility of all stress range within limit occurring with a corresponding expected number of load cycles. In addition, since a big portion of stress ranges caused by waves occurred during load cycles exceeding the criteria of high cycle loading, the difference in S-N curve would also influence the difference in results.

Chapter 7 Correlation study

The following chapter presents methodology of correlation study, in addition to the results that were performed for fatigue outputs from both codes. The meaning of correlation study were to assess how different loading impact the outcome comparatively between codes.

7.1 Methodology

With obtained results from fatigue analysis, the next step was to perform statistical analysis of the acquired data in order to gain a good comprehension of the differences between the two codes. The specific technique that was applied to evaluate these differences was a Pearson correlation matrix, which is a tool to determine impact of parameters on both outcome and other parameters. In this particular study, eight Pearson matrices was constructed, first portrayed the correlations between wave height, direction, number of cycles, displacements, stress range, and fatigue according to both codes. The second matrix determined the correlation between slugging loads and axial stress, bending stress, torsional stress, code stress, and fatigue according to both codes. The third Pearson matrix determined the correlation between displacements due to thermal fluctuations and axial stress, bending stress, torsional stress, code stress, and fatigue according to both codes. The fourth, and fifth matrix were utilized to determine correlation, for both codes, between each load case relevant to fatigue and total fatigue damage through design period. Matrix six provided the correlation between the same factors, however, with respect to weld class F2 according to PD5500. Lastly, matrix seven and eight presents result from correlation between sources of cyclic loading and design life, with respect to the additional factor of varying wall thickness.

Correlation parameters for relevant stress components, such as bending-, axial-, and torsional stress were in the cases of thermal expansion and slugging included in correlation study. This were partly to observe whether the fatigue outputs from codes resulted in significant difference in that regard; but also, to verify whether the outputs from stress analysis of an expansion load case, and occasional load case corresponds with fatigue output in an expected manner. In the case of slugging, number of load cycles were also included, due to it being a prevalent factor with a varying range. This were not the case with thermal expansion, where applied number of cycles varied between two numbers. Hence, cycles were excluded from correlation matrix of temperature variations.

The correlation factor which the Pearson matrix is based on is determined mathematically through equation 2.57, where variance and covariance of the parameters were determined through equation 2.59 and 2.58 respectively. Appliance of the formula for correlation factor will yield a result between -1 and 1, where a correlation factor of 1 or -1 will indicate full correlation, which mean that every change in one variable will be followed by a consistent change in corresponding variable (Walpole et al, 2012). An output of 0, however, means no relation between the variables, which can be interpreted as complete randomness between selected parameters. Negative sign of correlation factor indicates a decreasing trend, while positive sign shows an increasing trend of correlation between parameters (Kent state University, 2021). Table 2-4, from chapter 2.8.2, presents the categorization of correlation factors that were used during thesis along with paired coloring code, which is shown in figure 7-1, where output values are assigned definition based on how significantly the parameters affect other parameters.

By applying the Pearson correlation matrix for the mentioned scenarios, it was the intention to discover patterns and deviations regarding the application of different codes. Thus, gaining better comprehension of tendencies such as levels of conservativity integrated in the respective methods, and what level of conservatism applies for which specific load cases. Naturally, use of software is advantageous when handling large quantities of data, hence, correlation study was conducted through application of excel.

7.2 Effect of load cases

The following chapter includes results obtained from correlation study between various factors and the fatigue outputs from methodology according to both PD5500 and ASME B31.3. Figure 7-1 shows how correlation factor was categorized into coloring codes, based on both level of correlation and trend.

Colouring code
1
0.8
0.6
0.4
0.2
0
-0.2
-0.4
-0.6
-0.8
-1
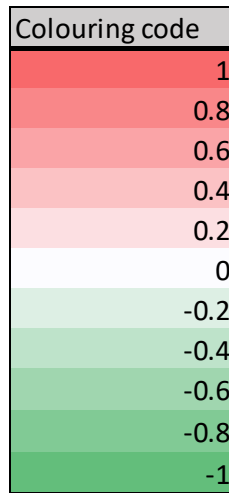
Figure 7-1: Coloring code correlation parameter

The main focus of study was that of load cases, and how factors associated with each respective load case affected the fatigue output from both codes. However, factors such as change in wall thickness, and weld class (for PD5500) were also taken into consideration.

7.3 Wave loads

Wave loads						
	Height	Direction	Cycles	Code stress range	Fatigue PD5500	Fatigue ASME
Height	1.000	-0.026	-0.513	0.782	-0.532	0.558
Direction	-0.026	1.000	0.017	-0.454	-0.075	-0.232
Cycles	-0.513	0.017	1.000	-0.312	-0.122	-0.143
Code stress range	0.782	-0.454	-0.312	1.000	-0.433	0.811
Fatigue PD5500	-0.532	-0.075	-0.122	-0.433	1.000	0.000
Fatigue ASME	0.558	-0.232	-0.143	0.811	0.000	1.000

Figure 7-2: Correlation wave displacements

Figure 7-2 shows the results from correlation study regarding different variables relevant to waves and fatigue. Specifically, wave heights for all directions with corresponding load cycles and stress ranges were evaluated against each other and fatigue output from both codes in regard to correlation parameter. Generally, there were a significant positive correlation between wave height and stress range, in addition to a significant negative correlation between wave height and cycles. This mean that as wave heights increase so does displacement range, furthermore, an increase in wave height also bring a reduction in number of wave cycles, which is a result that naturally makes sense and corresponds well with recorded wave data. When comparing the

factors of correlation related to calculated fatigue according to both codes, the table shows several noticeable differences. Firstly, regarding wave height, the magnitude of correlation factor is almost identical, however, PD5500 have a negative trend while ASME B31.3 have a positive trend. This indicates that the former experience a reduction in accumulated damage with increasing wave heights, and the latter oppositely experience an increase in damage with increasing wave height. This difference was likely due to the fundamental difference in executing the fatigue calculations with respect to wave loads. Thus, the damage caused by load cycles associated with every wave height and direction is determined individually and then added together, which means that 100-year waves, that by definition is estimated to only occur once every 100 year, have relatively few load cycles, thus lead to relatively low fatigue damage. The method of ASME B31.3, however, took the parameters derived from wave spectrum into consideration, and these parameters represented the tendencies of the wave field. Thus, an increase in wave height meant an increase in the maximum wave height representing field in calculation. A natural consequence of increase in wave height under mentioned considerations would be an increasing trend in fatigue. Secondly, the correlation between stress range and corresponding fatigue for the respective code is substantial, as with wave height, there is a difference in trend. Increased stress range resulted in a decrease in fatigue damage according to PD5500, and oppositely an increase for ASME B31.3, which could be explained similarly as the case with wave heights. However, more importantly was the difference in magnitude of correlation factor, where the matrix shows high correlation between stress range and fatigue according to ASME B31.3, while the correlation between stress range and PD5500 is merely moderate. Thirdly, ASME B31.3 shows a greater correlation between wave direction and estimated fatigue than that of PD5500, where the difference was -0.23 to -0.07. Lastly, both codes show a significantly low correlation between cycle number and fatigue, of -0.12 and -0.14, which are values of negligible difference. A possible reason for this might simply be the fact that a large number of the wave spectrum consists of waves of heights ranging from 1-3 meters and have low corresponding stress range. Furthermore, high stress ranges of the spectrum were generally paired with relatively low number of load cycles. Both situations mentioned will result in low accumulation of damage.

7.4 Slug loads

	Slugging							
	Loads	Axial Stress	Bending Stress	Torsion Stress	Cycles	Code Stress	Fatigue PD5500	Fatigue ASME B31.3
Loads	1.000	0.246	0.169	-0.189	-0.158	0.171	0.275	0.272
Axial Stress	0.246	1.000	0.390	0.544	-0.030	0.386	0.608	0.598
Bending Stress	0.169	0.390	1.000	-0.110	-0.148	1.000	0.662	0.672
Torsion Stress	-0.189	0.544	-0.110	1.000	0.110	-0.121	0.075	0.078
Cycles	-0.158	-0.030	-0.148	0.110	1.000	-0.150	0.036	0.028
Code Stress	0.171	0.386	1.000	-0.121	-0.150	1.000	0.662	0.671
Fatigue PD5500	0.275	0.608	0.662	0.075	0.036	0.662	1.000	0.000
Fatigue ASME	0.272	0.598	0.672	0.078	0.028	0.671	0.000	1.000

Figure 7-3: Correlation slug loads

Figure 7-3 displays the result from correlation study of various components related to slugging and fatigue. In this case, the included components were the loads exerted on elbows by slugging. The loads from all seven locations, and of all four categories were included for all elbow nodes in expansion loop. Furthermore, major stress components caused by the loading were also evaluated in study, in addition to the obtained code stress from these components. The last component that were considered in this correlation study were the number of load cycles paired with the different slug loads.

The following trends were gathered from this analysis. Axial stress had second highest correlation of the stress components, with a factor of 0.38 to code stress and 0.6 to fatigue according to both standards. However, bending stress were the stress component that represented the most significant influence on both code stress and fatigue due to slugging, which were the case for both ASME B31.3 and PD5500, where the factors of correlation between bending stress and fatigue for both standards were similar. The last stress component mentioned in the matrix, torsional stress, showed signs of negligible influence on accumulated damage. All these three mentioned parameters of correlation aligned reasonably with what could be expected for stresses caused by slug loads. This was because the slug causes the loop to leave its state of equilibrium which results in high cases of bending and axial stresses at bends. Furthermore, the number of load cycles showed a correlation that was equivalent to negligible with fatigue for both standards, which was a result that might seem counter intuitive. However, when comparing to data output from fatigue analysis, it was observed that most slug loads had a high load cycle number. This led to low accumulation of damage regarding stress ranges of low significance, even though these stress ranges were paired with high number of

96

load cycles. Additionally, significant stress ranges, which resulted in high instances of fatigue through analysis, were also generally paired with a large amount of load cycles, exceeding 10 000 000. Hence, for the scope of the analysis, it was mainly the magnitude of stress ranges that affected the fatigue with respect to slug loads.

7.5 Temperature

Temperature changes							
	Displacement range	Axial Stress	Bending Stress	Torsion Stress	Code Stress	Fatigue PD5500	Fatigue ASME B31.3
Displacement range	1.000	-0.071	-0.397	-0.452	-0.392	-0.617	-0.622
Axial Stress	-0.071	1.000	-0.246	0.134	-0.261	-0.225	-0.225
Bending Stress	-0.397	-0.246	1.000	0.139	1.000	0.946	0.942
Torsion Stress	-0.452	0.134	0.139	1.000	0.118	0.156	0.155
Code Stress	-0.392	-0.261	1.000	0.118	1.000	0.946	0.942
Fatigue PD5500	-0.617	-0.225	0.946	0.156	0.946	1.000	0.000
Fatigue ASME B31.3	-0.622	-0.225	0.942	0.155	0.942	0.000	1.000

Figure 7-4: Correlation changes in temperature

Figure 7-4 representing maximum temperature variation, shows that, similarly to the case of slug loading, there was little difference in correlation factors regarding outputs from the two standards. The factors included in this matrix were absolute values of displacement ranges caused by change in temperature, where the applied temperature range were both partial fluctuations and full range from maximum to minimum design temperature. As with slug loads, stress components representing axial, bending, and torsion stress were included in analysis, in addition to code stress, and fatigue output according to both codes. The results from figure 7-4 shows a high correlation between increase in displacement range due to thermal expansion and decreasing fatigue, which indicates that nodes under less restraint had lower instances of code stress and fatigue. Correspondingly, axial stress component was shown to have a small negative correlation with code stress. As with slugging the largest correlation between stress components and fatigue were due to bending.

7.6 Combined loading

Fatigue PD5500						
	Wave di	Slug di	Thermal di	Pressure di	Fatigue damage	Years
Wave di	1	0	0	0	-0.395870669	0.017890282
Slug di	0	1	0	0	0.995327039	-0.677258004
Thermal di	0	0	1	0	-0.387120872	-0.002739505
Pressure	0	0	0	1	-0.340017798	0.239025362
Fatigue damage	-0.395870669	0.99532704	-0.38712087	-0.340017798	1	-0.708279747
Years	0.017890282	-0.677258	-0.00273951	0.239025362	-0.708279747	1

Figure 7-5: Correlation combined loading for PD5500, weld class D

Fatigue ASME B31.3						
	Wave di	Slug di	Thermal di	Pressure di	Fatigue damage	Years
Wave di	1	0	0	0	-0.201733495	-0.385697541
Slug di	0	1	0	0	0.959721252	-0.47301635
Thermal di	0	0	1	0	-0.19290498	-0.390881685
Pressure	0	0	0	1	-0.433542112	0.753422539
Fatigue damage	-0.201733495	0.959721252	-0.19290498	-0.433542112	1	-0.64739143
Years	-0.385697541	-0.47301635	-0.39088168	0.753422539	-0.64739143	1

Figure 7-6: Correlation combined loading for ASME B31.3

Figure 7-5 and 7-6 present correlation parameters obtained from fatigue analysis according to PD5500 and ASME B31.3 respectively. Both tables show the correlation between fatigue caused by all four sources of stress ranges, and the total accumulated damage on each node, with corresponding design life.

Since fatigue due to pressure variations were the same over pipeline of the same geometry, the slot in the correlation matrix regarding fatigue and pressure were performed differently from the other load cases. While the other load cases represented fatigue damage from each respective load case on different node of the pipeline, correlation analysis regarding pressure change were conducted in the following way. Several analyses in Caesar were performed over different cases of pressure variations that deviated slightly from the 10 % pressure change. The reason for doing this was simply because variation in parameter was required to calculate correlation. For each range fatigue was calculated for fluctuations based on one load cycle per day. Hence, data relevant for pressure fluctuations was generated and applied in correlation study, which is presented in figures for correlation with regard to fatigue and all sources of loading. Pressure change was not considered separately with a correlation matrix presenting different components related to pressure change input and fatigue output. The reason for this

was the direct relation between internal pressure and resulting stress components. Hence, multiple pressure changes over the same cross section were expected to yield a perfectly linear result regarding correlation parameter.

The element of pressure variations was distributed randomly amongst different nodes, in which random fluctuations within the prescribed range were assigned. Thus, it was also random whether the higher or lower instances of fatigue due to pressure variation were paired with nodes exposed to high cases of accumulated fatigue from other sources. Hence, only the magnitude of correlation was considered, and not whether trend was positive or negative. This magnitude of correlation factor was high (0.75) for design life according to ASME B31.3, and low (0.24) for design life according to PD5500. Furthermore, fatigue from thermal expansion had similar pattern regarding correlation factor. To be specific, ASME B31.3 showed a moderate (-0.39) relation between thermal expansion and design life, whilst thermal expansion had negligible effect on outcome according to PD5500. The fact that fatigue outputs from both sources of loading had results that did not deviate that much from one another makes the outputs curious. One possible explanation, however, could be that the codes experienced different outcome regarding slugging and waves on design life. Hence, this factor would be participating in reducing the relative effect of pressure and temperature.

When comparing parameter output of damage caused by wave displacements between the two figures, the method of ASME B31.3 experienced a much greater impact from waves in regard to design life. This was an observation that were already made through evaluation of fatigue outputs. The correlation parameter from PD5500 indicated that the relation between design life and wave displacements were negligible. This low correlation could possibly be explained by the fact that nodes applied in study had varying exposure to the different sources of loading. For instance, node 470 experienced the largest instances of slug related fatigue but relatively little damage caused by waves. Comparatively, node 340 and 410 both experienced more wave related fatigue, and lower instances of slugging. However, damage from slugging were generally more evenly distributed amongst nodes, in addition to contributing to higher instances of fatigue. When combining this observation with the fact that slug loads had overall the greatest impact on design life of structure, it is more understandable that wave loads showed such low correlation with design life of weld.

Both methods gave a high correlation between slug loading and the total damage caused by cyclic loading, with 0.99 and 0.95 for PD5500 and ASME B31.3 respectively. The differences between these two values were basically negligible, especially considering the magnitude of correlation in both cases approaches that of perfect linear relation. However, when considering the difference in correlation, between the two codes, regarding slug induced fatigue and design life, the difference increased, where the correlation was -0.63 and -0.45 for PD5500 and ASME B31.3 respectively. This was not a difference of particular significance (Walpole et al, 2012), and likely due to the code's differences in conversion from accumulated damage to design life. PD5500 factor in wall thickness, due to the reason that fatigue strength of a component could decrease with increasing thickness (BSi, 2003). A reasonable assumption, based on the aforementioned point, would be that the method of PD5500 would be more conservative regarding design life output from slugging. However, when comparing outputs from fatigue analysis, it was found that the method of ASME B31.3 resulted in a shorter design life. It should also be noted that since fatigue outputs based on ASME B31.3 were generally more affected by wave displacements, this would impact the correlation between load case and fatigue output.

7.6.1 Effect of weld class

Fatigue PD5500 (weld class F2)					
	Wave di	Slug di	Thermal di	Pressure di	Fatigue damage	Years
Wave di	1	0	0	0	-0.277914175	0.037205464
Slug di	0	1	0	0	0.999940719	-0.373499787
Thermal di	0	0	1	0	-0.314870421	0.136887974
Pressure	0	0	0	1	-0.268564454	-0.192366945
Fatigue damage	-0.277914175	0.99994072	-0.31487042	-0.268564454	1	-0.3735251
Years	0.037205464	-0.37349979	0.13688797	-0.192366945	-0.3735251	1

Figure 7-7: Correlation combined loading for PD5500, weld class F2

As were discovered in fatigue analysis of supports in expansion loop, appliance of weld class F2 in accordance with PD5500 gave a more conservative output relative to that of ASME B31.3 for the same nodes. However, when comparing obtained results from correlation study regarding F2 weld class with that of class D, there were only slight differences. The most prevalent were the reduction of correlation between damage from slugging and design life from -0.677 to -0.37. This was likely due to low instances of stresses at supports relative to those estimated at elbows.

7.6.2 Effect of wall thickness

Figure 7-8 and 7-9 displays the correlation between change in wall thickness and fatigue for different sources, in addition to design life. The results from this study display tendencies coherent with an initial assumption, which states that a piping system subjected to both slugging, and expansion loads, such as wave displacements and thermal expansion, must compromise between rigidity and flexibility. The occurrence that support this assumption were the close to perfect linear relation shown between increasing wall thickness and increasing fatigue from both waves and effects of temperature. There was also a strong correlation between increasing wall thickness and a reduction in fatigue from slugging. Naturally, since a limited amount of simulations were done with different wall thicknesses, the resulting correlation were higher than if a wide range of values had been applied.

An interesting result from correlation study over wall thickness was that increasing wall thickness was connected by a decreasing trend of design life, according to both codes. Where PD5500 had a correlation parameter of -0.194, and ASME B31.3 showed the largest trend of -0.838. There were mainly two reasons for what causes the mentioned correlation factors. Firstly, as previously established, increased wall thickness led to increase in fatigue due to wave and temperature changes, and a decrease in fatigue from slugging. Hence, once the wall thickness went beyond a threshold, where stress ranges caused by expansion exceeded stress ranges from slugging, the structures design life would start to decrease. Secondly, the large difference in correlation factor for the two codes could be explained by the fact that results from ASME B31.3 generally were more effected by both wave loads and changes in temperature than PD5500. Thus, amplifying the described effect of increasing stress ranges due to expansion as a result of added structural stiffness.

PD5500					
	Wall thickness	Slug fatigue	Wave fatigue	Temperature fatigue	Design life
Wall thickness	1	-0.69669507	0.998084473	0.997588382	-0.193618411
Slug fatigue	-0.696695071	1	0	0	-0.556127576
Wave fatigue	0.998084473	0	1	0	-0.250284885
Temperature fatigue	0.997588382	0	0	1	-0.243741977
Design life	-0.193618411	-0.55612758	-0.250284885	-0.243741977	1

Figure 7-8: Correlation combined loading for PD5500, weld class D, with respect to wall thickness

ASME B31.3					
	Wall thickness	Slug fatigue	Wave fatigue	Temperature fatigue	Design life
Wall thickness	1	-0.690330595	0.998088219	0.997588382	-0.83813339
Slug fatigue	-0.690330595	1	0	0	0.231590762
Wave fatigue	0.998088219	0	1	0	-0.86830489
Temperature fatigue	0.997588382	0	0	1	-0.87323386
Design life	-0.838133394	0.231590762	-0.868304891	-0.87323386	1

Figure 7-9: Correlation combined loading for ASME B31.3, with respect to wall thickness

Chapter 8 Conclusion

8.1 Summary and conclusion

In this study, comparisons between the piping standards of PD5500 and ASME B31.3 were performed with respect to fatigue analysis. The execution of this study relied on an example case, where the methodologies from each standard were applied to estimations of design life. The example case of this thesis was specifically a bridge, constructed as an expansion loop between two platforms mounted at jack structures. This made it a highly relevant case study due to its exposure to different sources of loading relevant for fatigue, such as wave loads and slugging.

The applied method of processing loads was through the nodal software package Caesar 2. In this software, stress ranges from selected load cases were obtained and further applied for fatigue analysis. Additional statistical evaluation of fatigue outputs was also performed, through the utilization of a Pearson correlation matrix in the software excel. The work involved with this thesis resulted in the following observations regarding differences between codes.

Firstly, design life estimated solely from the effects of wave loads resulted in a ASME B31.3 to PD5500 ratio of 0.11. This result was much more conservative than results obtained from other load cases, such as variations in temperature and pressure. A suggested reason of which was that the method of ASME B31.3 relied on a probabilistic approach, based on expected values of both wave heights and number of cycles. As apposed to the methodology of PD5500, which applied actual recordings equivalent to design period. This was further emphasized when S-N curves for more conservative weld class were applied for different nodes of expansion loop. The results of which were an overall lower estimated design life than by ASME B31.3, which was mainly due to an increase in accumulated damage caused by slugging. However, damage caused by waves was still estimated to be lower by PD5500 than of ASME B31.3, by a ratio of 0.36.

Secondly, changes in wall thickness and diameter affected the codes differently. This was largely due to the fact that variation in wall thickness and diameter would impact both the influence of expansion load cases, and occasional loads such as slugging. In general, increased rigidity would cause higher stresses due to expansion, and correspondingly, less stresses due to

103

slugging. Since ASME B31.3 yielded in particular more conservative results regarding wave loads, thus change in wall thickness had more significant effect on said code, than to PD5500.

Lastly, an effect that showed large influence on the outcome of fatigue analysis, both from slugging and wave loads, was the constants representing the applied S-N curve. The difference in these coefficients resulted in a noticeable difference regarding design life, especially in the case of high cycle loading, which accounted for most of the slug loads. Coefficients of ASME B31.3 resulted in average design life corresponding to 85 % of PD5500, when solely considering the effect of stress ranges due to slugging. However, when applied with a more conservative weld class, such as F2, the ratio between the two codes regarding fatigue output changed in favor of a more conservative output for PD5500. It should also be noted that there were inconsistencies in ratios of fatigue outputs when estimations were based on high cyclic loading opposed to low cyclic loading. This might suggest that the codes have included different margins of safety for the transition between these states of load cycling. Specifically, the ratio between codes, with respect to PD5500, decreased from 1.05 to 0.85, for weld class D, and increased from 3.89 to 5.27 for weld class F2, when transitioning from low cyclic loading to high cyclic loading.

In conclusion, the analysis comparing codes generally resulted in more conservative outputs from ASME B31.3. This was particularly the case for wave loads, in addition to stress ranges with number of load cycles exceeding 10 000 000 cycles. The reason for the latter result was difference in S-N curves, where the curve constants of ASME B31.3 were more conservative than weld class D of PD5500. This was particularly the case for high cyclic loading.

8.2 Recommendation for future work

This thesis covered extensively the effect of load cases such as slugging and wave displacements, along with effects of change in pressure and temperature. Other than the impact of load cases included in this thesis, there are several additional factors that would be beneficial to include in further analysis.

Firstly, effects of corrosion. The example case of this thesis was a bridge located in air, thus making effects of corrosion negligeable. However, the standards take different approaches to incorporating effects of corrosion into the fatigue calculations. PD5500 does not allow for effects of corrosion, hence the standard demands that in order to use the presented steps, measures need to be taken to ensure that the structure is protected against corrosive effects. These measures include cathodic protection of pipeline in addition to routinely inspection of crack propagation. Unlike PD5500, ASME B31.3 actually factors in effects of corrosion through application of the environment factor, which specifies three different situations, in air, in seawater with cathodic protection and in seawater with free corrosion, where the environment factor is 1, 2.51 and 3 respectively. When applied with equation 2.38, the environment factor has large influence on number of load cycles until failure. Hence, a comparison study between the codes, where the case is a pipeline in sea water with cathodic protection would be one way to further evaluate the difference between the standards.

Secondly, effect of material. The evaluated bridge consisted of two different pipelines that had different materials, where one was duplex steel and the other was super duplex steel. Since the focus of this thesis was on the expansion loop, which solely consisted of the latter material type, choice of material and corresponding impact on fatigue was not explored. In addition, the standards have different approaches of incorporating material in calculations, where ASME B31.3 divide into two categories, namely ferritic steels and austenitic stainless steels, and aluminum, where the standard offers different SN-curve constants for the two categories. Furthermore, the equation for allowable cycles also includes an effect of temperature on material. In PD550, however, the presented SN-curves are also valid for the same categories of materials as with ASME B31.3, but there are no alterations to constants of the curves. The influence of material according to PD5500 is summed up as an adjustment of stress range with respect to measured stress and Youngs modulus of applied material under relevant conditions.

Hence, an analysis where both aluminum and steels of different properties are applied to fatigue calculations and further correlation studies could prove to be interesting.

Thirdly, further analysis regarding effect of pressure. Since effect of pressure fluctuations results in stress ranges that were homogenous, in accordance with geometry and material of pipe, numerous simulations were required to acquire large amounts of data. A result of which was that the analysis regarding pressure variation was somewhat limited throughout this thesis. Hence, a more thorough analysis specifically directed towards change in pressure could result in further insight.

Lastly, additional load cases. The work associated with this thesis included longitudinal displacements caused by waves. However, rotational displacements from waves was not considered. Hence, this could be an interesting addition to further comparison of the codes.

Bibliography

Artusi, R., Verderio, P., & Marubini, E. (2002). Bravais-Pearson and Spearman correlation coefficients: meaning, test of hypothesis and confidence interval. *The International Journal of Biological Markers*, 148-151.

Arveng Training and Engineering. (2021, June 1). *BASICS OF PIPING STRESS ANALYSIS*. Retrieved from arvengtraining.com/: https://arvengtraining.com/en/basics-of-piping-stress-analysis/

ASME . (2021, June 1). *Engineering History*. Retrieved from asme.org: https://www.asme.org/about-asme/engineering-history

ASME. (2018). *ASME Code for Pressure Piping, B31.3.* New York: The American society of Mechanical Engineers.

Barker, G. (2018). *The Engineer's Guide to Plant Layout and Piping Design for the Oil and Gas Industries.* Houston: Gulf Professional Publishing.

Bell, K. (2015). *Konstruksjonsmekanikk del 1 likevektslære.* Bergen: Fagbokforlaget Vigmostad & Bjørke AS.

Bell, K. (2015). *Konstruksjonsmekanikk Del 2 fasthetslære.* Bergen: Fagbokforlaget Vigmostad & Bjørke AS.

Berge, S., & Ås, S. K. (2017). *Fatigue and Fracture Design of Marine Structures.* Trondheim: NTNU, Faculty of Engineering Science and Technology.

Bjork, T., Samuelsson, J., & Marquis, G. (2008). *THE NEED FOR A WELD QUALITY SYSTEM FOR FATIGUE LOADED STRUCTURES.* Lappeenranta: Lappeenranta University of Technology.

Boresi, A. P., & Schmidt, R. J. (2003). *Advanced mechanics of materials.* Hoboken: John Wiley & sons, INC.

Braestrup, M. W., Andersen, J. B., Andersen, L. W., Bryndum, M., Christensen, C. J., & Nielsen, N.-J. R. (2005). *Design and Installation of Marine Pipelines.* Oxford: Blackwell Science Ltd.

BSi. (2003). *PD 5500.* London: British Standards institution .

BSI Group. (2021, June 1). *Our History*. Retrieved from bsigroup.com: https://www.bsigroup.com/en-GB/about-bsi/our-history/

Callister, W. D., & Rethwisch, D. G. (2011). *Materials Science and Engineering.* Hoboken: John Wiley & sons, Inc.

Chopra, O. K. (2000). Environmental Effects on Fatigue Crack Initiation in Piping and Pressure Vessel steels. *International Conference on Fatigue of Reactor Components.* Napa: Argonne National Laboratory.

Cook, R. D., Malkus, D. S., & Plesha, M. E. (1989). *Concepts and application of finite element analysis.* Madison: John Wiley & sons.

Dong, P. (2001). A structural stress definition and numerical implementation for. *International Journal of Fatigue*, 865–876.

Dong, P., & Hong, J. K. (2004). *THE MASTER S-N CURVE APPROACH TO FATIGUE OF PIPING AND VESSEL WELDS.* Battelle: Center for Welded Structures Research.

DST Group Limited. (2021, March 2). *Pipework and Expansion Guide: Flexibility of Pipe with Loop.* Retrieved from dstgroup.co.uk: https://www.dstgroup.co.uk/product/pipework-and-expansion-guide-flexibility-of-pipe-with-loop/#0

El-Reedy, M. A. (2015). *Marine Structural Design Calculations.* Oxford: Butterworth-Heinemann.

Engineering toolbox. (2021, March 10). *COefficients of friction.* Retrieved from engineeringtoolbox.com: https://www.engineeringtoolbox.com/friction-coefficients-d_778.html

Engineers Edge. (2021, May 21). *Pipe Expansion Thermal Loop Equations and Calculator.* Retrieved from engineersedge.com: https://www.engineersedge.com/calculators/pipe_expansion_thermal_loop_15035.htm

Gudmestad, O. (2015). *Marine Technology and Operations.* Southampton: WIT Press.

Gundersen, P. D., Andersen, T., & Haakonsen, R. (2012). METHODOLOGY FOR DETERMINING REMNANT FATIGUE LIFE OF FLEXIBLE. *ASME 2012 31st International Conference on Ocean, Offshore and Arctic Engineering.* Rio de Janeiro: ASME.

Hexagon. (2017). *CAESAR II Quick Reference <guide.* Madison: Intergraph Corporation.

Hexagon. (2017). *CAESAR II Application guide.* Madison: Intergraph corporation.

Hexagon AB. (2021, March 1). *Caesar 2 User Guide.* Retrieved from docs.hexagonppm.com: https://docs.hexagonppm.com/r/en-US/CAESAR-II-Users-Guide/Version-12/336074

Hou, D. Q., Tijsseling, A. S., & Bozkus, Z. (2014). Dynamic Force on an Elbow Caused by a Traveling Liquid Slug. *Journal of Pressure Vessel Technology*.

Hughes, T. J. (2000). *The Finite Element Method: Linear Static and Dynamic Finite Element Analysis.* Mineola: Dover publications, INC.

Hwang, S.-Y., Kim, M.-S., & Lee, J.-H. (2020). Thermal Stress Analysis of Process Piping System Installed on LNG Vessel Subject to Hull Design Loads. *Journal of Marine Science and Engineering*.

Irgens, F. (2008). Theory of Elasticity . In F. Irgens, *Continuum Mechanics* (pp. 199-301). Berlin: Springer-Verlag.

Journee, J., & Massie, W. (2001). *Offshore Hydromechanics.* Delft: Delft University of Technology.

Kansao, R., Blanco, A., Kenyery, F., Casanova, E., & Rivero, M. (2008). FATIGUE LIFE PREDICTION DUE TO SLUG FLOW IN EXTRA LONG SUBMARINE GAS PIPELINES. *International Conference on Offshore Mechanics and Arctic Engineering.* Estoril: ASME.

Kent state University. (2021, May 23). *University Library: Pearson correlation* . Retrieved from libguides.library.kent.edu: https://libguides.library.kent.edu/SPSS/PearsonCorr

Keprate, A., Chandima Ratnayake, R., & Sankararaman, S. (2016). Minimizing Hydrocarbon Release from Offshore Piping by Performing Probabilistic Fatigue Life Assessment. *Process Safety and Environment Protection*.

Lee, Y.-L., & Tjhung, T. (2012). *Metal Fatigue Analysis Handbook.* Oxford: Butterworth-Heinemann.

Løvås, G. G. (2013). *Statistikk for Universiteter og høgskoler.* Oslo: Universitetsforlaget.

MechniCalc. (2021). *Mechanical properties of materials*. Retrieved from mechanicalc.com: https://mechanicalc.com/reference/mechanical-properties-of-materials#stress-strain-approx

Mokhatab, S., & Towler, B. F. (2007). *Severe Slugging in Flexible Risers: Review of Experimental Investigations and OLGA Predictions.* London: Taylor & Francis.

Ortega, A., & Rivera, A. L. (2013). FLEXIBLE RISER RESPONSE INDUCED BY COMBINED SLUG FLOW AND WAVE LOADS. *International Conference on Ocean, Offshore and Arctic Engineering.* Nantes: ASME.

Paffumi, E., Nilsson, K. F., & Taylor, N. (2008). Simulation of thermal fatigue damage in a 316L model pipe component. *International Journal of Pressure Vessels and Piping*, 798-813.

Rezkallah, M. (2021, March 5). *Primary vs. Secondary Loads*. Retrieved from littlepeng.com: https://www.littlepeng.com/single-post/2020/04/07/151-primary-vs-secondary-loads

Roylance, D. (2001). *STRESS-STRAIN CURVES*. Cambridge: Massachusetts Institute of Technology: Department of Materials Science and Engineering.

Schreurs, P. (2013). *Applied Elasticity in Engineering*. Eindhoven: Eindhoven University of Technology, Departement of Mechanical Engineering.

Seipp, T. (2021, March 3). *Basics of Design By Analysis in ASME Section VIII, Division 2*. Retrieved from becht.com: https://becht.com/becht-blog/entry/basics-of-design-by-analysis-in-asme-section-viii-division-2/

Spirax Sarco. (2021, March 2). *PIPE EXPANSION AND SUPPORT*. Retrieved from spiraxsarco.com: https://www.spiraxsarco.com/learn-about-steam/steam-distribution/pipe-expansion-and-support

Stewart, M. (2016). *Surface Production Operations Volume 3: Facility Piping and Pipeline System* . Houston: Gulf Professional Publishing.

Sutton, I. (2017). *Plant Design and Operations*. Houston: Gulf professional publishing .

Tailtel, Y., Vierkandt, S., Shoham, O., & Brill, J. P. (1990). SEVERE SLUGGING IN A RISER SYSTEM: EXPERIMENTS AND MODELING. *Int. J. Multiphase Flow Vol. 16, No. I*, 57-68.

The Process Piping . (2, March 2021). *Piping Flexibility – Thermal Expansion in Piping*. Retrieved from theprocesspiping.com: https://www.theprocesspiping.com/piping-flexibility-thermal-expansion-in-piping/

Walpole, R. E., Myers, R. H., Myers, S. L., & Ye, K. (2012). *Probability & Statistics for Engineers & Scientists* . Boston: Pearson.

Ziegler, L., & Muskulus, M. (2016). *Comparing a fracture mechanics model to the SN-curve approach for jacket-supported*. New York: ASME .

Zienkiewicz, O., Taylor, R., & Zhu, J. (2005). *The Finite Element Method: Its Basis and Fundamentals*. Oxford: Elsevier Butterworth Heinemann.

Appendix

Table 0-1: Estimated displacement ranges with corresponding stress ranges and load cycles, for all elbow nodes. Method relevant for PD5500.

Wave height and directi on	Displacem ent range (mm)	Cycles No.	Node 250	Node 300	Node 340	Node 410	Node 430	Node 470
28 m at 65º and 245º	572	1	47.317 25	78.060 23	108.47 23	164.18 73	163.25 24	24.710 08
28 m at 20º and 200º	435.32743 36	0	36.011 36	59.408 67	82.554 11	124.95 67	124.24 52	18.805 9
28 m at 335º and 155º	62.768141 59	0	5.1923 36	8.5659 02	11.903 15	18.017 02	17.914 42	2.7115 48
28 m at 110º and 290º	426.21592 92	0	35.257 64	58.165 24	80.826 23	122.34 13	121.64 47	18.412 29
27 m at 65º and 245º	537.70710 44	0	44.480 46	73.380 32	101.96 91	154.34 39	153.46 5	23.228 64
27 m at 20º and 200º	409.22841 57	0	33.852 39	55.846 97	77.604 78	117.46 52	116.79 64	17.678 44
27 m at 335º	59.005027 38	1	4.8810 42	8.0523 53	11.189 53	16.936 85	16.840 41	2.5489 84

and 155º							
27 m at 110º and 290º	400.66316 98	1	33.143 85	54.678 08	75.980 49	115.00 67	114.35 18	17.308 42
26 m at 65º and 245º	504.29198 66	1	41.716 28	68.820 19	95.632 33	144.75 24	143.92 81	21.785 13
26 m at 20º and 200º	383.79744 11	1	31.748 67	52.376 43	72.782 13	110.16 55	109.53 82	16.579 83
26 m at 335º and 155º	55.338235 69	1	4.5777 16	7.5519 5	10.494 17	15.884 33	15.793 88	2.3905 8
26 m at 110º and 290º	375.76447 14	1	31.084 17	51.280 18	71.258 78	107.85 97	107.24 55	16.232 81
25 m at 65º and 245º	471.76464 43	1	39.025 54	64.381 22	89.463 95	135.41 57	134.64 46	20.379 97
25 m at 20º and 200º	359.04211 87	2	29.700 85	48.998 1	68.087 61	103.05 97	102.47 29	15.510 42
25 m at 335º and 155º	51.768863 63	2	4.2824 48	7.0648 42	9.8172 83	14.859 77	14.775 16	2.2363 86
25 m at 110º	351.52728 37	2	29.079 21	47.972 56	66.662 52	100.90 27	100.32 81	15.185 78

and 290º							
24 m at 65º and 245º	440.13558 87	2	36.409 1	60.064 84	83.465 91	126.33 69	125.61 75	19.013 61
24 m at 20º and 200º	334.97044 81	3	27.709 58	45.713 06	63.522 73	96.150 17	95.602 67	14.470 53
24 m at 335º and 155º	48.298064 61	3	3.9953 35	6.5911 86	9.1590 92	13.863 51	13.784 57	2.0864 49
24 m at 110º and 290º	327.95943 87	4	27.129 62	44.756 28	62.193 19	94.137 73	93.601 68	14.167 66
23 m at 65º and 245º	409.41589 24	4	33.867 9	55.872 55	77.640 33	117.51 91	116.84 99	17.686 53
23 m at 20º and 200º	311.59085 61	5	25.775 57	42.522 47	59.089 1	89.439 28	88.929 99	13.460 55
23 m at 335º and 155º	44.927053 68	6	3.7164 77	6.1311 47	8.5198 24	12.895 9	12.822 46	1.9408 23
23 m at 110º and 290º	305.06918 71	7	25.236 08	41.632 47	57.852 35	87.567 29	87.068 66	13.178 82
22 m at 65º and 245º	379.61724 49	7	31.402 88	51.805 96	71.989 41	108.96 56	108.34 51	16.399 25

22 m at 20º and 200º	288.91223 95	10	23.899 54	39.427 55	54.788 4	82.929 59	82.457 37	12.480 85
22 m at 335º and 155º	41.657113 6	11	3.4459 79	5.6849 02	7.8997 23	11.957 29	11.889 2	1.7995 64
22 m at 110º and 290º	282.86523 91	13	23.399 31	38.602 32	53.641 67	81.193 85	80.731 51	12.219 62
21 m at 65º and 245º	350.75201 65	14	29.015 07	47.866 76	66.515 5	100.68 01	100.10 68	15.152 29
21 m at 20º and 200º	266.94401 26	19	22.082 27	36.429 57	50.622 41	76.623 81	76.187 5	11.531 83
21 m at 335º and 155º	38.489601 82	20	3.1839 55	5.2526 35	7.2990 46	11.048 08	10.985 17	1.6627 29
21 m at 110º and 290º	261.35681 23	23	21.620 08	35.667 09	49.562 88	75.020 06	74.592 87	11.290 47
20 m at 65º and 245º	322.83333 17	26	26.705 57	44.056 72	61.221 09	92.666 33	92.138 66	13.946 22
20 m at 20º and 200º	245.69616 39	34	20.324 59	33.529 89	46.593 04	70.524 81	70.123 23	10.613 94

20 m at 335º and 155º	35.425958 52	37	2.9305 23	4.8345 43	6.7180 66	10.168 69	10.110 79	1.5303 81
20 m at 110º and 290º	240.55368 61	43	19.899 2	32.828 11	45.617 84	69.048 71	68.655 53	10.391 78
19 m at 65º and 245º	295.87515 41	47	24.475 52	40.377 77	56.108 82	84.928 23	84.444 63	12.781 64
19 m at 20º and 200º	225.17932 08	64	18.627 39	30.729 98	42.702 29	64.635 64	64.267 59	9.7276 19
19 m at 335º and 155º	32.467716 03	69	2.6858 1	4.4308 35	6.1570 74	9.3195 58	9.2664 9	1.4025 87
19 m at 110º and 290º	220.46626 53	81	18.237 51	30.086 8	41.808 52	63.282 8	62.922 46	9.5240 18
18 m at 65º and 245º	269.89238 69	88	22.326 17	36.831 93	51.181 53	77.470 12	77.028 98	11.659 2
18 m at 20º and 200º	205.40482 54	121	16.991 6	28.031 38	38.952 32	58.959 56	58.623 83	8.8733 72
18 m at 335º and 155º	29.616509 71	129	2.4499 51	4.0417 34	5.6163 81	8.5011 46	8.4527 38	1.2794 16

18 m at 110º and 290º	201.1056547	153	16.63596	27.44468	38.13704	57.72552	57.39682	8.68765
17 m at 65º and 245º	244.9009906	166	20.25882	33.42138	46.44225	70.29657	69.89628	10.57958
17 m at 20º and 200º	186.3848247	228	15.41821	25.43574	35.34543	53.50004	53.1954	8.051719
17 m at 335º and 155º	26.87409101	245	2.223091	3.667479	5.096317	7.71396	7.670034	1.160946
17 m at 110º and 290º	182.483747	291	15.09551	24.90336	34.60564	52.38027	52.08201	7.883194
16 m at 65º and 245º	220.9181237	313	18.27489	30.14846	41.89421	63.41251	63.05142	9.543538
16 m at 20º and 200º	168.1323773	434	13.90833	22.94485	31.88409	48.26085	47.98604	7.263223
16 m at 335º and 155º	24.24234278	465	2.005387	3.308327	4.597241	6.958541	6.918917	1.047255
16 m at 110º and 290º	164.6133276	559	13.61722	22.46461	31.21675	47.25074	46.98168	7.111203

15 m at 65º and 245º	197.9623114	596	16.37593	27.01571	37.54094	56.82325	56.49969	8.55186
15 m at 20º and 200º	150.6615821	833	12.4631	20.56063	28.57098	43.24602	42.99976	6.508495
15 m at 335º and 155º	21.72329788	893	1.797005	2.964555	4.119537	6.235472	6.199966	0.938434
15 m at 110º and 290º	147.5082002	1083	12.20224	20.13029	27.97299	42.34087	42.09977	6.372271
14 m at 65º and 245º	176.0536511	1144	14.56359	24.02585	33.38625	50.53457	50.24682	7.605418
14 m at 20º and 200º	133.9877345	1612	11.0838	18.28516	25.40901	38.45994	38.24094	5.788194
14 m at 335º and 155º	19.31916171	1728	1.598129	2.636465	3.663624	5.545387	5.51381	0.834577
14 m at 110º and 290º	131.18334	2117	10.85181	17.90245	24.87719	37.65497	37.44055	5.667046
13 m at 65º and 245º	155.2140655	2214	12.83969	21.1819	29.4343	44.55276	44.29907	6.70516

13 m at 20º and 200º	118.1275189	3151	9.771801	16.12074	22.40133	33.90741	33.71434	5.103042
13 m at 335º and 155º	17.03233993	3378	1.408957	2.324385	3.229959	4.888976	4.861137	0.735787
13 m at 110º and 290º	115.6550824	4180	9.567274	15.78333	21.93246	33.19772	33.00869	4.996234
12 m at 65º and 245º	135.4676178	4327	11.20622	18.48712	25.68965	38.88473	38.66331	5.852124
12 m at 20º and 200º	103.0992489	6222	8.528625	14.06985	19.55141	29.59369	29.42517	4.453829
12 m at 335º and 155º	14.8654731	6670	1.229709	2.028675	2.819041	4.266997	4.242699	0.64218
12 m at 110º and 290º	100.9413577	8347	8.350119	13.77536	19.1422	28.97428	28.8093	4.360609
11 m at 65º and 245º	116.8409126	8545	9.665369	15.94516	22.15734	33.5381	33.34713	5.047461
11 m at 20º and 200º	88.92317239	12424	7.355945	12.13525	16.86311	25.52458	25.37923	3.841431

11 m at 335° and 155°	12.82148067	13319	1.060625	1.749734	2.431425	3.680288	3.659331	0.553881
11 m at 110° and 290°	87.06198971	16880	7.201983	11.88126	16.51016	24.99034	24.84804	3.761029
10 m at 65° and 245°	99.36361319	17063	8.219604	13.56005	18.843	28.52141	28.359	4.292452
10 m at 20° and 200°	75.62186491	25124	6.255628	10.32004	14.34069	21.70656	21.58295	3.266822
10 m at 335° and 155°	10.90361773	26934	0.901974	1.488005	2.067727	3.129783	3.111961	0.47103
10 m at 110° and 290°	74.03908169	34506	6.124696	10.10403	14.04054	21.25223	21.13122	3.198446
9 m at 65° and 245°	83.06912608	34630	6.871684	11.33636	15.75297	23.84423	23.70845	3.588539
9 m at 20° and 200°	63.22075082	51541	5.229777	8.627669	11.98898	18.14693	18.0436	2.731101
9 m at 335° and 155°	9.11555019	55255	0.754061	1.243989	1.728644	2.616534	2.601635	0.393787

9 m at 110º and 290º	61.897525 81	70787	5.1203 16	8.4470 9	11.738 05	17.767 11	17.665 94	2.6739 38
8 m at 65º and 245º	67.995528 45	72256	5.6247 58	9.2792 78	12.894 46	19.517 49	19.406 35	2.9373 68
8 m at 20º and 200º	51.748809 26	107543	4.2807 89	7.0621 05	9.8134 8	14.854 02	14.769 43	2.2355 19
8 m at 335º and 155º	7.4614562 19	115292	0.6172 3	1.0182 57	1.4149 67	2.1417 42	2.1295 46	0.3223 31
8 m at 110º and 290º	50.665694 65	147701	4.1911 92	6.9142 94	9.6080 81	14.543 12	14.460 31	2.1887 29
7 m at 65º and 245º	54.186867 25	154150	4.4824 72	7.3948 24	10.275 83	15.553 84	15.465 27	2.3408 42
7 m at 20º and 200º	41.239562 69	229430	3.4114 39	5.6279 19	7.8205 4	11.837 44	11.770 03	1.7815 26
7 m at 335º and 155º	5.9461695 04	245960	0.4918 82	0.8114 67	1.1276 13	1.7067 93	1.6970 74	0.2568 71
7 m at 110º and 290º	40.376409 05	315100	3.3400 36	5.5101 26	7.6568 54	11.589 68	11.523 68	1.7442 38

6 m at 65º and 245º	41.69505021	338635	3.449118	5.690079	7.906917	11.96818	11.90003	1.801203
6 m at 20º and 200º	31.73251609	504009	2.624992	4.330503	6.017654	9.108526	9.056659	1.370827
6 m at 335º and 155º	4.575386041	540321	0.378487	0.624398	0.867662	1.313322	1.305844	0.197654
6 m at 110º and 290º	31.06834715	692209	2.570051	4.239864	5.891703	8.917882	8.867101	1.342135
5 m at 65º and 245º	30.58273932	775393	2.52988	4.173594	5.799614	8.778493	8.728506	1.321157
5 m at 20º and 200º	23.27535913	1154062	1.925395	3.176364	4.413865	6.680977	6.642934	1.005482
5 m at 335º and 155º	3.355982014	1237208	0.277615	0.457987	0.636418	0.963304	0.957818	0.144977
5 m at 110º and 290º	22.78820045	1584995	1.885096	3.109882	4.321482	6.541142	6.503895	0.984437
4 m at 65º and 245º	20.92807875	1892979	1.731222	2.856033	3.968734	6.007212	5.973005	0.904081

4 m at 20º and 200º	15.927564 36	281743 0	1.3175 68	2.1736 18	3.0204 53	4.5718 6	4.5458 27	0.6880 62
4 m at 335º and 155º	2.2965325 35	302041 4	0.1899 75	0.3134 05	0.4355 07	0.6591 98	0.6554 45	0.0992 09
4 m at 110º and 290º	15.594196 73	386947 1	1.2899 91	2.1281 23	2.9572 34	4.4761 7	4.4506 82	0.6736 6
3 m at 65º and 245º	12.833157 03	482864 3	1.0615 9	1.7513 27	2.4336 39	3.6836 39	3.6626 64	0.5543 85
3 m at 20º and 200º	9.7668274 76	718674 9	0.8079 36	1.3328 69	1.8521 5	2.8034 78	2.7875 14	0.4219 21
3 m at 335º and 155º	1.4082402 41	770452 6	0.1164 93	0.1921 81	0.2670 54	0.4042 22	0.4019 21	0.0608 35
3 m at 110º and 290º	9.5624055 06	987031 5	0.7910 26	1.3049 71	1.8133 84	2.7448	2.7291 71	0.4130 91
2 m at 65º and 245º	6.4413718 08	132804 69	0.5328 46	0.8790 47	1.2215 21	1.8489 36	1.8384 08	0.2782 64
2 m at 20º and 200º	4.9022829 69	197660 90	0.4055 29	0.6690 09	0.9296 53	1.4071 55	1.3991 42	0.2117 76

2 m at 335° and 155°	0.7068408	19885989	0.058472	0.096462	0.134043	0.202892	0.201737	0.030535
2 m at 110° and 290°	4.799677046	21190160	0.397041	0.655007	0.910196	1.377703	1.369858	0.207343
1 m at 65° and 245°	1.982564729	27146841	0.164003	0.270559	0.375967	0.569077	0.565836	0.085646
1 m at 20° and 200°	1.508854572	29597467	0.124816	0.205912	0.286134	0.433103	0.430637	0.065182
1 m at 335° and 155°	0.217555776	31729849	0.017997	0.02969	0.041257	0.062447	0.062092	0.009398
1 m at 110° and 290°	1.477273895	40649300	0.122204	0.201602	0.280146	0.424038	0.421623	0.063817

Table 0-2: Inputs for correlation analysis for varying wall thickness

Wall thickness	Diameter	Slug fatigue	Wave fatigue	Temperature fatigue	Design life
16.66	406.4	1.413511659	7.40843E-05	4.94303E-05	26.14235301
19.05	457.2	9.918792411	0.000371242	0.000169727	3.72562836

20.62	508	0.744201759	0.000999838	0.000407205	49.56452996
24.61	610	0.044131805	0.004220706	0.002133896	731.9940614
30	711	1.930144501	0.004057533	0.001895664	19.08775047
16.66	406.4	47.64529622	6.82913E-06	5.75714E-06	0.775642989
19.05	457.2	0.248322394	0.000106934	6.81958E-05	134.4915392
20.62	508	1.848218573	0.000529001	0.000245307	18.07514506
24.61	610	0.139002729	0.001419276	0.000585298	237.0147774
30	711	0.008749886	0.005723689	0.002899713	1923.689717
16.66	406.4	0.340700171	0.005537179	0.002629951	95.7980712
19.05	457.2	8.648168844	1.11306E-05	9.16766E-06	3.864487002
20.62	508	0.061285933	0.000150167	9.23078E-05	511.8539903
24.61	610	0.462984108	0.000711882	0.00034954	67.86739451
30	711	0.034751615	0.001924438	0.000833948	839.6043731
16.66	406.4	0.002489243	0.007312241	0.003877538	2302.325569
19.05	457.2	0.085963249	0.007113328	0.003578663	325.8339758
20.62	508	2.108657206	1.77799E-05	1.47431E-05	14.93513275

24.61	610	0.005010056	0.000152614	0.000166735	5175.183822
30	711	0.036994403	0.001207052	0.00063008	710.2643256
16.66	406.4	0.002913207	0.003238908	0.001479852	3613.832454
19.05	457.2	0.000345471	0.011232072	0.006203706	1551.108878
20.62	508	0.008583237	0.011041294	0.005899636	1080.57014
24.61	610	0.161158227	3.8289E-05	3.25638E-05	171.0650073
30	711	0.00061669	0.000437379	0.000270037	17954.55162
16.66	406.4	0.003829301	0.001955766	0.00101023	3498.555978
19.05	457.2	0.00033754	0.005068312	0.002293651	3087.696469
20.62	508	7.87061E-05	0.016582811	0.008919384	929.3546445
24.61	610	0.001439496	0.016454981	0.008706363	893.7210049
30	711	0.016302561	7.01226E-05	6.07413E-05	1446.669212